IMPROVING SAMPLE COLLECTION AND TIME SERIES ANALYSES OF
ENVIRONMENTAL DATA IN HE´EIA FISHPOND, OʻAHU, HAWAIʻI, FROM
2007 - 2011

A THESIS SUBMITTED TO THE GLOBAL ENVIRONMENTAL SCIENCE
UNDERGRADUATE IN PARTIAL FULFILLMENT OF THE REQUIREMENTS
FOR

BACHELOR OF SCIENCE
IN
GLOBAL ENVIRONMENTAL SCIENCE

DECEMBER 2011

By
Daniel E. McCoy

Thesis Advisors:
Kathleen C. Ruttenberg
Margaret McManus

ACKNOWLEGEMENTS

ABSTRACT

Since 2007, the He'eia Observatory Project, conducted under the supervision of Kathleen Ruttenberg, Margaret McManus, and initiated by Charles Young, has attempted to quantify the spatial and temporal variability of the chemical and physical properties of He'eia Fishpond. This was accomplished by monthly characterization of the surface and deep water column throughout the interior and exterior of the pond, as well as through the continuous deployment of in-situ temperature and water level sensors. As the project evolved, monthly sampling methods, routines, protocols, and in-situ instrument deployment schemes have changed, at times causing interruptions in data collection. This thesis project evaluated the suitability of previous deployment strategies and found that they were not optimal. The efforts made to evaluate and improve this strategy are documented in this undergraduate thesis.

In addition to improving the collection of data at He'eia Fishpond, archived temperature data (2007 – 2010) were combined with data from 2010 – 2011 to create temperature time-series plots of He'eia Fishpond. Coupled with spatial contour maps and environmental time series plots, the seasonal temperature changes within He'eia in the past four years were examined, with special attention given to the effects of the El Niño/Southern Oscillation phenomenon.

TABLE OF CONTENTS

LIST OF TABLES

LIST OF FIGURES

CHAPTER 1

INTRODUCTION TO HE'EIA FISHPOND AND RESEARCH GOALS

1.1 Introduction

Ancient Hawaiian fishponds were part of a complex Hawaiian subsistence economy that integrated freshwater, brackish, and oceanic-based aquatic farming systems. Creating these fishponds required the Hawaiian people to adapt their *ahupua'a*, or land divisions, into diverse plots based on their location between sea (*makai)* and mountain (*mauka)* (Fig 1.1). These were incredibly productive systems, and are believed to originate as far back as 1,500 – 1,800 years ago (Costa-Pierce 1987). Several different structures were known to have existed (Fig 1.2):

A) *loko wai* - Freshwater fishpond.

B) *loko 'ume'iki* - Seashore pond, with numerous stone lanes, which led fish into areas where they could be netted with the ebb and flow of the tide.

C) *loko pu'uone* - Coastal body of brackish water isolated from the sea by sand dunes, and fed by springs or streams.

D) *loko i'a kalo* - Freshwater, taro fishpond.

E) *loko kuapā* - Seashore pond bounded by a constructed wall with sluice gates, artificially enclosing the coastal reef with a stone wall. (Apple and Kikuchi 1975; Henry 1993; Kikuchi 1976).

He'eia Fishpond is a 0.356 km^2 (88 acre) *loko kuapā* (Fig 1.2, panel "D") located on the windward side of the Hawaiian island of Oahu (Fig 1.3), and is the site of the

research conducted for this thesis. It is estimated to be almost 800 years old (Kelly 1975), and has major cultural significance to the Hawaiian population that still influences its usage today. After Kamehameha conquered Oʻahu, He'eia Fishpond became known as the "King's Pond." He'eia Fishpond was later turned over to Abner Paki by Kamehameha III during The Great Mahele of 1848 (Kelly 1975). Today the pond is managed by the nonprofit organization Paepae o He'eia, whose goal is to restore the fishpond to its non-impacted ecological state and to "implement values and concepts from the model of a traditional fishpond to provide physical, intellectual, and spiritual sustenance for [their] community" (www.paepaeoheeia.org). The continued perseverance of Paepae o He'eia towards reconstructing He'eia Fishpond to its original form is a tremendous cultural achievement, and improving their knowledge of how the fishpond functions is crucial to achieving success.

1.2 Research Goals

In order to benefit the scientific community as well as the ongoing work at He'eia Fishpond, the goal of the research for this thesis was to provide data on some of the physical aspects of He'eia Fishpond. Specific objectives of this undergraduate research project are listed below:

Objective 1: Improve the monthly sampling methods utilized in the He'eia Observatory System (Chapter 2).

The He'eia Observatory System (HObS) is a research project that requires monthly water sample collection and water quality measurements. The project dates

back to 2007, and throughout the years has been modified significantly to achieve different collection goals. Primary goals of this thesis are to review, evaluate, and summarize past practices, create a final sampling scheme for data collection in order to achieve a systematic approach to water quality assessment for future studies, and to establish a more consistent record of the chemical and physical behavior of He'eia Fishpond. Additionally, tests conducted to optimize the quality of data collected by the YSI® 6600 V2 multi-parameter water quality sonde will aid future researchers in collecting data in the most efficient and effective way possible.

Objective 2: Establish an efficient in-situ sampling scheme (Chapter 3).

Having designed a more efficient and systematic approach to data collection in He'eia Fishpond (Objective 1), this project undertook to evaluate the placement of in-situ instruments utilized throughout the pond. TidbiT® v2 temperature sensors (Fig 1.4) and HOBO® water level loggers (Fig 1.5) have been deployed in a sporadic manner since 2007, and thus archived time-series temperature and pressure data is not consistent temporally and spatially. In order to improve the in-situ time series of He'eia Fishpond, a statistical approach to evaluate an optimal deployment scheme was conducted.

Objective 3: Evaluate a climate recording station at He'eia since 2007 (Chapter 4).

Physical oceanographic data have been collected at He'eia Fishpond since 2007 and extend into the present, in the form of monthly temperature and salinity profiles, and in-situ temperature data. Coupled with data available from the Kane'ohe

3

Bay Marine Corps Base (Mesowest 2011), a further objective of the present study was to determine whether data from in-situ instruments deployed in He'eia Fishpond are capable of detecting seasonal changes as well as longer term climate patterns such as El Niño and La Niña. Biogeochemical research conducted in He'eia Fishpond will benefit from the background knowledge of seasonal and interannual patterns of pond temperature, rainfall, air temperature, and wind. Additionally, establishing a systematic routine for collecting physical oceanographic data will result in a more complete data set that will aid Paepae o He'eia in understanding the seasonal and yearly changes that occur within He'eia Fishpond.

1.3 Overview of Study Site

He'eia Fishpond is located adjacent to He'eia stream, a freshwater source to Kane'ohe Bay that originates in the mountains that rise at the back of the He'eia *ahupua'a,* immediately *mauka* of the pond (Fig 1.6). The stream passes through 410.2 km^2 (Young 2011) of ancient taro farmland, where waters were historically diverted to flood the numerous *lo'i* (taro patch) plots. The stream originally carried a far smaller sediment load than it does today, as suspended particles had more time to sift out and deposit over the taro patches (Henry 1975; Kelly 1975). As a consequence of an increase in land usage over the past century, increased sediment loading into the pond overwhelms the natural flushing mechanisms, resulting in progressive accumulation of the terrigenous particulate load on the pond bottom (Young 2011). Each year the pond becomes shallower, an issue that reveals the ever apparent forces that change the environment of He'eia Fishpond.

The pond is fully surrounded by an ancient 2.5 km *kuapā* (fishpond wall),

interrupted by three freshwater *mākāhā* (sluice gates) (Fig 1.7) along the northern

edge of the pond, five saltwater *mākāhā* along the eastern wall, and a break in the

pond's eastern wall known as OB (ocean break, Fig 1.8). Each *mākāhā* is a flume

with a horizontal concrete floor and vertical basalt rock or concrete mortar walls

(Young 2011). A groove on either side of the *mākāhā* walls allows for a gate to be

placed into the *mākāhā*, preventing large fish from entering or exiting the pond, and

preventing outside water sources from entering the pond.

He'eia stream flows into the pond through the freshwater sluice gates known

as River *Mākāhā* 1 (RM1), River *Mākāhā* 2 (RM2), and River *Mākāhā* 3 (RM3)

before running into Kane'ohe Bay at the river mouth northeast of the pond (Fig 1.8).

RM1 and RM2 are above the normal tidal range of He'eia Fishpond, resulting in

unidirectional flow of He'eia stream into the pond. RM3 is positioned at a lower

elevation, and thus allows bi-directional flow based on the semidiurnal tidal cycle

(Young 2011).

The remaining *mākāhā* are all seawater sluice gates which, depending on tidal

height, either discharge or permit water flow out of/into the pond. The northernmost

mākāhā is a series of three closely placed *mākāhā* known as Triple *Mākāhā* (TM),

which often are treated as a single *mākāhā* due to their narrow widths (1.85 m, 1.50

m, 1.63 m) in comparison to the other seaward gates. Ocean *Mākāhā* 1 (OM1) is the

largest *mākāhā* in the fishpond at 6.60 m wide, located halfway down the *kuapā* on

the eastward side of He'eia Fishpond. The final sluice gate, Ocean *Mākāhā* 2 (OM2),

is the southern most *mākāhā* in the fishpond and furthest from the mouth of He'eia

stream. While only 1.82 m wide, OM2 is the only gate that features a guard house (Fig 1.7).

Breaks in the fishpond wall (apart from *mākāhā*) such as OB, as well as the island towards the northwestern corner of the pond (Fig 1.8), are a result of a major flooding event in 1965, which affected the entire east coast of Oahu. The island was formed from the remnants of the *kuapā* that was used for a freshwater *mākāhā* to the northwest (known as RM1), transforming that area of the fishpond into a "diffuse flow region" rather than a sluice gate (Young 2011). A 50 m gap in the *kuapā* at OB was replaced with a temporary 79 m wall that elbows into the pond while repairs are currently being conducted. While accomplishing the task of retaining pond water, the height of the surrounding intact *kuapā* is 1.20 m high, while the replacement wall measures 0.90 m. Spring tides in Kane'ohe Bay thus cause water to overflow the replacement wall and enter He'eia Fishpond at OB at significant rates (Young 2011).

He'eia Fishpond contains twenty ~3 m tall PVC stakes driven into the seabed that form the sampling grid used in this thesis, as well as in previous studies. Each stake is given a number based on its position in the pond. Starting from just north of OM2 (pond 1), the stakes are numbered following the eastward *kuapā* until reaching the northern most stake 7 in the pond (pond 1 - 7). The stake numbering then follows a transect south, bisecting the pond, before reaching an area to the northwest of the boat dock (pond 8 – 13). From there, the stakes follow the westward *kuapā* (currently covered with mangrove) until reaching an area just to the south of RM2 (pond 14 – 19). A final stake (pond 20) is placed to the northeast of the pond dock, just southeast of OM2. Locations and abbreviated names are outline in Fig 1.9.

6

The last two sites occupied in this thesis research are two ocean sites, originally included in the He'eia sampling scheme in order to characterize the oceanic contribution to the nutrient dynamics of He'eia Fishpond, following the study conducted by Young (2011). The first ocean site is located just southeast of the He'eia river mouth, labeled as Ocean 1 (OCN1), and was chosen by Young (2011) to represent "a less confounded water sample from Kane'ohe Bay". To the north of OM2, outside the *kuapā*, is another ocean site known as Ocean 2 (OCN2), chosen to represent Kane'ohe Bay water. These sites are sampled monthly for archival purposes, and data recorded were excluded from this thesis. Their locations are noted in Fig 1.8.

1.4 Sampling Methods

He'eia Fishpond data were obtained through three primary methods: monthly discrete water sampling, monthly YSI® profiling, and in-situ instrumentation. Monthly profiles were obtained at pond stakes and *mākāhā* using a YSI® 6600v2 Multi-parameter Water Quality Sonde, a portable instrument set to record water column temperature, depth, conductivity (salinity), pH, dissolved oxygen, fluorescence (a proxy for chlorophyll-a), and turbidity to a handheld recorder every second (Fig 1.10). The sites that were sampled have varied since 2007, and the different sampling schemes (1 - 6) are outlined in Table 1.1. In-situ instruments deployed in He'eia Fishpond include HOBO® water level loggers (Fig 1.5) and TidbiT® v2 temperature sensors (Fig 1.4). Deployment methods, timelines, and schemes are outlined further in Chapter 3.

Along with YSI and in-situ raw data, water was collected in acid washed (H+) 1 liter HDPE (high density polyethylene) and 250 ml amber HDPE bottles at all *mākāhā,* ocean sites, and a group of preselected stakes during the sampling effort. Depending on the site, water was collected at both the surface and sediment water interface, or at the surface only. The collection scheme has varied since 2007, and is outlined in Table 1.2.

After collection, samples were placed on ice, brought back to the lab, and filtered as soon as possible. Depending on the water quality factor being sought, different filtering methods were utilized to obtain archive samples. Young (2011) summarized the different filtering methods used to obtain these samples. For the purpose of this thesis, only TSS (total suspended solids) and fluorescence (a proxy for chlorophyll-a) samples were collected, which are discussed further in Chapter 2. Collection schemes utilized since 2007 are outlined in Table 1.3. Different schemes and each date the scheme was utilized are summarized in Table 1.4.

The following chapters discuss the methods and findings on improving the monthly sampling routine employed at He'eia Fishpond (Chapter 2), the rationale used for establishing a permanent in-situ sampling scheme (Chapter 3), and the methods and preliminary results of the climate monitoring within He'eia Fishpond since 2007 (Chapter 4). This thesis will expand our knowledge on the physical environment of He'eia Fishpond and will provide future researchers with a more consistent data collection routine to benefit long-term, time-series studies on the influences of physical, biological, and chemical changes to this small coastal mesocosm.

Table 1.1: YSI sampling site schemes from 2007 – 2011. For each scheme, (x) indicates sites that were profiled. Refer to Table 1.4 for dates each scheme was utilized.

YSI Profile Sites	Scheme P1	Scheme P2	Scheme P3	Scheme P4	Scheme P5	Scheme P6
OM2	X		X	X	X	X
OCN2	X		X	X	X	X
OB	X		X	X	X	X
OM1	X		X	X	X	X
TM	X		X	X	X	X
OCN1	X		X	X	X	X
RM3	X			X	X	X
RM2	X			X	X	X
RM1	X			X	X	X
River						
Pond 1	X				X	X
Pond 2						X
Pond 3	X				X	X
Pond 4						X
Pond 5						X
Pond 6	X	X			X	X
Pond 7	X	X			X	X
Pond 8	X				X	X
Pond 9	X	X		X	X	X
Pond 10						X
Pond 11		X			X	X
Pond 12						X
Pond 13	X	X		X	X	X
Pond 14						X
Pond 15	X				X	X
Pond 16	X				X	X
Pond 17						X
Pond 18	X	X			X	X
Pond 19						X
Pond 20						X
Dates	8/11/07 - 11/5/07 11/17/07 - 2/11/10 except 3/15/2009	11/6/07 - 11/11/07	3/15/09	3/4/10	4/29/10 - 9/16/10	10/14/10 - present

Table 1.2: Monthly bottle grab sampling schemes. SFC denotes that only surface water bottle samples were taken (top 25 cm of water column), where SFC/DEEP notes that bottle samples were taken at the pond surface as well as near the sediment water interface (bottom 25 cm of water column). Refer to Table 1.4 for dates each scheme was utilized.

Sampling Sites	Scheme WC1	Scheme WC2	Scheme WC3	Scheme WC4	Scheme WC5	Scheme WC6
OM2	SFC		SFC	SFC	SFC	SFC
OCN2	SFC		SFC	SFC	SFC	SFC
OB	SFC		SFC	SFC	SFC	SFC
OM1	SFC		SFC	SFC	SFC	SFC
TM	SFC		SFC	SFC	SFC	SFC
OCN1	SFC		SFC	SFC	SFC	SFC
RM3	SFC		SFC	SFC	SFC	SFC
RM2	SFC		SFC	SFC	SFC	SFC
RM1	SFC		SFC	SFC	SFC	SFC
River	SFC		SFC	SFC	SFC	SFC
Pond 1	SFC/DEEP		SFC		SFC	
Pond 2						
Pond 3	SFC/DEEP		SFC		SFC	
Pond 4						
Pond 5						
Pond 6	SFC/DEEP	SFC	SFC		SFC	SFC/DEEP
Pond 7	SFC/DEEP	SFC	SFC		SFC	SFC/DEEP
Pond 8	SFC/DEEP		SFC		SFC	
Pond 9	SFC/DEEP	SFC	SFC	SFC	SFC	SFC/DEEP
Pond 10						
Pond 11		SFC			SFC	SFC/DEEP
Pond 12						
Pond 13	SFC/DEEP	SFC	SFC	SFC	SFC	SFC/DEEP
Pond 14						
Pond 15	SFC/DEEP		SFC		SFC	
Pond 16	SFC/DEEP		SFC		SFC	
Pond 17						
Pond 18	SFC/DEEP	SFC	SFC		SFC	SFC/DEEP
Pond 19						
Pond 20						
Dates	8/11/07 - 11/05/07 11/17/07 - 8/30/08	11/06/07 - 11/11/07	7/2/09 - 2/11/10	3/4/10	4/29/10 - 10/14/10	11/11/10 - present

Table 1.3: Monthly sampling schemes for grab sample filtering. Refer to Table 1.4 for dates each scheme was utilized. Abbreviations: TSS (Total Suspended Solids), Chl-A (Chlorophyll A/Fluorescence), SEDEX (Sediment Sequential Extraction for phosphorus), Fe-Ox (selective extraction for Iron Oxyhdryoxide), DIC (Dissolved Inorganic Carbon), DOC/TDN (Dissolved Organic Carbon and Total Dissolved Nitrogen), Nutrients (Dissolved Inorganic Nutrients), Nuts-Acidified (Total Dissolved Phosphorus), CN (Carbon Nitrogen), Phytocount (Commercial Enumeration of Cell Type at Genus Level).

Sample Taken/Filtered	Scheme F1	Scheme F2	Scheme F3	Scheme F4	Scheme F5	Scheme F6
TSS	X	X	X	X	X	X
Chl-A	X	X	X	X	X	X
Sedex	X	X	X	X	X	
Fe-Ox	X	X	X	X	X	
DIC	X		X			
DOC/TDN	X	X				X
Nutrients	X	X	X	X	X	X
Nuts-Acidified	X	X	X	X	X	X
CHNorg	X	X				
CHNtotal	X	X				
Phytocount	X	X		X		
Dates	8/11/07 + 11/05/07 11/17/07 - 3/15/08 5/17/08 - 8/30/08	9/15/07 + 10/13/07 11/06/07 - 11/11/07 4/19/08	9/28/09	8/9/10	7/02/09 + 8/12/09 10/22/09 - 7/29/10 9/16/10 - 10/14/10	11/11/10 – present

11

Table 1.4: YSI schemes (sites profiled, Table 1.1), water column sample schemes (surface or surface/deep grab sample locations, Table 1.2), and filtering schemes (grab sample filtering byproducts, Table 1.3) for each monthly sampling date since 8/11/2007.

DATES	YSI SCHEME	SAMPLE SCHEME	FILTER SCHEME
8/11/2007	P1	WC1	F1
9/15/2007	P1	WC1	F2
10/13/2007	P1	WC1	F2
11/5/2007	P1	WC1	F1
11/6/2007	P2	WC2	F2
11/7/2007	P2	WC2	F2
11/8/2007	P2	WC2	F2
11/11/2007	P2	WC2	F2
11/17/2007	P1	WC1	F1
12/9/2007	P1	WC1	F1
1/12/2008	P1	WC1	F1
2/16/2008	P1	WC1	F1
3/15/2008	P3	WC1	F1
4/19/2008	P1	WC1	F2
5/17/2008	P1	WC1	F1
6/14/2008	P1	WC1	F1
7/26/2008	P1	WC1	F1
8/30/2008	P1	WC1	F1
7/2/2009	P1	WC3	F5
8/12/2009	P1	WC3	F5
9/28/2009	P1	WC3	F3
10/22/2009	P1	WC3	F5
11/22/2009	P1	WC3	F5
12/14/2009	P1	WC3	F5
1/28/2010	P1	WC3	F5
2/11/2010	P1	WC3	F5
3/4/2010	P4	WC4	F5
4/29/2010	P5	WC5	F5
5/20/2010	P5	WC5	F5
6/18/2010	P5	WC5	F5
7/29/2010	P5	WC5	F5
8/9/2010	P5	WC5	F4
9/16/2010	P5	WC5	F5
10/14/2010	P6	WC5	F5
11/11/2010	P6	WC6	F6
12/2/2010	P6	WC6	F6
1/27/2011	P6	WC6	F6
2/17/2011	P6	WC6	F6
4/29/2011	P6	WC6	F6

Figure 1.1: Generalized Hawaiian ahupua'a. Rainwater from the forest watershed was redirected into various taro plots before entering the coastal region, where fishponds would intercept the river waters and create productive fish farms. Figure from Costa-Pierce (1987).
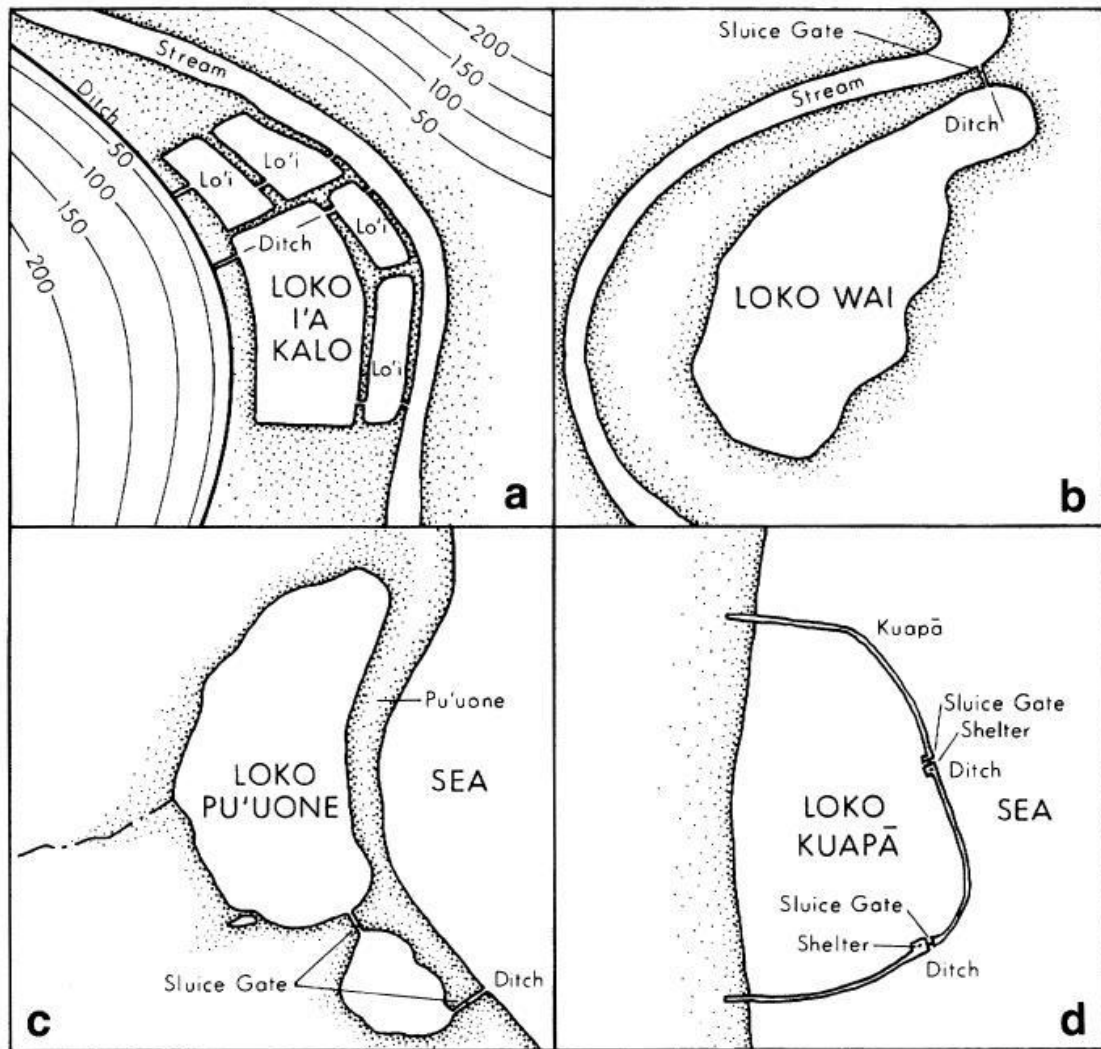
Figure 1.2: The main types of Hawaiian farming systems. (a) Lo'i are taro patches constructed in the valleys. (b) *Loko wai* are freshwater ponds used for aquaculture. (c) *Loko pu'uone* were brackish-water lakes separated by a spit of land and connected to the sea by a ditch that had grates to trap and hold large fish. (d) *Loko Kuapā* were the fishponds, built along the shoreline, usually on top of a flat reef. Figure from Costa-Pierce (1987).
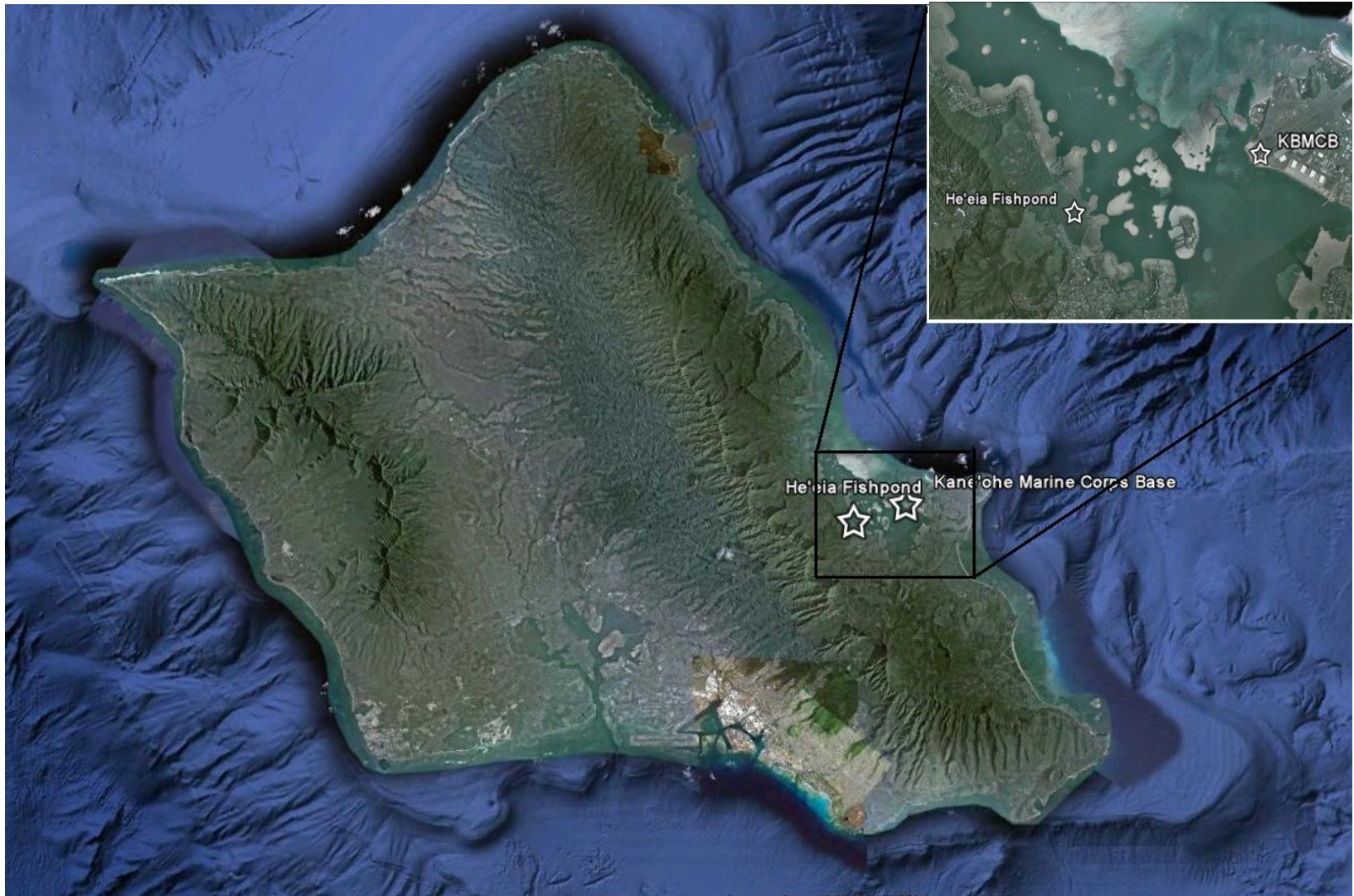
Figure 1.3: Map of Oahu with Kane'ohe Bay inset. He'eia Fishpond and Kane'ohe Marine Corps Base are shown.

Temperature Sensor
Operation range:*
-20° to 70°C (-4° to 158°F) in air;
maximum sustained temperature of 30°C (86°F) in water*

Accuracy: 0.2°C over 0° to 50°C (0.36°F over 32° to 122°F)

Resolution: 0.02°C at 25°C (0.04°F at 77°F)

Response time: 5 minutes in water; 12 minutes in air moving 2 m/sec; 20 minutes in air moving 1 m/sec (typical to 90%)

Stability (drift): 0.1°C (0.18°F) per year

Logger
Real-time clock: ± 1 minute per month 0° to 50°C (32° to 122°F)

Battery: 3 Volt lithium, non-replaceable

Battery life (typical use): 5 years with 1 minute or greater logging interval

Memory (non-volatile): 64K bytes memory (approx. 42,000 12-bit temperature measurements)

Weight: 19.5 g (0.68 oz)

Dimensions: 3.0 × 4.1 × 1.7 cm (1.2 × 1.6 × 0.65 in.); mounting bail 4.6 mm (3/16 in.) diameter

Figure 1.4: TidbiT® v2 Temperature Logger with sensor specs (for more information visit www.OnsetComp.com).

Pressure Sensor

Operation range: 0 to 207 kPa (0 to 30 psia); approximately 0 to 9 m (0 to 30 ft) of water depth at sea level, or 0 to 12 m (0 to 40 ft) of water at 3,000 m (10,000 ft) of altitude

Factory calibrated range: 69 to 207 kPa (10 to 30 psia), 0° to 40°C (32° to 104°F)

Burst pressure: 310 kPa (45 psia) or 18 m (60 ft) depth

Water level accuracy*: Typical error - 0.05% FS, 0.5 cm (0.015 ft) water

Maximum error: - 0.1% FS, 1.0 cm (0.03 ft) water

Raw pressure accuracy**: 0.3% FS, 0.62 kPa (0.09 psi) maximum error

Resolution: < 0.02 kPa (0.003 psi), 0.21 cm (0.007 ft) water

Pressure response time: 90% < 1 second

Thermal response time (90%)†: Approximately 10 minutes in water to achieve full temperature compensation of the pressure sensor

* With accurate reference water level measurement and Barometric Compensation Assistant data
** Absolute pressure sensor accuracy includes all pressure drift, temperature, and hysteresis-induced errors
† Maximum error due to rapid thermal changes is approximately 0.5%

Temperature Sensor
Operation range: -20° to 50°C (-4° to 122°F)

Accuracy: 0.37°C at 20°C (0.67°F at 68°F), see Plot A

Resolution: 0.1°C at 20°C (0.18°F at 68°F) (10-bit)

Response time (90%): 3.5 minutes in water (typical)

Stability (drift): 0.1°C (0.18°F) per year

Figure 1.5: HOBO® water level logger (0 – 30ft) in-situ instrument with pressure and temperature sensor operation ranges and specs (for more information, visit www.OnsetComp.com)

17

Figure 1.6: He'eia Fishpond (black outline) with the ahupua'a (land division) of He'eia in grey, He'eia stream in blue. Ahupua'a outline taken from Young (2011).

NORMAL TIDE RANGE   GRATE

ROCKS

VIEW OF MAKAHĀ FROM SEAWARD

GUARD HOUSE   AUWAI O KA MAKAHĀ   NETTERS AREA

SEAWARD
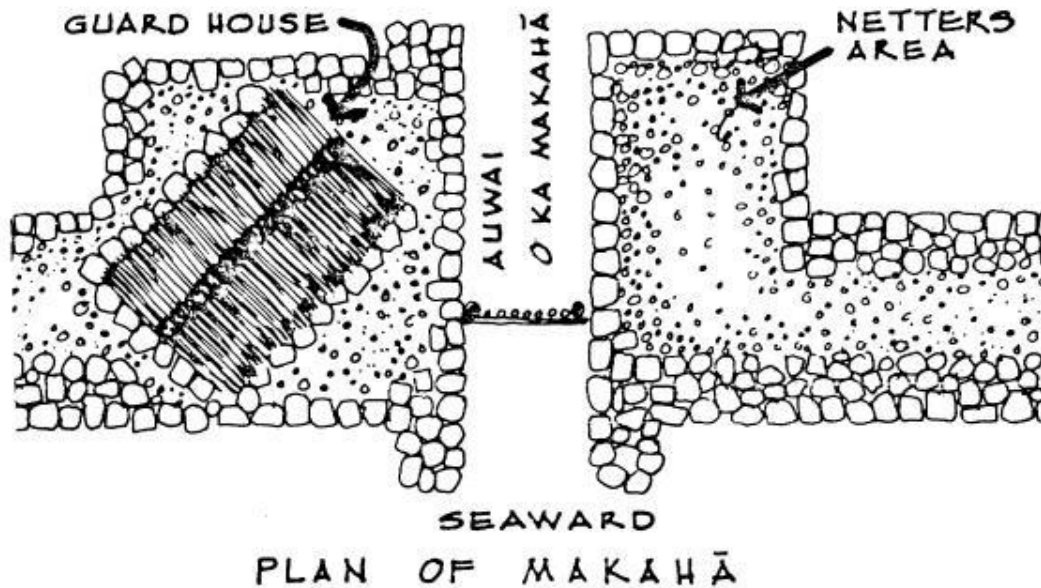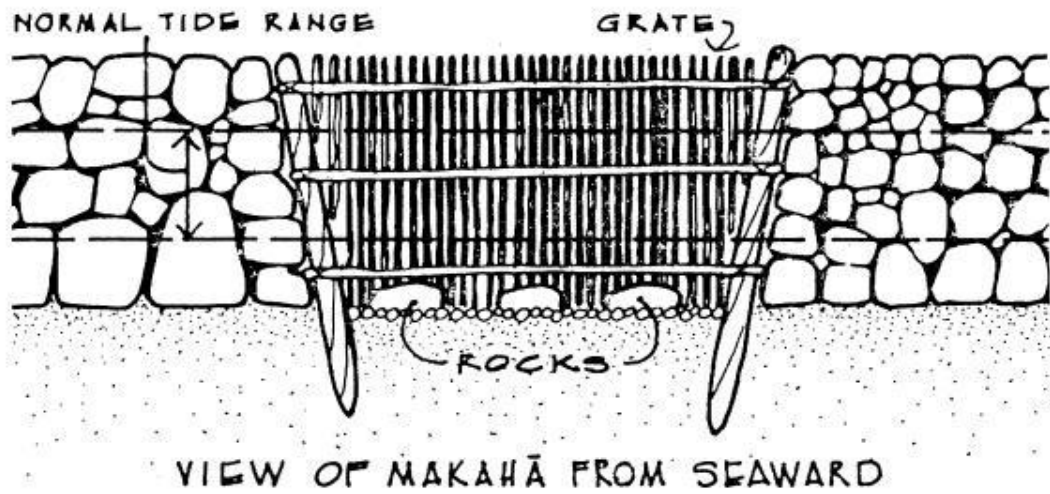
PLAN OF MAKAHĀ

Figure 1.7: Sketches of *mākāhā* plans taken from Costa-Pierce (1987). The sluice gates allow water to pass through, although at a much slower pace then without the gates present.

Figure 1.8: He'eia Fishpond with He'eia stream (blue line) and each of the sluice gates (*mākāhā*) and ocean sites (OCN1 and OCN2). RM1, RM2, and RM3 are freshwater sluice gates permitting He'eia stream water to flow into He'eia. OM1, OM2, and TM are ocean sluice gates permitting Kane'ohe Bay waters to flow into the pond. OB is a break in the pond wall that currently allows Kane'ohe Bay waters to flood into the pond at high tide. The black circle just to the right of RM1 is a small mangrove island that was created from debris washed into the pond during the 1965 flood (see text). Site names from Young (2011)

Figure 1.9: He'eia Fishpond and He'eia stream (blue line) with all sampling stakes (pond 1 – 20). Site names from Young (2011).

YSI 6600 V2 Sensor Specifications

	Range	Resolution	Accuracy
ROX™ Optical Dissolved Oxygen* % Saturation	0 to 500%	0.1%	0 to 200%: ±1% of reading or 1% air saturation, whichever is greater; 200 to 500%: ±15% of reading
ROX™ Optical Dissolved Oxygen* mg/L	0 to 50 mg/L	0.01 mg/L	0 to 20 mg/L: ± 0.1 mg/L or 1% of reading, whichever is greater; 20 to 50 mg/L: ±15% of reading
Dissolved Oxygen** % Saturation ETV✓ 6562 Rapid Pulse™ Sensor*	0 to 500%	0.1%	0 to 200%: ±2% of reading or 2% air saturation, whichever is greater; 200 to 500%: ±6% of reading
Dissolved Oxygen** mg/L ETV✓ 6562 Rapid Pulse™ Sensor*	0 to 50 mg/L	0.01 mg/L	0 to 20 mg/L: ± 0.2 mg/L or 2% of reading, whichever is greater; 20 to 50 mg/L: ±6% of reading
Conductivity*** 6560 Sensor* ETV✓	0 to 100 mS/cm	0.001 to 0.1 mS/cm (range dependent)	±0.5% of reading + 0.001 mS/cm
Salinity	0 to 70 ppt	0.01 ppt	±1% of reading or 0.1 ppt, whichever is greater
Temperature 6560 Sensor* ETV✓	-5 to +50°C	0.01°C	±0.15°C
pH 6561 Sensor* ETV✓	0 to 14 units	0.01 unit	±0.2 unit
ORP	-999 to +999 mV	0.1 mV	±20 mV
Depth Deep	0 to 656 ft, 200 m	0.001 ft, 0.001 m	±1 ft, ±0.3 m
Medium	0 to 200 ft, 61 m	0.001 ft, 0.001 m	±0.4 ft, ±0.12 m
Shallow	0 to 30 ft, 9.1 m	0.001 ft, 0.001 m	±0.06 ft, ±0.02 m
Vented Level	0 to 30 ft, 9.1 m	0.001 ft, 0.001 m	±0.01 ft, 0.003 m
Turbidity* 6136 Sensor* ETV✓	0 to 1,000 NTU	0.1 NTU	±2% of reading or 0.3 NTU, whichever is greater**
Nitrate/nitrogen****	0 to 200 mg/L-N	0.001 to 1 mg/L-N (range dependent)	±10% of reading or 2 mg/L, whichever is greater
Ammonium/ammonia/ nitrogen****	0 to 200 mg/L-N	0.001 to 1 mg/L-N (range dependent)	±10% of reading or 2 mg/L, whichever is greater
Chloride****	0 to 1000 mg/L	0.001 to 1 mg/L (range dependent)	±15% of reading or 5 mg/L, whichever is greater
Rhodamine*	0-200 µg/L	0.1 µg/L	±5% reading or 1 µg/L, whichever is greater

Figure 1.10: YSI 660v2 Multiparameter Water Quality Sonde image with individual sensor specifications (for more specifications, visit www.YSI.com)

22

CHAPTER 2

ASSESSMENT OF MONTHLY SAMPLING FIELD METHODS AT

HE'EIA FISHPOND

2.1 Introduction

Water quality assessment at He'eia Fishpond is of interest to both Paepae o He'eia, the non-profit organization that works to restore the pond to its original conditions, and for the biogeochemical research being conducted there. Remediation of He'eia Fishpond to pre-contact conditions required, as a first step, a full characterization of current conditions including present-day nutrient loading and physical oceanographic parameters. The He'eia Observing System (HObS) was initiated to characterize He'eia Fishpond by investigating month-to-month fluctuations in biogeochemical and physical parameters. These included dissolved inorganic nutrients, TDN (total dissolved nitrogen), DON (dissolved organic nitrogen), TDP (total dissolved phosphorous), DOP (dissolved organic phosphorus), DOC (dissolved organic carbon), chlorophyll-a, dissolved oxygen, pH, and turbidity, as well as salinity and temperature. Water column profiling and discrete sample collection efforts were conducted each month, beginning in August 2007, to accomplish this task. By completing monthly sample inventories, broad seasonal patterns in nutrient loading behavior were characterized by Young (2011).

In addition to monthly profiling and sampling, Young (2011) deployed in-situ temperature sensors that have resulted in the availability of an archived data set that was used in this thesis research to analyze the climate of He'eia Fishpond (discussed

in Chapter 4). Having been in operation since August 2007, it was timely to evaluate

the efficiency of the profiling, sampling, and in-situ deployment schemes employed

by HObS to date. A major goal of this thesis was to evaluate past practices, and make

recommendations for improving the efficiency and accuracy of data collected by

HObS.

The monthly sampling protocol for the HObS has been inconsistent since it's

inception in 2007. As with many pilot projects, collecting accurate primary data

requires trial and error in protocol, sampling and filtering methods, and supply

purchases. A large focus of this thesis work was centered on significantly improving

the monthly sampling routine utilized at He'eia Fishpond in order to create more

reliable data in the future. This chapter documents such efforts, including the

following:

1) Finalize a YSI® sonde deployment strategy. The sampling grid used for

    YSI® water column profiling varied among six unique schemes since

    2007 (Table 1.1). Using past data to formulate the ideal deployment grid

    throughout the pond will allow for more accurate month-to-month

    comparisons in YSI® data and aid in creating smoother contour plots used

    to characterize the spatial distribution of a variety of properties of He'eia

    Fishpond .

2) Evaluate the mode of YSI® deployment in order to determine how to best

    deploy the sonde in order to eliminate instability and inaccuracy. Two

tests were conducted: the first to ascertain the ideal deployment time

required to stabilize YSI® probes in order to reduce error. The second test

was to determine whether continuous vertical profiling was superior to

static data collection to characterize the properties of the surface and deep

water column.

3) Limit sampling supplies. Grab samples are made each month to achieve

TSS (total suspended solids) and chlorophyll-a values at each stake. The

YSI® simultaneously records similar values using optical probes.

Performing standardization curves each month could significantly reduce

the amount of bottles and filters normally used to ascertain TSS and

chlorophyll-a values via grab samples.

2.2 Methods

Monthly Sampling: Beginning in August 2007, field-sampling efforts within

He'eia Fishpond focused on the collection of YSI® water column profile data at

selected sites (see below) and the collection of discrete water column samples at all

mākāhā, ocean sites, and selected transect stakes. While filtered water and filtered

particles have been collected for different analyses in the past (see Young (2011) for a

more in depth explanation of water column sampling and analyses conducted), the

current field sampling strategy follows a reduced sampling regime, focused mainly

around the collection of TSS, dissolved inorganic nutrients, total dissolved

phosphorus, dissolved organic carbon, total dissolved nitrogen, and chlorophyll-a.

From the initiation of the HObS project, the twelve monthly sampling dates within a calendar year were divided between the four tidal cycles; neap-flood, neap-ebb, spring-flood, and spring-ebb. The initial focus of HobS was on nutrient loading from Kane'ohe Bay and He'eia stream, so examining the effects of different tidal states on nutrient loading seemed practical (Young 2011). After the completion of Young's thesis work, however, the focus shifted to characterizing long-term environmental patterns. Therefore, under the reduced sampling scheme (October 2010-present), a decision was made to sample at the same tidal height, midway between high and low tide, rather than at the extremes of the tidal cycle, in order to facilitate comparisons between monthly water quality data sets.

Pre-sampling Preparation:

- Sampling supplies were washed with phosphate free soap and reverse osmosis (RO) water, then submerged in a 10% hydrochloric acid (H^+) bath. The supplies consisted of 1 L HDPE (high density polyethylene) bottles for TSS, 250 ml amber HDPE fluorescence/chlorophyll-a bottles, 500 ml and 250 ml filtering rigs, and 250 ml graduated cylinders.

- Pre-weighed duplicate 47 mm, 0.2 um hydrophilic polypropylene membrane filters were placed in pitri dishes and labeled for each site at which TSS samples were collected.

- "Nutrients" (dissolved inorganic nutrients) and "nutrients acidified" (TDP) 60 ml bottles for filtered water collection were washed (as described above) and organized. The TDP bottles required 600 ul of concentrated

trace metal clean hydrochloric acid to be carefully pipetted into each bottle (with a 600 ul acid: 60 ml sample ratio, all samples are assumed to be pH 1 when stored).

- Vials were prepared for chlorophyll-a filter storage by wrapping 13x100mm Fisher-Brand® culture tubes with aluminum foil to prevent light penetration that would otherwise allow photodecomposition of samples.

- The 40 cc glass vials to be used in DOC (dissolved organic carbon)/TDN (total dissolved nitrogen) collection were soap, RO, and acid washed (H^+) before being muffled in a 550C° furnace for two hours to remove hydrocarbon build-up.

- The YSI® was calibrated 24 hours before sampling began. All probes were calibrated according to instructions in the YSI® 6-series multi-parameter water quality sonde user manual (See appendix A for simplified instructions).

Sampling Protocol:

- The last of the YSI® calibrations, dissolved oxygen and pressure, were completed once at pond level.

- The YSI® was placed in a bucket of pond water in the front of the boat to keep all probes hydrated. In particular, the pH and dissolved oxygen probes must be in a humid environment for probe calibrations to be maintained.

- The boat was slowly driven to each sampling site. Each site was approached from downwind in order to prevent the engine motor, which often disturbs the SWI (sediment water interface), from contaminating the samples.

- Each H^+ clean bottle was rinsed three times with pond water at the site to condition the bottles to the sample water, and a water sample was then taken by fully submerging the bottle into the water column. "Deep" sampling bottles were inverted, and then lowered to the SWI to prevent surface water from contaminating the samples.

- The YSI® was left submerged in the water for at least 60 seconds (rationale discussed later) while bottle samples were taken. After all probes were stabilized, data were collected for a ~30 second time period at the surface of the pond water column. The YSI® was then lowered to the SWI, and data were collected for a ~30 second time period (rationale discussed below) to characterize the deep-water column.

Sample Processing:

- HDPE bottle samples for TSS were filtered through a 47 mm, 0.2 um hydrophilic filter mounted on a filtration rig to remove suspended solids, yet allow for filtrate collection for nutrient samples. For each 1000 ml bottle, 500 ml was used for the first of the duplicate TSS samples. After the first round of filtering was completed, the filter was saved and all filtrate discarded. The second of the duplicate TSS filters from the same

site was placed in the filtering rig, and 250 ml of water was allowed to filter through. The filtrate was discarded (due to a suspicion that the hydrophilic polypropylene filters themselves aren't perfectly clean), and another 250 ml was filtered through the same TSS filter. The filter was saved, and the 250 ml of filtrate was also saved and poured into the nutrient, nutrient acidified, and DOC/TDN vials, and the latter two were stored in a freezer for future analysis; the acidified samples were stored refrigerated.

- Chlorophyll-a samples were filtered through a separate filtration rig, with 150 ml of water filtered through a 25 mm, 0.2 um glass microfiber filter (GP/P). The filter was then stored in the prepared aluminum wrapped vials, capped, and stored in a freezer for future analysis.

- TSS filter samples were placed in a drying oven at 60ºC after sampling was completed and given a few days to evaporate all humidity from the filter. After drying, the samples were weighed at least three more times. The initial TSS weight (before sampling) was subtracted from the final weight, and a TSS g/L value was recorded.

- YSI® data was organized on spread sheets and binned into top 25 cm surface and bottom 25 cm deep profiles for each site.

Evaluations of YSI Profiling Grid Using Matlab® Contouring: Spatial contouring creates images of the physical oceanographic parameters of He'eia Fishpond, and is a great tool for drawing conclusions about how the fishpond

29

functions. Work by Benjamin (2010) and Young (2011) attempted to accurately contour He'eia Fishpond by using a selected group of sites (Fig 2.1) from sampling scheme P5 (see Table 1.1). Since October 2010, the reduced sampling regime (outlined in Chapter 1) profiled the water column at all sites of He'eia Fishpond (Fig 3.5). In order to evaluate whether the additional sites profiled by the reduced sampling scheme led to superior contour plots of He'eia Fishpond, relative to the original scheme, a direct comparison was made. YSI® sonde data were offloaded into Microsoft Excel® using Ecowatch® software, and organized into surface and deep water based on the YSI® depth (two different methods were used to achieve this, discussed below).

Table 1.1 summarizes the various YSI® sampling schemes from 2007 to the present; "scheme 5" was the dominant deployment grid used over the past four years. Surface contour maps of temperature in He'eia Fishpond from the April 2011 sampling were created using Matlab®, with one contour plot using only the sites that "scheme 5" would have sampled, and a second plot using the full twenty stake grid (along with all six *mākāhā*) that "scheme 6" describes (see appendix for script). Visual analysis of the old ("scheme 5") and new ("scheme 6") sampling grid for YSI® deployment, as revealed in the spatial contour plots, permits objective evaluation of the relative superiority of the new scheme over the old scheme for faithfully capturing the spatial distribution of surface water temperatures within the pond.

YSI® Standardization Experiment: Standardization experiments were conducted to determine whether TSS and Chl-a filtering at each sampling site could be replaced by a standard curve established by the optical NTU (nephelometric unit, a proxy for TSS) and fluorescence probes on the YSI®. Two experiments were run, one each for Chl-a and TSS. Each of these is described below.

Chlorophyll standardization curves were constructed using YSI® fluorescence data and chlorophyll-a concentrations determined via fluorometer on extracted filtered particles from the December 2010 monthly sampling. All filters collected were allowed to thaw overnight, after which 5 ml of a 90% acetone solution was then added to the chlorophyll vials containing the filters. The next day the sample extracts were run on a fluorometer to determine chlorophyll-a concentrations in units of g/L. These experimental values were compared to the fluorescence data from the YSI fluorescence probe for each site and a standard curve was constructed (Young 2011).

The TSS standardization experiment was conducted by preparing triplicate TSS 47 mm, 0.2 um hydrophilic polypropylene membrane filters for four sites in He'eia Fishpond; a river *mākāhā* site (RM3), a pond site (Pond 20), an ocean *mākāhā* site (OM2), and an ocean site (OCN2) (Fig 2.2). Sites were chosen based on NTU values from previous deployments in order to sample at the NTU value extremes. The river *mākāhā* (RM3) tends to carry a lot of suspended sediment into the pond and usually has the highest NTU and TSS values, thus making it the best candidate for the high end of the standard curve. The ocean site (OCN2) generally has much less suspended sediment, and was selected as the low end. The remaining sites were chosen as mid-range sites based on analysis of previous deployments (OM2 and Pond

31

20). Three acid washed HDPE 1 L bottles were prepared for each site, into which only the surface water was collected. Sample water was then filtered through the pre-weighed filters. Left to air dry for two days, the filters were then weighed for a g/L value. These values were compared to NTU readings off the YSI® sonde, taken at the same time sample waters were collected for TSS, and a standard curve was created.

YSI® Probe Stabilization Experiment: An experiment was conducted to determine optimal YSI® deployment time to allow all probes to stabilize, and whether sampling the entire column via continuous profiling was equivalent to static deployment in the surface and deep waters in terms of signal stability, accuracy, and precision. The YSI® sonde was deployed at each site for a prolonged period of time (98 – 197 seconds) in order to determine the length of time required for each probe to stabilize in a variety of oceanic conditions. Time series plots were created and analyzed to determine the amount of time the probes needed to be conditioned in the water column before stable and accurate data could be taken. Three tables were constructed (Tables 2.1 – 2.3) that summarize the probe accuracies from beginning to end (Table 2.1), the beginning to the middle of the deployment period (Table 2.2), and the middle of the deployment to the end (Table 2.3) in order to determine whether probe reading stability increases over time.

Finally, a YSI® deployment test was conducted to determine how to best sample the water column to achieve data that accurately describe conditions at the surface and sediment water interface. A new method was utilized in this test, hereafter called the "static deployment mode", in which the YSI® was left submerged

in the top 25 cm of the water column for a 30 second deployment (after the YSI® had

been conditioned to the water for over a minute), then lowered to the sediment water

interface for an additional 30 second deployment. Following the first deployment, the

YSI was then lowered at the same site in continuous profiling mode, at a rate of 1

inch per second, until the sonde reached the SWI. The data were offloaded and

separated into two different deployment files. Both deployments were analyzed for

"surface" and "deep" water samples, with the latter deployment strategy requiring

that the entire data set be separated into the top 25 cm (using depth sensor data) and

the bottom 25 cm. Analysis of the two different deployment methods was used to

determine which strategy achieved a data set that most accurately characterized the

surface and deep-water column. The new strategy would only be utilized if the

accuracy improvements outweighed the increase in time spent at each stake that is

required for the static deployment mode.

2.3 Results

YSI® Profiling Grid: Two surface temperature contour plots were created

from the April 2011 monthly sampling, with the first plot only using sites from

"scheme 5" (Table 1.1), referred to as the old method, and the other plot using the full

sampling method proposed in "scheme 6", here referred to as the full grid sampling

method (Fig 2.3). In the old scheme plot, where contours were constrained by fewer

data points, the cold pool in the northern corner of He'eia Fishpond, adjacent to RM2,

stretches farther towards the island than it does in the new "full grid" scheme. The

warmest area of the pond is similar in both plots, located just to the right of the island

near stake 9. Near the perimeter of the pond, where TM and OM1 are located, the old scheme plot exhibits colder water than is evident in the full grid scheme. Because of the more extensive YSI® data in the vicinity of TM and OM1, the contour plot constructed for the full grid scheme clearly reveals much warmer temperatures than was estimated by the old scheme, which interpolates over fewer grid points. The contour shapes, formed from temperatures in similar areas of the pond, are very different in the two plots. The old method shows a rapid decline in temperature from the warmest area of the pond to the adjacent stakes. In the plot constructed from the full grid scheme, the gradation of temperature contours is more gradual from the warmest spot in the north-central pond (near stakes 8 and 9) to areas close to the pond perimeter. Finally, by including more stakes in the full grid scheme, the plotted contour extends closer to the perimeter of the fishpond, especially at the southern end of the fishpond, near stake 20.

Probe Stabilization: Probe stabilization data were organized into several different figures and tables. Tables 2.1 – 2.3 were constructed by dividing each deployment period (N) in half, and reporting the data from the full time period (Table 2.1), the first half of the deployment time period (Table 2.2), and the last half of the time period (Table 2.3). By creating three tables, identifying which time slice exhibited the lowest standard deviation about the mean, and therefore the lowest % variance, would permit determination of the ideal stabilization time.

For each probe, a time series plot was constructed with time on the x-axis, and probe readings on the y-axis for each site. The mean value, standard deviation, and

percent variation was calculated for each time slice of the time series using Microsoft Excel®.

Individual probes responded differently over time. The YSI® 6560 temperature (Fig 2.4) and pressure (data not shown) probes which do not require calibration, displayed only minor drift over time at all sites with time-series slopes near zero (ranging from (0.0004) to (0.0011)). No sampling site exhibited significantly greater drift with respect to the other sites (Fig 2.4). The 6560 probe also measures salinity via a conductivity reading. The time-series slopes for salinity at all sites were equally small, ranging from (-0.00009) to (0.0014) (Fig 2.5). Throughout the three deployment intervals (Tables 2.1 – 2.3), the pond, ocean, and ocean *mākāhā* sites exhibited less than 0.1% variance, whereas the river *mākāhā* site displayed variations of 0.45% from the beginning to the end of the deployment (Table 2.1) and 0.48% from the beginning to the middle of the deployment (Table 2.2). However, the middle to the end of the deployment exhibited a much lower percent variation at 0.12%.

The stability of the YSI® 6561 pH (Fig 2.6) probe varied at each site, but was more stable towards the end of the deployment. The time series slopes for the ocean site, the pond site, and the river *mākāhā* site were small, ranging from (0.0003 – 0.0007). The ocean *mākāhā* site clearly exhibited more drift than the other sites, with a slope of (0.0023) (Fig 2.6). This is confirmed in Table 2.1, where the ocean *mākāhā* site exhibited 1.37% variance over the entire deployment. However, the pH readings at all sites improved with time. From the beginning to the middle of the deployment period, the pond, ocean, ocean *mākāhā*, and river *mākāhā* sites showed variations of

35

0.11%, 0.43%, 0.94%, and 0.33% respectively (Table 2.2). When analyzed from the middle to the end of the deployment period, the calculated variation lowered to 0.07%, 0.16%, 0.48%, and 0.04% respectively (Table 2.3).

The optical probes (ODO%, turbidity, and chlorophyll) exhibited much greater variability during the time series deployment in comparison to the other probes, yet in most cases improved greatly as more time passed. Time series slopes for the ROX™ optical dissolved oxygen probe were larger in comparison to the other probes (Fig 2.7), with the ocean *mākāhā*, ocean, river *mākāhā*, and pond sites exhibiting slopes of 0.012, (-0.0096), (-0.0295), and 0.0234, respectively. The pond, ocean, and river *mākāhā* site readings all improved in accuracy with time, with %variation improving from 1.44% to 0.55% (pond site), 0.41% to 0.23% (ocean site), and 3.92% to 0.08% (river *mākāhā*). However, the ocean *mākāhā* site readings were more stable from the beginning to the middle of the deployment (0.22%) than they were from the middle to the end of the deployment period (0.66%) (Tables 2.2 and 2.3). It is important to note that the ODO% was still changing at the end of the time series deployment for the ocean *mākāhā* and ocean sites, suggesting that the ROX probe had still not stabilized by the end of the deployment (Fig 2.7).

The YSI® 6136 turbidity probe exhibited different degrees of drifts throughout the entire deployment period (Fig 2.8). The ocean *mākāhā* and the ocean site showed minimal slopes of 0.00008 and (-0.001) respectively, whereas the river *mākāhā* and pond site displayed slightly large slopes of 0.0109 and (-0.0224), respectively (Fig 2.8). From the beginning to the middle of the deployment (Table 2.2), standard deviations about average values were larger at the pond site (±1.43),

ocean site (±1.36), and the ocean *mākāhā* (±0.28) than from the middle to the end of

the deployment (±1.18, ±1.32, and ±0.26, respectively). The river *mākāhā* was more

stable towards the beginning of the deployment (standard deviation of ±1.67, Table

2.2) than from the middle to the end of the deployment (±1.98, Table 2.3). The ocean

mākāhā site displayed much smaller deviations (~±0.3) in comparison to the other

sites (±1.18-1.92, Tables 2.1 – 2.3).

The last probe, the YSI® 6025 fluorescence probe, exhibited minimal drift

during the time series drifts at the ocean *mākāhā* (slope of 0.0015), ocean site (-

0.0013), and river *mākāhā* site (-0.0012), whereas the drift at the pond site was larger

by comparison (0.0115) (Fig 2.9). There was no clear improvement in stability at any

point during the deployment. The pond site variation improved from 148.65% from

the beginning to the middle down to 103.09% from the middle to the end (Table 2.3).

The ocean *mākāhā*'s variation responded similarly (239.85% down to 196.43%).

However, variation at the ocean site was greater towards the end of the deployment

(76.51%) than from the beginning to the middle (73.40%), whereas the river *mākāhā*

displayed similar variation throughout the entire deployment (50.11%, 49.54%, and

50.37% for beginning to end, beginning to mid, and mid to end, respectively) (Tables

2.1 - 2.3). Deviations from average values were extremely high in some cases, such as

the ocean *mākāha,* where the standard deviation was ±1.53 with respect to a 0.70

average value (217% variance, table 2.1).

NTU and Chl-A Standard Curves: Comparison of chlorophyll-a determined

on extracted samples to that derived from the YSI fluorescence probe from the

December 2010 monthly sampling is shown in Figure 2.10. The chlorophyll comparison was moderately successful for all sites with the exception of the river *mākāhā* (RM1, RM2, and RM3), which is clearly displayed in the differences between the plots with and without the *mākāhā* included (Figure 2.10). An XY scatter plot was constructed (Fig 2.11) that included a linear regression line to estimate the feasibility of constructing a standard curve from, which exhibited an R^2 value of 0.76 (Fig 2.11).

Probe NTU and TSS data from 1/27/2011 and 2/17/2011 (Fig 2.12) appear to correlate moderately well with one another. XY scatter plots for the same two months are shown in figure 2.13, with the 1/27/2011 sampling exhibiting an R^2 value of 0.33 and the 2/17/2011 sampling showing an R^2 of 0.42. In a dedicated standardization experiment, triplicate TSS g/L values from each site were averaged and placed into a XY scatter plot to compare with the NTU values from the YSI®. An R^2 value of 0.98 accompanied the best-fit linear regression, a very strong correlation (Figure 2.14). Thus, results of the dedicated standardization experiment showed a much stronger relationship between probe (NTU) and discrete samples (TSS) than did a similar comparison constructed from monthly data (Fig 2.13).

YSI® Water Column Sampling: Results from the YSI® sonde deployment with regards to NTU showed that the stability of the 6136 turbidity probe increased when held stationary in the surface and deep water column for ~30 seconds relative to stability observed in continuous profiling mode (Figure 2.15). The new static method exhibited lower standard deviation from average NTU values when compared to the

old, continuous profiling method, from ±0.57 down to ±0.44 for the surface, and

±1.19 down to ±0.97 for the deep water measurements. Visual analysis of the static

deployment time series plot displays two distinct data populations, one representing

surface (0-50 seconds) and the other deep (50 – 141 seconds), whereas the continuous

profiling time series plot exhibits a continuously rising NTU value throughout the

deployment.

2.4 Discussion

YSI® Profiling Grid: After comparison of the two temperature contour images

from April 2011 (Fig 2.3), which show the distribution of temperature contour lines

resulting from the old scheme 5 (all makaha sites and stakes 1, 3, 6 ,7 ,8, 9, 11, 13,

15, 16, and 18) versus the new scheme 6 (all sites of He'eia fishpond with exception

to OB, OCN1 and OCN2) profiling grids, it was concluded that deploying the YSI®

at all stakes is critical for making accurate contour maps of He'eia Fishpond (Table

1.1). Specifically, the old, scheme 5 sampling grid doesn't allow proper interpolation

of the physical properties of He'eia Fishpond in the areas that are highly variable. The

inaccuracies in contours that result from the scheme 5 profiling grid most likely

originate from the distance between YSI® profiling sites, which are larger than the

scale of temperature variability within the pond. This is especially important in the

region around RM2 and RM1 (Fig 2.3), which exhibits the largest variability in

temperature and salinity over short distances. The interpolation based on the scheme

5 grid suggested that water temperature gradually changes from the cold, fresh waters

of RM2 and RM1 to the warm, brackish waters of stakes 7, 9, and 18. When the full

grid is used to create a contour plot, in contrast, it became clear that stake 19, the stake closest to RM2, as well as stakes 4 and 5 were actually much warmer than the scheme 5 grid plot interpolated they would be. Because temperature is likely a marker for water mass type, and a proxy for other water column parameters, it follows that higher resolution profiling will improve contouring results for other parameters as well.

Stakes 1, 2, 4, 5, 10, 12, 14, 17, 19, and 20 were originally left out of the scheme 5 sampling grid (Table 1.1) in order to quickly complete monthly sampling before the tide changed the physical and chemical properties of He'eia Fishpond. Travel time between each site takes approximately two minutes, and it takes another three minutes to profile. Removing ten sites from the sampling grid, as was done for the reduced scheme 5 grid, shortened sampling time by roughly an hour. However, after viewing the inaccurate contour plots that this old, scheme 5 grid established, it is recommended that the full sampling grid (scheme 6) be reinstated permanently. Establishing a more accurate understanding of the spatial properties of He'eia Fishpond is of higher priority than saving an hour of sampling time.

Probe Stabilization: After evaluating the stability of the individual probes over a time series, it became clear that the YSI® needs to be submerged in the water column for at least a minute before reliable data can be recorded. The stability, conducted by comparing standard deviation about average values, and percent variation over three distinct time slices within a single deployment (beginning to end, beginning to middle, and middle to end of deployment, Tables 2.1 – 2.3), revealed

that most probes were more stable towards the end of the deployment. Specifically, the pH (Fig 2.6), salinity (Fig 2.5), and dissolved oxygen (Fig 2.7) probes stabilized more effectively with longer deployment times. In fact, it is likely that the pH and dissolved oxygen probes were not submerged long enough for the readings to completely stabilize. YSI Incorporated® estimates that the pH probe readings have a standard deviation of ±0.02 from recorded values, which three out of four sites (with exception of the ocean *mākāhā*) achieved (YSI 2006). Therefore, based on our analysis, probe readings are significantly more stable after a minute of static deployment in the water column.

The optical turbidity (Fig 2.8) and fluorescence (Fig 2.9) probes displayed more instability than anticipated based on specifications advertized by YSI Incorporated®. YSI® estimates that the 6136 turbidity probe has a precision range of ±0.03NTU units (YSI 2006). Only the ocean *mākāhā* achieved precision with this range, and only when the probe was deployed for the full 190 second deployment period (Fig 2.8). The other three sites displayed greater deviations, from ±1.20 to ±1.98, towards the end of the deployment period (Table 2.3). It is important to note that the pond site, river *mākāhā* site, and the ocean site are characterized by higher turbidity than the ocean *mākāhā*. This could explain the pooer probe stability and higher variability about the mean. However, it is concluded based on the small slopes associated with the time series plot from each site that turbidity drift readings are small, and that the probes respond quickly to the condition of the water column, despite the fact that they do not necessarily provide more stable readings over time.

41

Similar to the turbidity probe (Fig 2.8), the low-level drift associated with the fluorescence probe (Fig 2.9) suggests that probe values do not necessarily improve with increased deployment time. The large standard deviation about average fluorescence readings remained throughout all three deployment period analyses. It is clear that the probe quickly responds to the changing water column fluorescence, similar to the way in which the turbidity probe functions, but displays substantial oscillation about mean values. The oscillation range appears constant for the duration of the entire deployment, however, leading to the conclusions that the recommended thirty-second deployment should provide sufficient data to obtain reasonable precision about the average value.

YSI® Water Column Profiling: The static deployment strategy is more accurate than the continuous deployment strategy (Fig 2.15). As long as the sonde is first submerged for 60 seconds to stabilize the probes, most of the probes will respond quickly to the small changes between the surface and deep water column. The optical turbidity and fluorescence probes will likely benefit the most from static deployment. As was shown in the fluorescence (Fig 2.9) and turbidity (Fig 2.8) time series plots, the drift associated with the optical probes is very small. Thus, allowing the probe to establish a long term average in an unchanging environment (as the static deployment would allow) will result in a more reliable value, and will help benefit TSS vs. NTU and chlorophyll vs. extracted evaluations.

Chlorophyll Standardization: The December 2010 chlorophyll value comparison was precise enough (R^2 value of .77) to suggest that a standard curve constructed from a small number of grab samples that cover the fluorescence range of values observed in He'eia Fishpond can be employed. However, upon further analysis, the standard curve results were inconclusive. There appeared to be two populations of data, one with low fluorescence and extraction results and the other with high fluorescence and extraction results (Fig 2.11). Because the standard curve is heavily influenced by these two populations, it is not possible to conclude, decisively, that the standard curve approach is viable. In order for chlorophyll standardizations to be plausible, more research is needed.

Turbidity Standardization: While the experimental TSS vs NTU standard curve produced a successful standard curve R^2 value of 0.98 (Fig 2.14), monthly sampling values failed to achieve results anywhere near this experimental value (Fig 2.13). The discrepancy between the results could be due to the limited number of samples used in the experimental test, or to the fact that central He'eia Fishpond wasn't sampled at all during the YSI® standardization experiment, where more than half of the sites in He'eia are located. YSI Incorporated® states that the turbidity probe is capable of estimating TSS concentrations by establishing a standard curve similar to the one discussed in the previous section on chlorophyll-a. However, given the imperfect results from the monthly sampling trials (Fig 2.13), and despite the promise suggested by the experimental trial (Fig 2.14), it is recommended that water filtering should remain the preferred method for determining a TSS.

2.5 Summary and Recommendations

Evaluation of past deployment routines and practices at He'eia Fishpond have revealed that data collection schemes have not been optimal for generating representative and precise data for a number of key parameters in He'eia Fishpond. The incomplete sampling grid (scheme 5, Table 1.1), established in the interest of saving time spent sampling, failed to produce accurate contours plots of the physical properties of He'eia Fishpond (Fig 2.3). The manner in which the YSI® was deployed also caused unnecessary imprecision by continuously profiling the entire water column, when only the surface and deep water column was of interest in sampling efforts. Additionally, the YSI® wasn't left in the water long enough to condition the sonde probes to the environment of each site.

By sampling at all grid and makaha sites of He'eia Fishpond, utilizing the static deployment method, instead of the continuous profiling method, and conditioning probes for at least 60 seconds before profiling begins more accurate surface and deep contour plots can be achieved. Additionally, the use of chlorophyll-a standardization curves could reduce the sample preparation and filtration efforts during each monthly sampling, but would require more extensive fluorescence probe chlorophyll extraction data comparisons in order to be conclusive enough to recommend this approach. If these recommendations are adopted by future researchers at He'eia Fishpond, data quality will improve, and will permit more accurate characterization of the environment of this ancient Hawaiian fishpond.

Table 2.1: Probe drift readings for the entire deployment period of the YSI stabilization experiment.

POND SITE

Probe	Time	# N	AVG	STDev	% Variation
Turbidity	1:END	98	4.79	1.54	32.07
Flourescence	1:END	98	1.49	1.81	121.18
pH	1:END	98	7.72	0.02	0.20
Salinity	1:END	98	29.29	0.03	0.10
ODO%	1:END	98	86.62	1.12	1.30

OCEAN SITE

Probe	Time	# N	AVG	STDev	% Variation
Turbidity	1:END	195	19.43	1.34	6.89
Flourescence	1:END	195	2.06	1.54	74.53
pH	1:END	195	7.71	0.04	0.55
Salinity	1:END	195	28.66	0.01	0.05
ODO%	1:END	195	86.42	0.56	0.65

OCEAN MĀKĀHĀ

Probe	Time	# N	AVG	STDev	% Variation
Turbidity	1:END	153	0.76	0.27	35.73
Flourescence	1:END	153	0.70	1.53	217.07
pH	1:END	153	7.45	0.10	1.37
Salinity	1:END	153	29.33	0.02	0.05
ODO%	1:END	153	96.45	0.62	0.64

RIVER MĀKĀHĀ

Probe	Time	# N	AVG	STDev	% Variation
Turbidity	1:END	197	25.23	1.92	7.60
Flourescence	1:END	197	2.89	1.45	50.11
pH	1:END	197	7.70	0.02	0.31
Salinity	1:END	197	22.38	0.10	0.45
ODO%	1:END	197	88.09	2.72	3.09

POND SITE

Probe	Time	# N	AVG	STDev	% Variation
Turbidity	1:MID	49	5.59	1.43	25.61
Flourescence	1:MID	49	1.20	1.79	148.65
pH	1:MID	49	7.70	0.01	0.11
Salinity	1:MID	49	29.31	0.02	0.08
ODO%	1:MID	49	85.99	1.24	1.44

OCEAN SITE

Probe	Time	# N	AVG	STDev	% Variation
Turbidity	1:MID	97	19.37	1.36	7.02
Flourescence	1:MID	97	2.12	1.56	73.40
pH	1:MID	97	7.67	0.03	0.43
Salinity	1:MID	97	28.67	0.02	0.06
ODO%	1:MID	97	86.89	0.35	0.41

OCEAN MĀKĀHĀ

Probe	Time	# N	AVG	STDev	% Variation
Turbidity	1:MID	76	0.76	0.28	37.49
Flourescence	1:MID	76	0.60	1.44	239.85
pH	1:MID	76	7.36	0.07	0.94
Salinity	1:MID	76	29.36	0.02	0.05
ODO%	1:MID	76	96.06	0.21	0.22

RIVER MĀKĀHĀ

Probe	Time	# N	AVG	STDev	% Variation
Turbidity	1:MID	98	24.67	1.67	6.77
Flourescence	1:MID	98	2.99	1.48	49.54
pH	1:MID	98	7.69	0.02	0.33
Salinity	1:MID	98	22.32	0.11	0.48
ODO%	1:MID	98	89.23	3.50	3.92

Table 2.3: Probe drift readings from middle to end of deployment period of the YSI stabilization experiment.

POND SITE

Probe	Time	# N	AVG	STDev	% Variation
Turbidity	MID:END	49	3.99	1.18	29.53
Flourescence	MID:END	49	1.76	1.81	103.09
pH	MID:END	49	7.73	0.01	0.07
Salinity	MID:END	49	29.27	0.02	0.08
ODO%	MID:END	49	87.26	0.48	0.55

OCEAN SITE

Probe	Time	# N	AVG	STDev	% Variation
Turbidity	MID:END	98	19.49	1.32	6.77
Flourescence	MID:END	98	2.04	1.56	76.51
pH	MID:END	98	7.74	0.01	0.16
Salinity	MID:END	98	28.65	0.00	0.01
ODO%	MID:END	98	85.94	0.20	0.23

OCEAN MĀKĀHĀ

Probe	Time	# N	AVG	STDev	% Variation
Turbidity	MID:END	77	0.76	0.26	33.94
Flourescence	MID:END	77	0.82	1.61	196.43
pH	MID:END	77	7.53	0.04	0.48
Salinity	MID:END	77	29.38	0.00	0.01
ODO%	MID:END	77	96.84	0.64	0.66

RIVER MĀKĀHĀ

Probe	Time	# N	AVG	STDev	% Variation
Turbidity	MID:END	99	25.79	1.98	7.69
Flourescence	MID:END	99	2.79	1.40	50.37
pH	MID:END	99	7.72	0.00	0.04
Salinity	MID:END	99	22.45	0.03	0.12
ODO%	MID:END	99	86.95	0.07	0.08

Figure 2.1: Sampling scheme 5 (Table 1.1) used prior to October 2010. This scheme was used from 2007 – 2010. Sites sampled include OM2, OCN2, OB, OM1, TM, OCN1, RM3, RM2, RM1, and stakes 1, 3 ,6 ,7, 8, 9, 11, 13, 15, 16, and 18. Sites from Young (2011).

Figure 2.2: Sampling sites used to determine ideal deployment time to allow for YSI probe stabilization and the sites used to create NTU vs. TSS standardization curves. The sites that were sampled included a pond site (Pond 20), an ocean *mākāhā* (OM2), an ocean site (OB), and a river *mākāhā* (RM3). Sites from Young (2011).
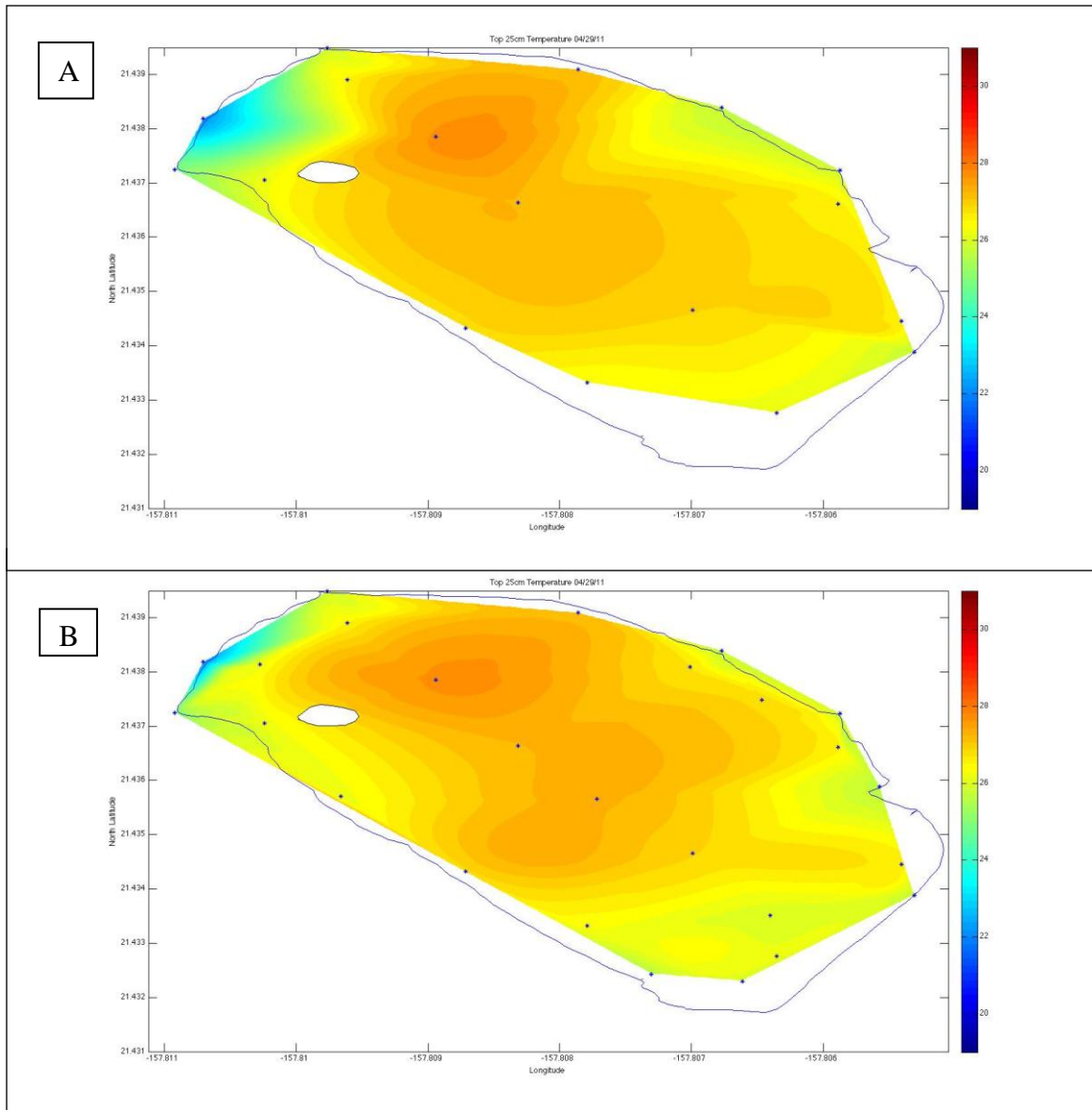
Figure 2.3: Matlab® temperature contour plots for the April 2011 sampling. The top figure (A) is a plot using the reduced "old" sampling scheme (OM2, OM1, TM, RM3, RM2, RM1, Stakes 1, 3, 6, 7, 8, 9, 11, 13, 15, 16, and 18) (sites from Fig 2.1), where as the "new" method, shown on the bottom plot (B), uses OM2, OM1, TM, RM3, RM2, RM1, and all stakes in He'eia Fishpond (Fig 3.5). Sites from Young (2011).
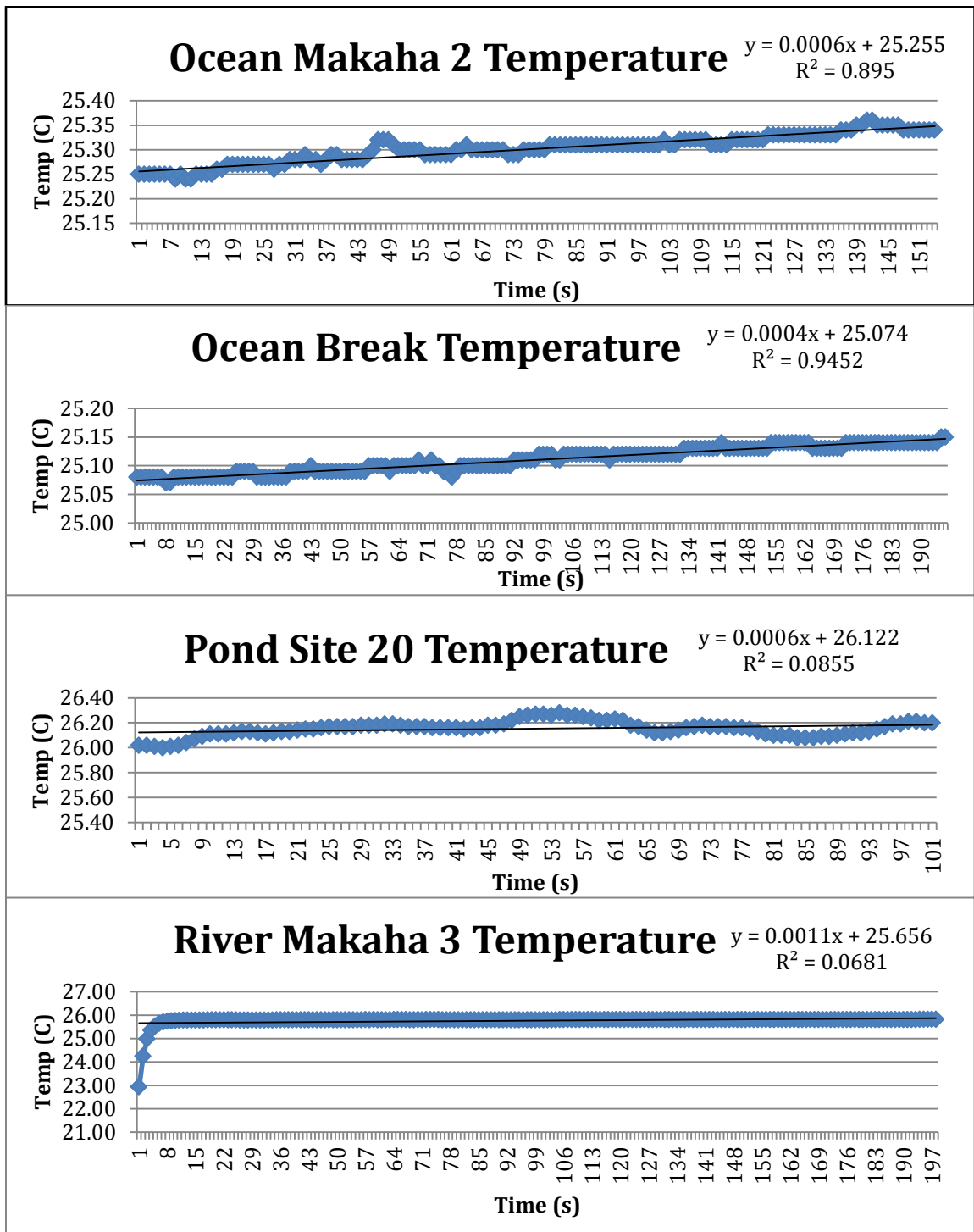
Figure 2.4: YSI 6560 temperature probe readings from four sites (OB, Pond 20, RM3, OM2) in He'eia Fishpond. The sonde was left in the water for up to 193 seconds to determine the minimum time required for the temperature probe to stabilize.
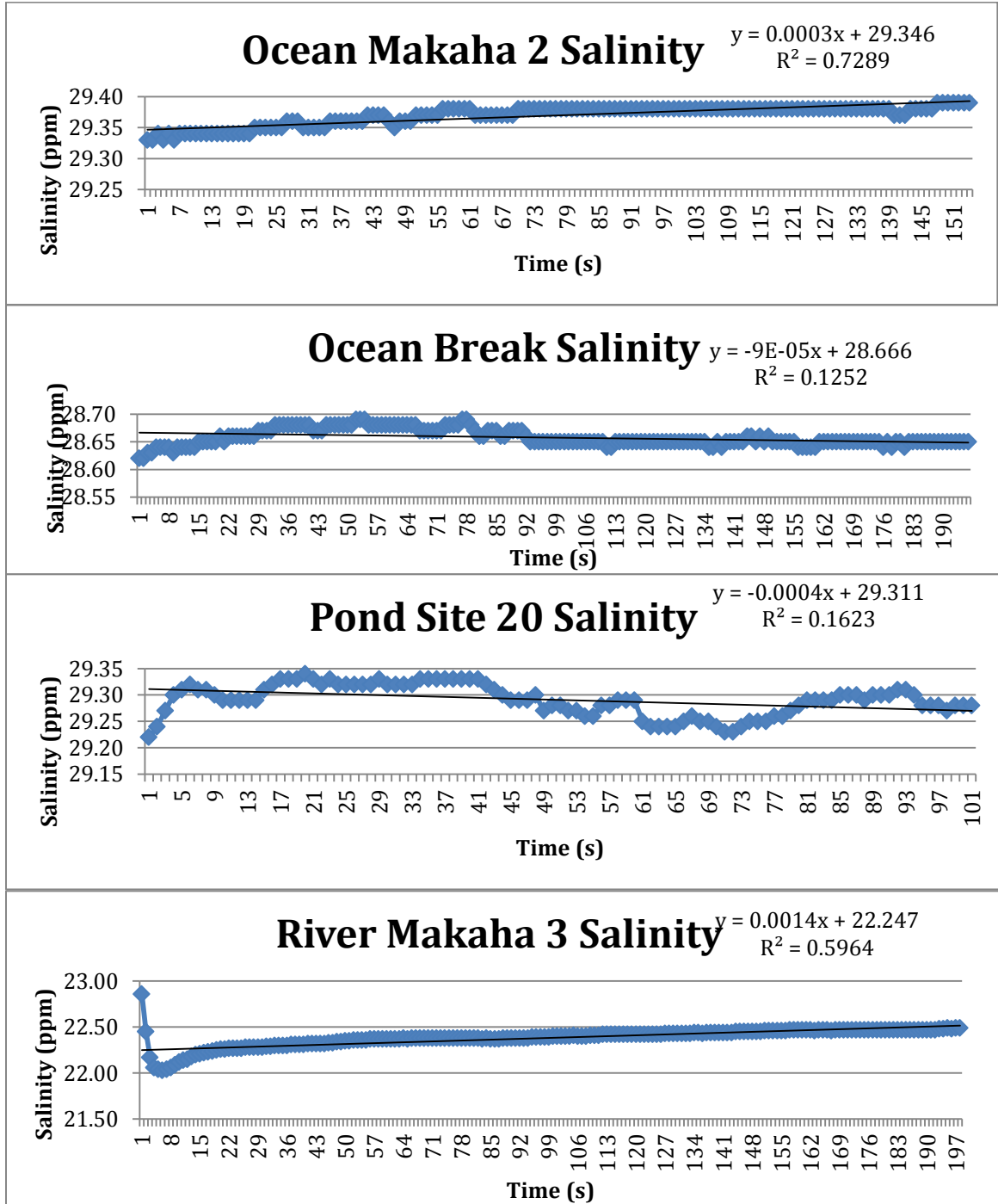
Fig 2.5: YSI 6560 salinity sonde probe readings from four sites (OM2, OB, Pond 20, RM3) in He'eia Fishpond. The sonde was left in the water for up to 193 seconds to determine the minimum time required for the salinity probe to stabilize.
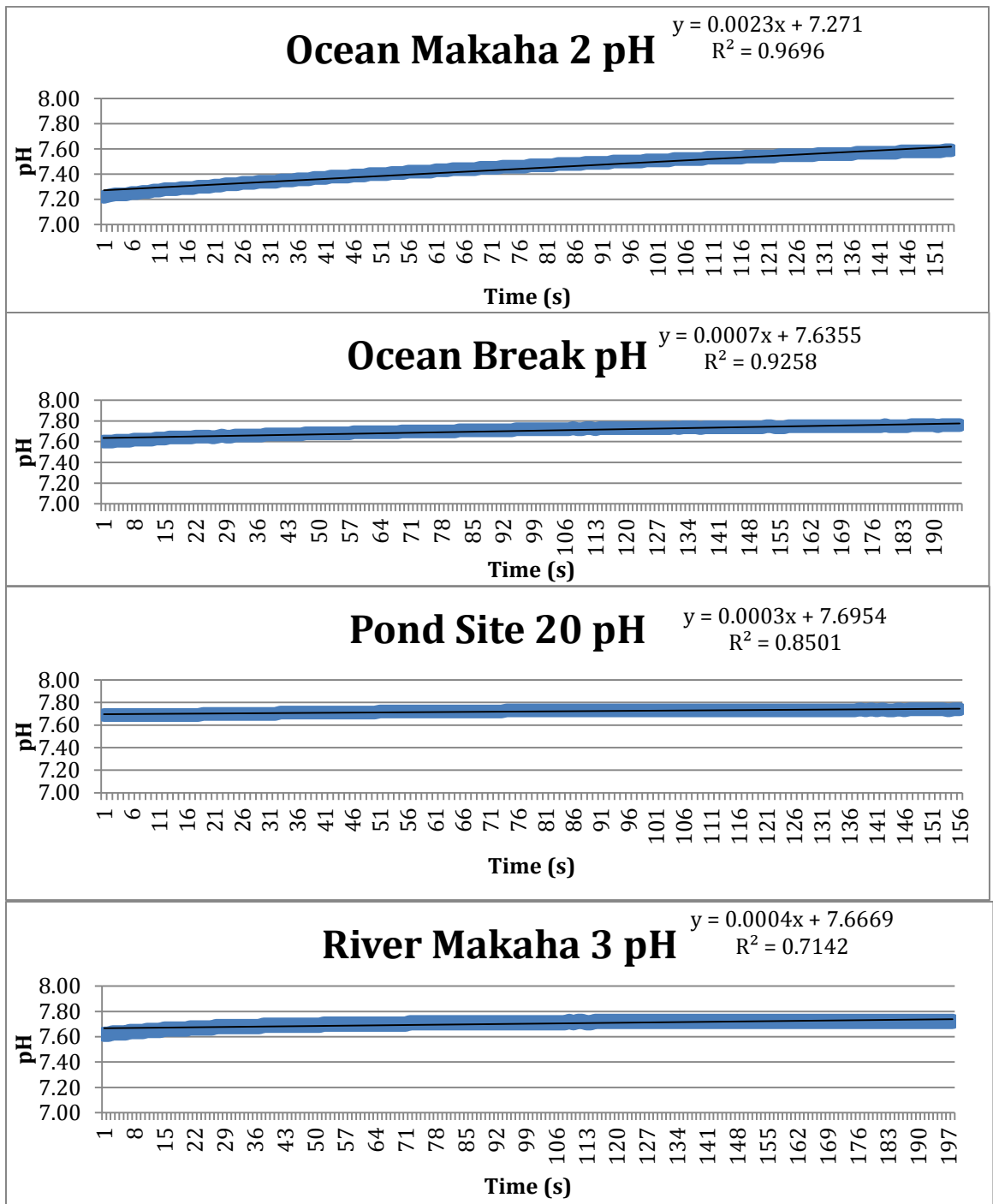
Figure 2.6: YSI 6561 pH probe readings from four sites (OM2, OB, Pond 20, RM3) in He'eia Fishpond. The sonde was left in the water for up to 193 seconds to determine the minimum time required for the pH probe to stabilize.
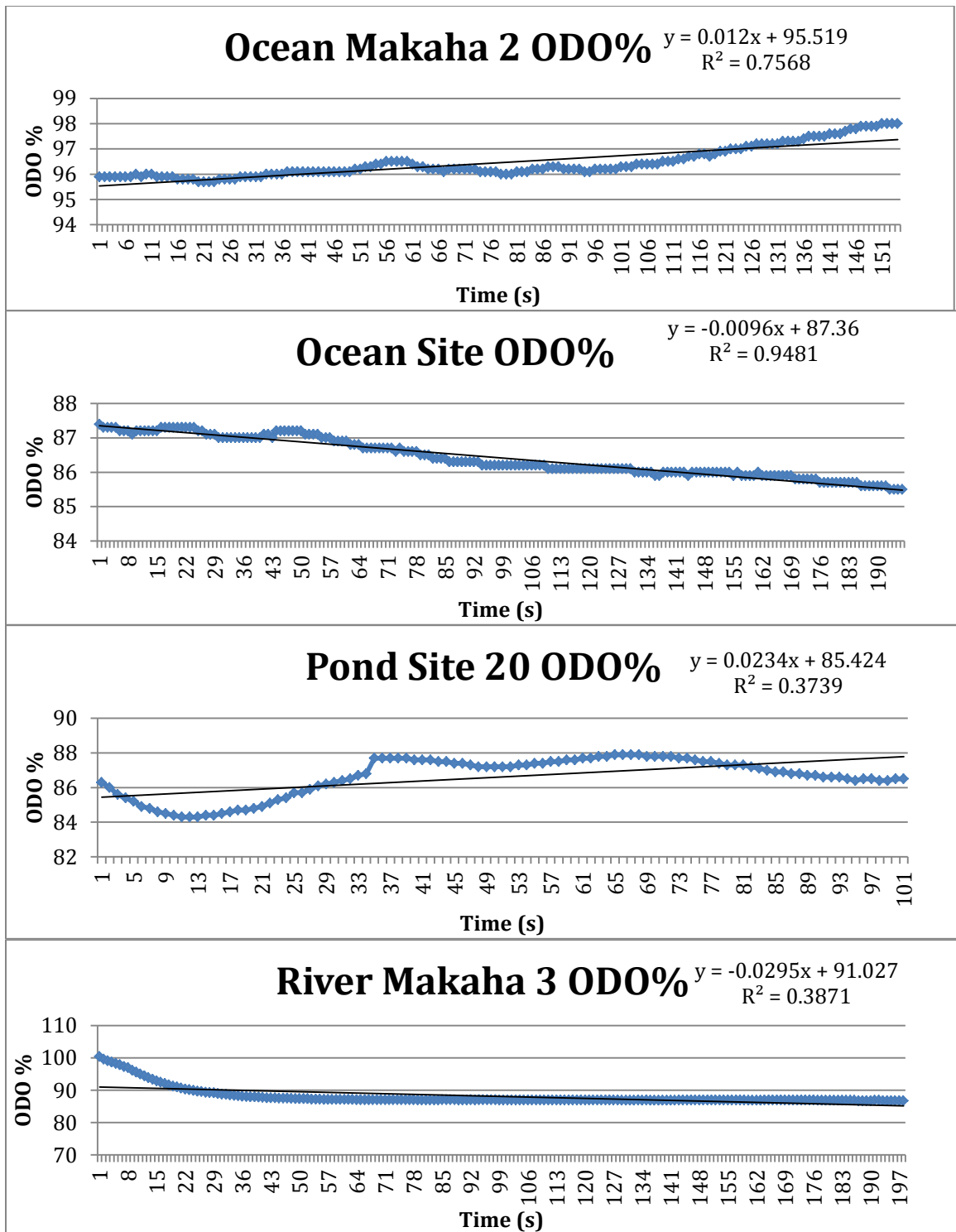
Fig 2.7: YSI ROX™ Optical Dissolved Oxygen probe readings from four sites (OM2, OB, RM3, Pond 20) in He'eia Fishpond. The sonde was left in the water for up to 193 seconds to determine the minimum time required for the dissolve oxygen probe to stabilize.

54
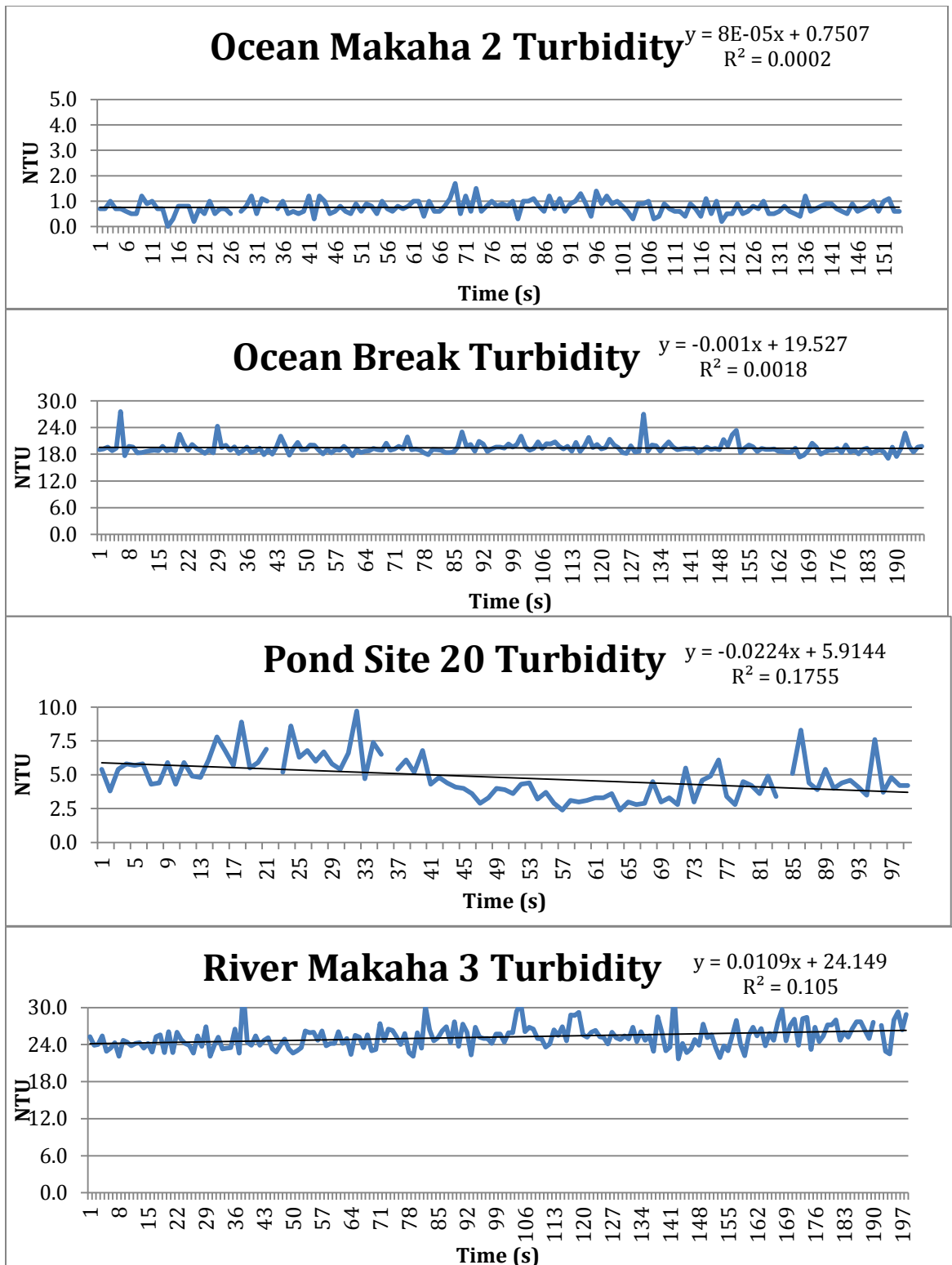
Figure 2.8: YSI 6136 turbidity probe readings from four sites (OM2, OB, Pond 20, RM3) in He'eia Fishpond. The sonde was left in the water for up to 193 seconds to determine the minimum time required for the turbidity probe to stabilize.
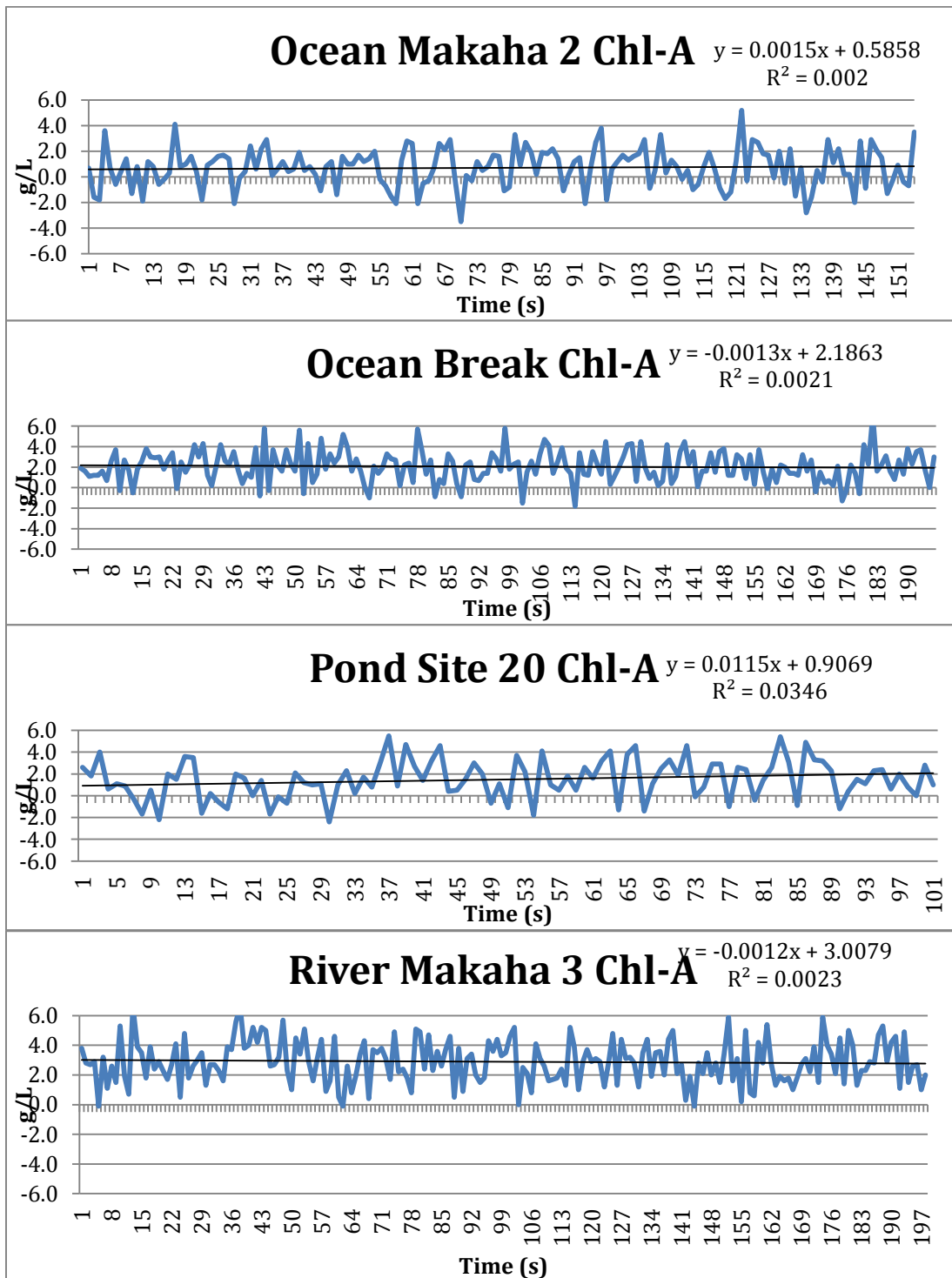
Figure 2.9: YSI 6025 chlorophyll probe readings from four sites (OM2, OB, Pond 20, RM3) in He'eia Fishpond. The sonde was left in the water for up to 193 seconds to determine the minimum time required for the chlorophyll probe to stabilize.
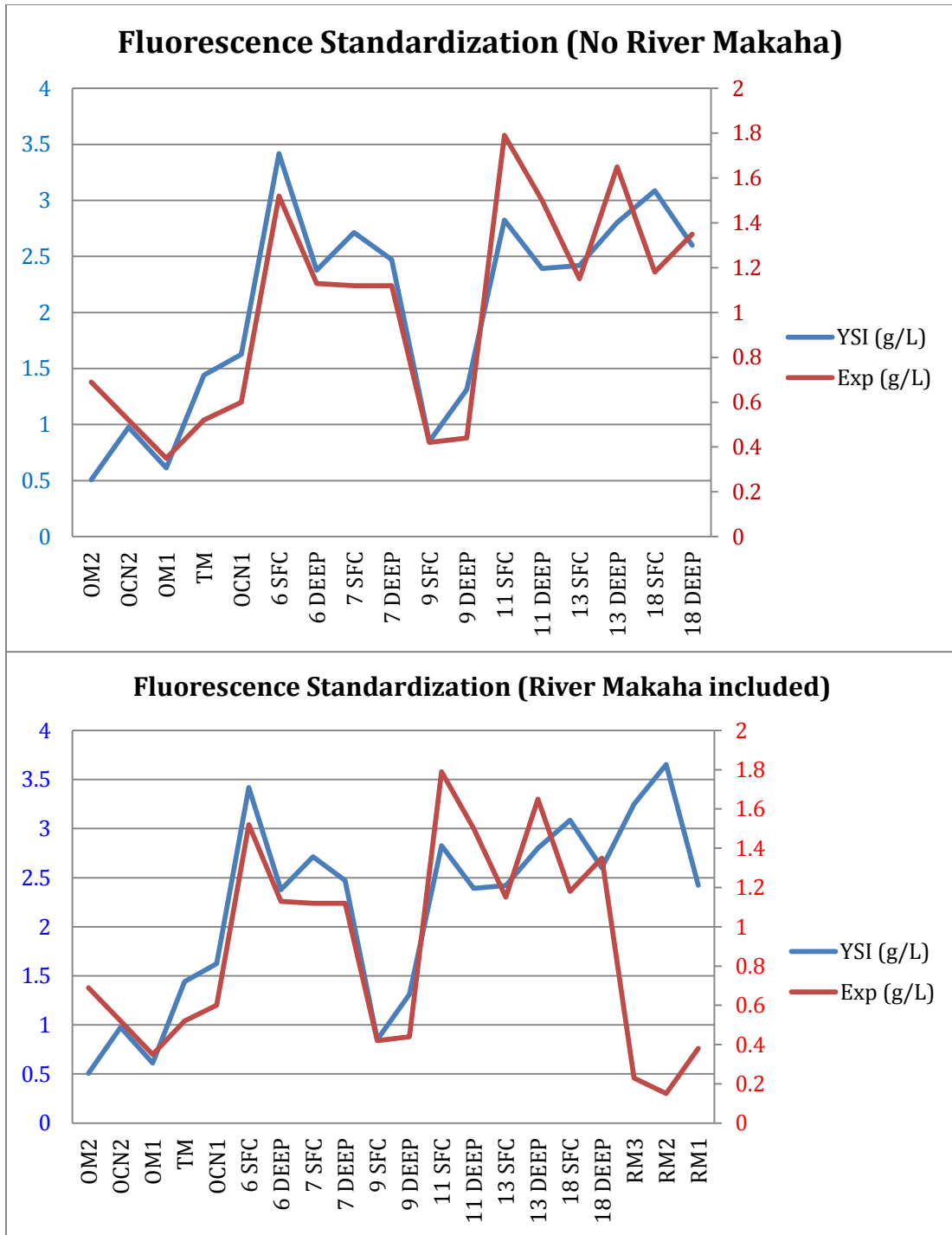
Figure 2.10: December 2010 chlorophyll-a site comparison curves. The top graph excludes the river makaha (RM3, RM2, RM1), which were found to have no correlation between experimental values, found from analyzing filtered samples on a fluorometer, and readings from the fluorescence probe. The bottom curve, which includes the freshwater sites, shows this poor correlation.
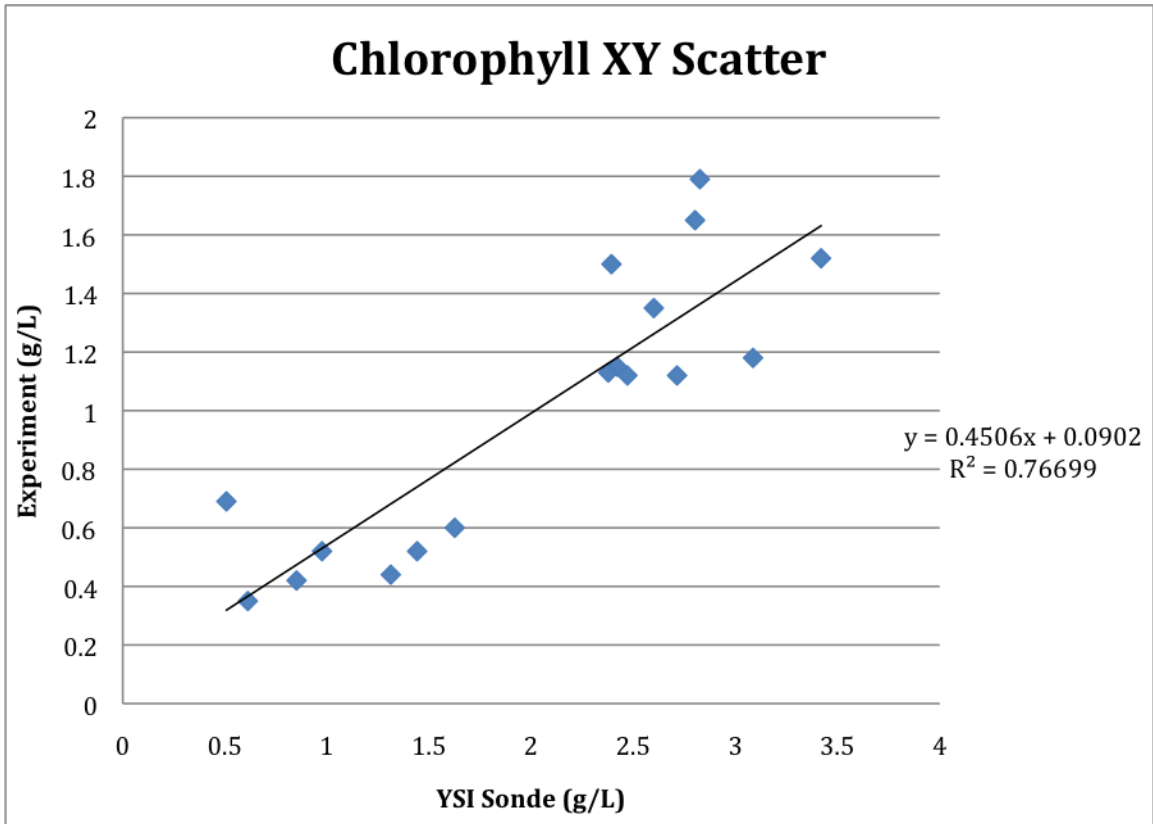
Figure 2.11: XY scatter plot of December 2010 chlorophyll data. The X axis represents values from the YSI fluorescence probe, whereas the Y axis represents values from filtered water samples, which were analyzed on a fluorometer to achieve a chlorophyll value in g/L.
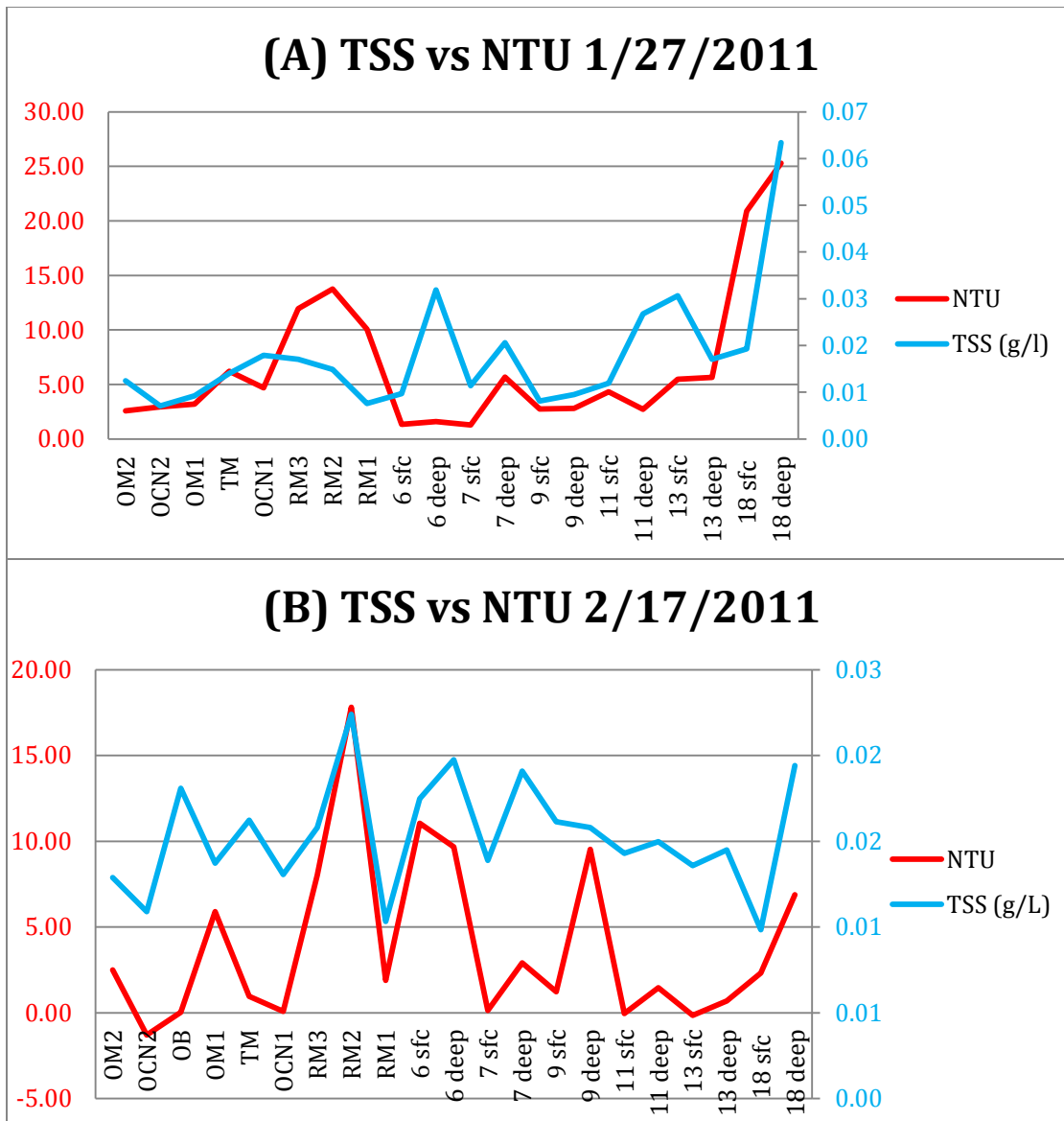
Figure 2.12: TSS vs. NTU plots for 1/27/2011 and 2/17/2011. TSS values were averaged over duplicate filter samples. NTU values are from the YSI 6136 turbidity probe. The left Y axis represents NTU values whereas the right Y axis represents TSS (g/L) values.

(A) TSS vs NTU XY Scatter (1/27/2011)

TSS (g/L)

y = 295.8x + 1.4272
$R^2 = 0.3381$

NT

(B) TSS vs NTU XY Scatter (2/17/2011)

TSS (g/L)

y = 987.91x - 11.269
$R^2 = 0.4235$

NTU
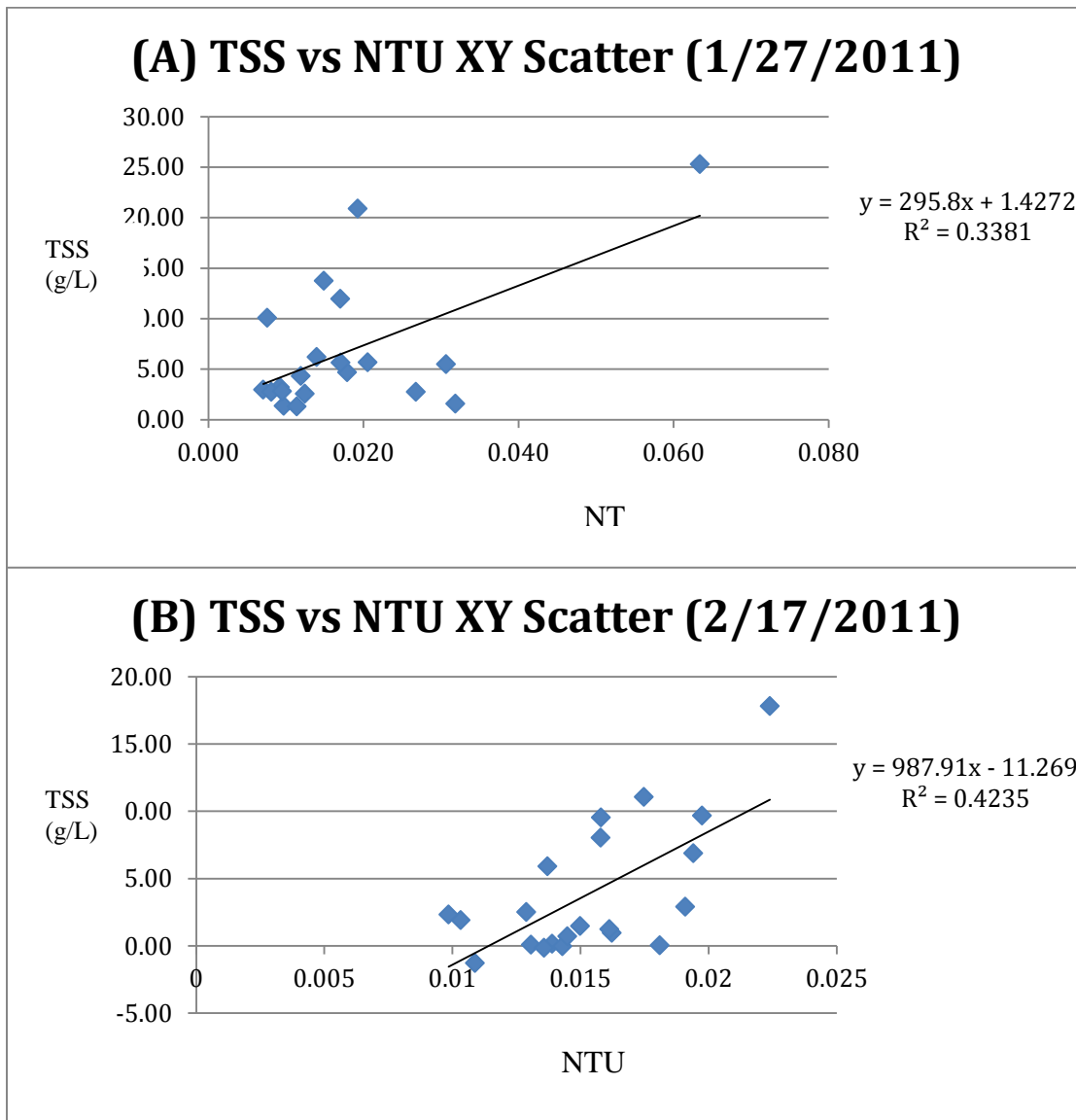
Figure 2.13: TSS vs. NTU XY scatter plots from 1/27/2011 (A) and 2/17/2011 (B). Each graph is accompanied with a linear best-fit line, along with an R^2 value. See figure 2.12 for line plots.
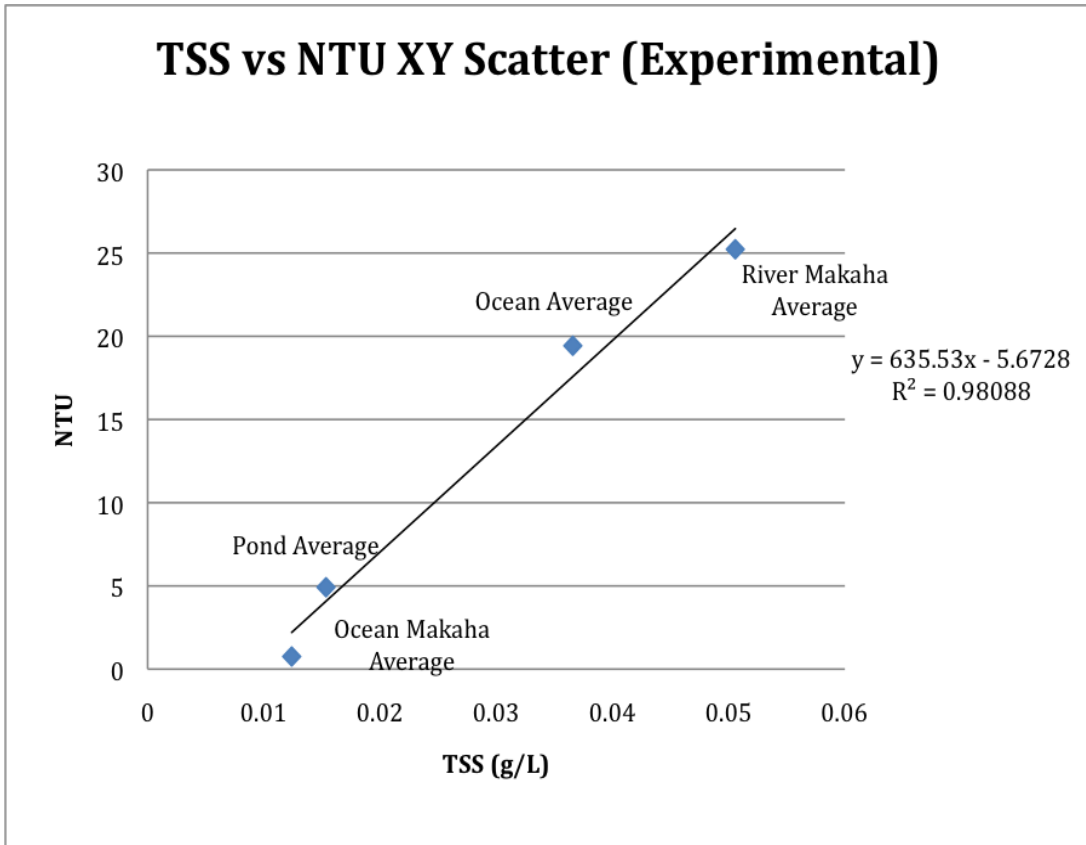
Figure 2.14: TSS vs. NTU XY scatter plot from the four sites used to establish YSI probe stabilizations (see figures 2.4 – 2.9). Each TSS value was achieved by taking triplicate filter samples from individual sites and determining an average TSS weight.

Continuous Profiling Method

	Surface	Deep
AVG	3.58	4.57
STDEV	0.57	1.19
% ERR	15.98	25.99

Static Profiling Method

	Surface	Deep
AVG	2.62	4.88
STDEV	0.44	0.97
% ERR	16.71	19.85
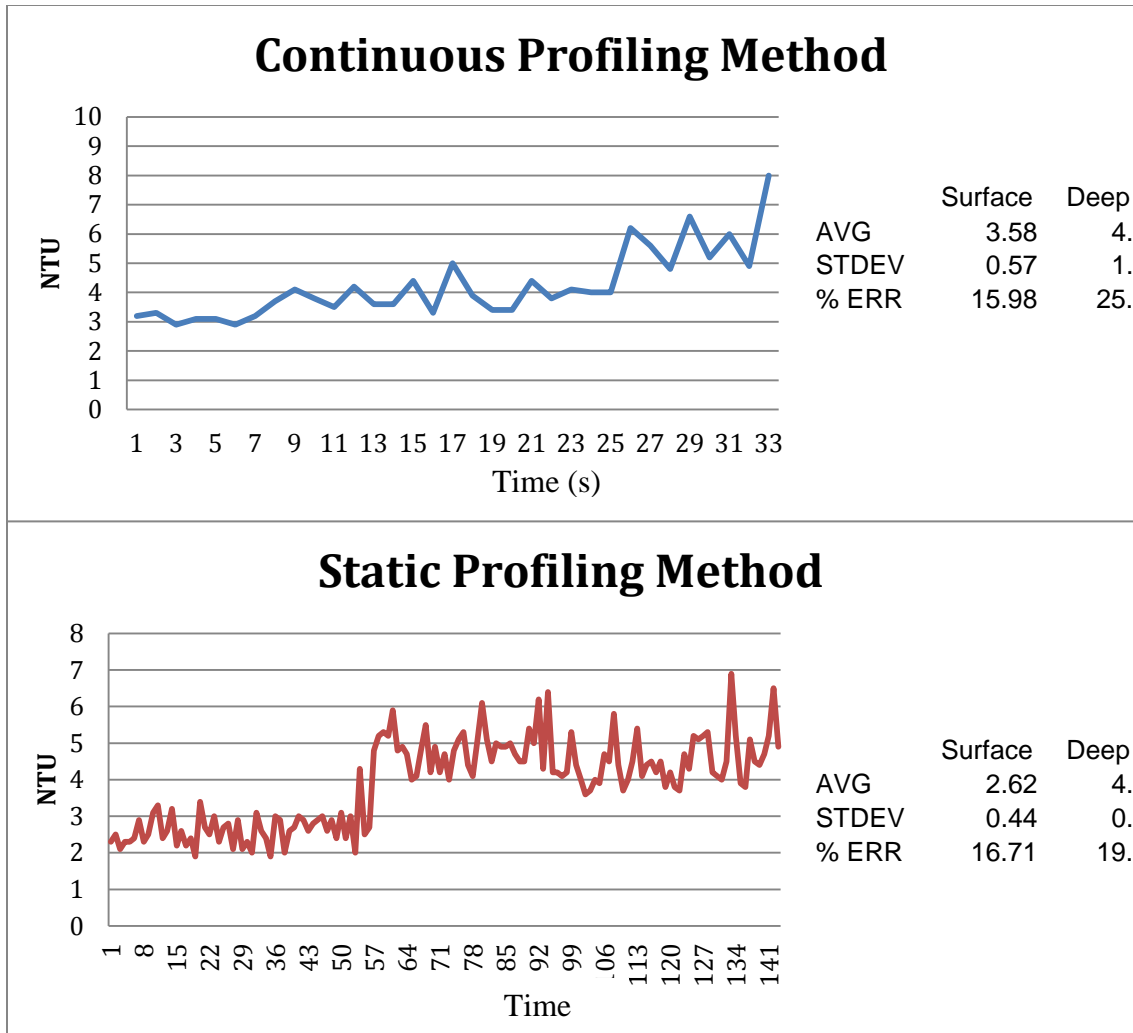
Figure 2.15: YSI turbidity probe readings after two different deployment strategies. The top graph represents a method in which the YSI is slowly lowered in the water column at ~1 inch per second. The bottom graph represents a method where the YSI is held stationary in the surface water column for up to a minute, then lowered to the sediment water interface. The average, standard deviation, and % variance is displayed to the right of each graph.

CHAPTER 3

IMPROVING IN SITU INSTRUMENT DEPLOYMENT METHODS

3.1 Introduction

In-situ instruments are a vital part of the oceanographic monitoring that takes place at He'eia Fishpond. Understanding the temporal and spatial fluctuations in temperature and tidal height allows for accurate descriptions of the physical processes that affect the pond. Since 2007, He'eia Fishpond has been equipped with a variety of in-situ instruments to: (1) record the water flowing through each *mākāhā* and (2) measure water temperature over the entire extent of the fishpond. Young (2011) utilized flow in and out of the pond, through in-situ instrument analysis, to describe nutrient fluctuations during the wet season. In this thesis, in-situ temperature sensors were analyzed to describe seasonal and climate-driven changes, as well as the spatial variability of He'eia Fishpond physical characteristics (see Chapter 4). However, the lack of consistency in deployment strategy impairs our ability to utilize archived data to analyze temperature at He'eia Fishpond. Recognizing that past deployment practices were not optimal, an effort to improve the in-situ deployment strategy utilized throughout the pond was undertaken. The following chapter describes the methodology employed to evaluate past practices and devise a final deployment strategy to be used for the foreseeable future.

3.2 Instrument Descriptions and Deployment Routines:

TidbiT® v2 Temperature Sensors: The TidbiT® v2 precision sensor is a waterproof (up to 300 m), epoxy-enclosed instrument manufactured by ONSET®, and is used to accurately measure water and air temperature (Fig 1.4). The v2 has an operation range of -20º to 70ºC in air and a maximum temperature of 30ºC in water, with an accuracy of ±0.2ºC (Fig 1.4). Each sensor has dimensions of 3.0 cm (L) x 4.1 cm (W) x 1.7 cm (H), and weighs less than 23 g. Fixed-rate or variable logging interval options are available with the TidbiT® temperature sensor series, with intervals from 1 second to 18 hours (OnsetComp.com)

The sensors deployed within He'eia Fishpond are programmed to record temperature readings to onboard memory every 20 minutes to allow for several month long deployments without draining the battery. At 20 minute logging intervals, the limited onboard memory is not sufficient to have permanent deployments in the pond, thus requiring periodic data offloading and instrument cleaning. Sensors are attached inside perforated PVC cylinders to protect against biota, while still allowing water to flow freely through the open ends and numerous drilled holes within the PVC pipe. Cylinders and sensors are attached ~20 cm above the sediment water interface, which is deep enough to remain submerged over the fullest extent of tidal range and deep enough to be unaffected by daily surface water heating due to solar radiation (Young 2011). TidbiT® loggers are deployed throughout the pond in order to capture the fullest possible record of spatial and temporal temperature variation in He'eia Fishpond (see below for rationale used to select TidbiT® deployment locations). Upon instrument retrieval, sensors are cleaned before data were offloaded.

HOBO® Water Level Loggers: HOBO® water level data loggers are high accuracy water pressure based sensors manufactured by ONSET Computer Corporation for use in a variety of water column depth ranges. The loggers deployed in He'eia Fishpond are part of the U20-001-01-Ti series (Fig 1.5), which features titanium housing for use in salt-water environments. The sensor itself is a durable ceramic pressure sensor with an accuracy of ±0.01 ft (Fig 1.5). Such accurate readings make the HOBO® loggers ideal for use in shallow, tidally dominated areas like He'eia Fishpond, where water level can fluctuate by several feet throughout the day. Each sensor has the capability of recording temperature as well as pressure. Pressure operation range is approximately 0 to 30 ft while temperature operation ranges is from -20º to 50ºC (OnsetComp.com).

Each individual instrument is attached to 10 cm or 20 cm tall cinderblock anchors and is deployed on either side of the *mākāhā* in order to create a weir for the purpose of estimating water discharge (description below). An air reference HOBO® pressure logger was placed onshore near the boating dock at He'eia Fishpond to establish an air pressure barometric assistant. This sensor increases the accuracy of pressure readings by factoring in temporal fluctuations in air pressure, which has a significant effect on water depth pressure in the shallow waters of He'eia Fishpond.

3.3 History of Instrument Deployment

TidbiT® Placement History: TidbiT® v2 temperature loggers were first deployed in He'eia Fishpond (initially only stake 13) starting on 8/08/2007. By

2/08/08, an additional five TidbiT® sensors were deployed for a total of six instruments. Since then, the number of sensors has fluctuated between seven and five sensors; TidbiT® placement schemes would frequently change before the next deployment. The TidbiT® temperature grid established by Young (2011) was subject to modification if additional loggers were purchased, or if sensors were damaged (or lost) upon retrieval. From 3/05/2008 to 9/02/2008, TidbiT® loggers were placed at stakes 3, 6, 9, 13, 15, and 18. This was the general pattern of deployment for most of the subsequent years. Stakes 13, 15, and 18 were TidbiT® sites throughout the entire period, while stakes 3, 6, and 9 were deployed more sporadically (Fig 3.1). Periodic removal of sensors from the pond for weeks to months at a time, either for the aforementioned cleaning and reprogramming, or for the winter holidays, has caused significant interruptions in climatic temperature records. The result is a sporadic history of sensor deployment.

From 6/18/2010 to 2/08/2011, seven TidbiT® loggers were deployed (stakes 3, 6, 9, 11, 13, 15, 18), a deployment pattern that achieved maximum coverage of the fishpond. Upon retrieval on 2/08/2011, we discovered that three TidbiT® loggers were lost or damaged. As a consequence, only four functional TidbiT® loggers remain for in-situ temperature studies. In an effort to maximize the efficiency of the residual sensors, a project was devised to determine an optimal deployment strategy for the temperature loggers. This new strategy is outlined in section 3.4.

HOBO® Logger History: A continuous, in-situ record of water discharge into and out of He'eia Fishpond is a pre-requisite for determining residence time within

He'eia Fishpond. A better understanding of the water sources of the pond has permitted calculation of nutrient loading to the pond (Young 2011), and will also benefit any studies which attempt to characterize the physical and chemical properties of the pond as a whole. Fully enclosed by the *kuapā*, water flows into He'eia Fishpond through six *mākāhā* and a break in the wall known as ocean break (OB). In order to calculate water fluctuations, Young (2011) established rating curves for each *mākāhā* and the ocean break by characterizing the dimension of each site and deploying several acoustic Doppler current profilers (ADCP) at these sites over several tide cycles. With knowledge of water fluctuations and the dimensions of each *mākāhā*, it has been possible to calculate flow rates.

Two types of ADCP instruments were available for use in initial water flux calculations: Nortek Aquadopp current meters (used to measure single point current direction and magnitude) and Sontek Argonaut-SW current profilers (which integrate water column current direction and magnitude). With fewer current/flow meters than *mākāhā,* a Nortek Aquadopp was periodically deployed at RM3 and TM whereas a Sontek Argonaut was periodically deployed at OM1, OM2, OB, and RM2, assuming that the different ADCPs produced similar data. Data from each ADCP was used to create a rating curve (Fig 3.2) that compared flow against pressure. After each site had an established rating curve over the entire tidal cycle, a pair of HOBO® water level loggers would then be deployed on either side of the *mākāhā* to establish a weir. The difference between the water level of each sensor yields a pressure value, which can be plugged into the rating curve equation of the *mākāhā* to calculate flow.

During Young's (2011) work to establish rating curves, HOBO® water level loggers were placed at the *mākāhā* with established rating curves while the ADCPs were being deployed systematically at other *mākāhā (*Fig 3.3) which had not yet been characterized by rating curves. The completion of each *mākāhā's* rating curve was accomplished by Young (2011). Funds were then made available to equip each *mākāhā* (and the ocean break) with a pair of HOBO® sensors to ensure future discharge rates could be calculated by making use of the rating curves determined by Young (2011). Exceptions to this deployment strategy are RM2, which is an elevated river *mākāhā* that only permits flow into He'eia Fishpond (thus requiring only one HOBO® sensor), and RM1, a destroyed river *mākāhā* that now functions as a diffuse flow region. This distinct *mākāhā* (RM1) thus requires a permanent ADCP to establish accurate flow rates. The final pressure scheme is outlined in figure 3.4.

3.4 Methods

Criteria for Instrument Placement: In an effort to improve future temperature time series data, a study was conducted to determine the most effective placement of TidbiT® v2 sensors throughout the pond. Ideally, all twenty stakes in the pond would be equipped with a permanent TidbiT® sensor to create an accurate representation of the spatial temperature ranges of He'eia Fishpond. However, given the limited resources of this project, only four TidbiT® V2 sensors are currently available for distribution throughout the pond. In order to achieve the best understanding of pond temperature variability, each stake was evaluated for possible TidbiT® sensor placement according to the following criteria:

A) Identify stakes that exhibit similar temperatures month to month so that redundancies can be eliminated by selecting a particular stake that records temperature that is representative of temperatures observed at multiple stakes.

B) Identify the stakes that exhibit the highest standard deviations from monthly average temperatures. This analysis will allow us to eliminate stakes that show little variability in temperature from month to month and instead instrument stakes that display broader temperature ranges. A goal of the TidbiT® loggers is to accurately show the full range of temperatures that characterize He'eia Fishpond.

C) Once stakes that satisfy the criteria of (A) and (B) have been identified, the stake selections must still provide maximum spatial coverage of He'eia Fishpond.

The data utilized to evaluate which stakes best satisfied the three criteria defined for optimal TidbiT® sensor deployment were derived from monthly surface YSI profiles at each of the twenty stakes within the pond (Fig 3.5). Since YSI® profiles from all stakes began 10/14/2010, the data were limited to the 6 monthly samplings through 4/29/2011. Surface temperature data from the six deployments were systematically evaluated in order to identity which of the 20 stakes within He'eia Fishpond best met the selection criteria. The goal was to identify sites that exhibit a large temperature range (criteria B) while simultaneously representing a multitude of stakes that tend to exhibit similar temperatures (criteria A). The small

group of stakes that fit both criteria was then assessed to determine which four stakes would also satisfy criteria C, spatial maximum coverage of He'eia Fishpond. The evaluations conducted to determine this optimal deployment strategy are discussed in the next section.

Evaluation of Characteristic Mean Temperature at Each Stake: The primary goal of the TidbiT® v2 sensors deployed in He'eia Fishpond is to establish an understanding of seasonal temperature variability and to accurately represent the spatial distribution of temperature in the pond as a whole. The pond receives cold, fresh water flux from the river *mākāhā* and warm, saline water flux from the ocean *mākāhā*, resulting in distinct temperature zones throughout He'eia Fishpond (Fig 3.6). The objective of this study was to identify the four stakes that would best represent temperature variability of He'eia Fishpond. To achieve this objective, an analysis of mean temperature variability at each stake, as indicated by the magnitude of the standard deviation about the mean temperature of a stake, was used to identify those stakes that consistently displayed distinct mean temperatures. The ideal result would identify four stakes within He'eia Fishpond that continuously, from month to month, represent the maximum range of mean temperatures. In order to evaluate the temperature range experienced for each stake, and to identify those stakes with similar temperature ranges, the following analysis was undertaken using TidbiT® temperature data from October – December 2010 and January, February, and April of 2011.

A)   The minimum and maximum surface temperatures from each monthly sampling were identified.

B)   The difference between the minimum and maximum temperatures was divided by four.

$(T_{max} - T_{min}) / 4$

C)   The $[(T_{max} - T_{min}) / 4]$ value was used to separate the stakes into four groups, each characterized by distinct temperature ranges.

D)   Each stake was then identified as belonging to one of four temperature zones (cold, cool, warm, and hot) and organized into Table 3.1.

Visual inspection of Table 3.1 should permit identification of stakes that differ from each other with respect to temperature. This would allow us to assume the remaining stakes and their temperatures would be represented by one of the four candidates. It was not a requirement that candidate stakes remain in the same temperature "group" month to month.

Evaluation of Natural Standard deviation of YSI Monthly Data: The temperature data, as organized in Table 3.1, were used to evaluate the natural standard deviation displayed by each stake over the 6-month sampling period. To achieve this analysis, standard deviations of mean YSI water column surface temperatures were organized into a table (Table 3.2). The objective was to identify stakes with the broadest range of temperature between monthly sampling dates. Sites

that displayed maximum standard deviation were given priority as TidbiT® sensor

candidates over those that displayed smaller variability, to ensure that the extreme

temperature ranges were accounted for. Recall from Chapter 2 that each month, YSI

water quality data at individual sites were binned into the surface (top 25 cm) and

bottom (lower 25 cm) water column. For the purpose of this analysis, only surface

temperature data was evaluated. In addition to overall averages from all deployments,

sampling dates were grouped by season in order to account for natural fluctuations in

pond temperature due to seasonal effects (Table 3.3).

Evaluation of the Physical Location of TidbiT® Candidates in He'eia

Fishpond: Pond stake locations are spread over the entire area of He'eia Fishpond,

with fifteen perimeter sites following the ancient pond wall and five sites that follow

a transect line that passes over the center of the oval shaped pond (Fig 3.5). Having

already evaluated the temperature ranges and groups of stakes with distinct mean

temperature groups, it is important to also consider He'eia Fishpond spatially so that

none of the stakes selected are in close proximity to each other. Temperature contour

maps dating back to 2007, created in Matlab® based on YSI® data (see Chapter 4 for

all contour maps), were visually evaluated in order to divide the pond into four

temperature zones every month. After all months were evaluated, the zones were

placed on a figure (Fig 3.6) based on common occurrences. The stakes that were

candidates for TidbiT® sensor deployment were evaluated using Figure 3.6 to

strategically place four TidbiT® sensors within the four common temperature zones.

In this manner, the four sites would represent He'eia Fishpond spatially.

3.4 Results

Redundant Stake Temperatures: No stake was located in the same temperature group throughout the entire 6-month period. Stakes 3, 6, 8, 12, 13, 16, and 18 appeared in all four temperature groups during the study. Stakes 7 and 15 only appeared in two groups. The remaining stakes varied greatly month to month. Table 3.4 highlights in which temperature group each stake fall in throughout the 6 months, including the overall average group for each stake. The red group (hottest) and the yellow group (cooler) contained the most stakes throughout the study, while the green group (coldest) and orange group (warmer) showed fewer stakes per month. The overall average for all stakes exhibits the opposite observation, with more stakes appearing in the orange and green group while the red and yellow group included fewer stakes.

Assessment of Stake Standard Deviations: Winter standard deviations were typically below 1.0 for most stakes, with pond 6 exhibiting the only significant deviation (± 1.58). Spring, although data was from a reduced sampling pool, displayed the highest standard deviations, up to ± 2.44 for pond 18. No stake showed standard deviations lower than ± 1.01, with most deviations above ± 1.5. Summer months (similar to spring in reduced stake sites) displayed uniform standard deviations, with most stakes exhibiting a standard deviation around ± 1.0. Fall months typically displayed deviations of ± 1.3, but lower deviations, down to ± 0.18 (Pond 14) and ± 0.30 (Pond 20), were also present. Annual standard deviation showed a significant division between stakes, with stakes 1, 3, 6, 7, 8, 9, 13, 15, 16, and 18 all being above

a standard deviation of ±1.5 whereas the remaining stakes (2, 4, 5, 10, 11, 12, 14, 17, 19, and 20) did not deviate above ±1.06 (Table 3.2).

3.5 Discussion

Redundant Stake Temperatures: Visual inspection of Table 3.4 resulted in a selection of a set of four stakes that best met the criterion most accurately. Stakes 1, 9, 13, and 18 were in distinct temperature ranges for 4 out of the 6 months. While 4/29/2011 demonstrated stakes 1, 13, and 18 in the same group, these four stakes also fell into separate groups on the basis of temperature average for all 6 months. Apart from 4/29/2011, the only other month in which stakes 1, 9, 13, and 18 were not partitioned into separate temperature groups was 11/11/2010, which placed stakes 9 and 13 in the orange (warm) group. There was no obvious substitute to replace any of the four described stakes, since no two of the remaining stakes were in the same temperature group for more than 3 months throughout the study.

Assessment of Stake Standard deviation: Standard deviation about mean temperatures varied significantly from season to season (Table 3.2). Without the complete 20-stake evaluation for spring and summer, annual data provide the best representation of pond temperature deviations. The fact that stakes 1, 3, 6, 7, 8, 9, 13, 15, 16, and 18 all displayed a standard deviation at or greater than ±1.5, while no other stake was in the vicinity of that value, suggests that a standard deviation cutoff of 1.50 is an appropriate criterion for a stake to be a TidbiT® sensor candidate.

3.6 Conclusion

TidbiT® Sensor Placement: Both statistical analyses suggested stakes 1, 9, 13, and 18 as ideal TidbiT® locations based on their large standard deviation from monthly means and their consistent placement in different temperature zones from month to month. The four ideal candidates are not distributed to achieve maximum spatial coverage across the pond grid, however, as there is a large section in northeast He'eia Fishpond without an in-situ temperature sensor. With four TidbiT® sensors available for deployment, the last location was determined to be stake 6, rather than stake 1, based on its large standard deviation between monthly means (±1.91) and the need for a sensor in that section of the pond. The three stakes (9, 13, 18) alone do not efficiently cover the whole span of the 88-acre pond, and despite stake 1 having met two out of three criteria for placement, all three original criteria must be met for the future benefit of climatic temperature data collection in He'eia Fishpond.

An added benefit of including stakes 6, 13, and 18 is that these stakes had the most uninterrupted deployments within the 2008-2011 time series (Figure 3.1). It would be of greater benefit for future climate studies to continue monitoring stakes 6, 13, and 18 in order to continue the longest uninterrupted climate time series. Therefore, based on the analyses conducted above, and the criteria defined for proper placement, stakes 6, 9, 13, and 18 were identified as optimal sites for future TidbiT® sensor placements. Should funding exist in the future for an additional TidbiT® v2 sensor, stake 1 would make an ideal location for deployment due to its large standard deviation from monthly means, its habit to be in different temperature groups than stakes 9, 13, and 18, and its physical location in southeastern He'eia Fishpon

Table 3.1: Six-month Analysis of temperature zones in He'eia Fishpond based on YSI profiling data. Sites were binned for minimum and maximum sites, and the difference was divided by four to create each division. Site names from Young (2011)

SITE	10/14/10	11/11/10	12/2/10	1/27/11	2/17/11	4/29/11	AVERAGE
Pond1	25.46	24.22	24.36	25.09	25.04	26.56	25.12
Pond2	26.35	24.34	24.05	24.24	25.01	25.64	24.94
Pond3	26.83	24.46	24.38	24.51	25.53	26.53	25.37
Pond4	26.66	24.96	24.65	24.44	25.32	26.78	25.47
Pond5	26.68	24.97	24.71	24.36	25.39	26.69	25.46
Pond6	26.22	24.98	24.44	23.22	25.87	27.14	25.31
Pond7	26.04	24.72	24.36	23.48	24.99	26.51	25.02
Pond8	25.83	25.16	24.79	23.35	25.15	27.66	25.32
Pond9	26.31	25.21	24.67	24.36	25.62	27.24	25.57
Pond10	26.71	25.07	24.73	24.87	25.66	27.29	25.72
Pond11	26.00	24.72	24.76	24.66	25.68	26.89	25.45
Pond12	25.87	24.81	24.64	24.96	25.84	25.98	25.35
Pond13	26.06	25.13	24.95	25.62	24.66	26.18	25.43
Pond14	26.05	25.80	24.37	25.68	25.69	25.50	25.51
Pond15	25.91	24.94	24.35	24.65	25.74	26.36	25.32
Pond16	26.52	24.87	24.31	23.36	25.58	26.81	25.24
Pond17	26.01	24.58	24.32	23.90	25.55	26.23	25.10
Pond18	26.58	24.85	24.15	23.97	25.41	26.23	25.20
Pond19	26.47	24.90	23.93	24.36	24.71	26.24	25.10
Pond20	26.32	25.89	24.91	26.41	24.69	25.90	25.69
MIN	25.46	24.22	23.93	23.22	24.66	25.50	24.94
MAX	26.83	25.89	24.95	26.41	25.87	27.66	25.72
DIFF/4	0.34	0.42	0.25	0.80	0.30	0.54	0.20
Hot	26.49	25.48	24.70	25.61	25.57	27.12	25.53
Warm	26.15+	25.06+	24.44+	24.81+	25.27+	26.58+	25.33+
Cool	25.80+	24.64+	24.19+	24.02+	24.96+	26.04+	25.13+
Cold	25.46+	24.22+	23.93+	23.22+	24.66+	25.50+	24.94+

Table 3.2: A seasonal comparison of standard deviations about the mean temperatures from each individual stake. Starred sites indicate potential TitbiT locations based on a yearly standard deviation greater than ±1.5. Averages are from same six-month period as Table 3.1

STDEV	ALL	WINTER	SPRING	SUMMER	FALL
Pond1*	1.78	0.94	1.42	1.00	1.34
Pond2	0.91	0.51	NaN	NaN	1.42
Pond3*	1.51	1.12	1.18	0.95	1.34
Pond4	1.02	0.46	NaN	NaN	1.20
Pond5	1.00	0.52	NaN	NaN	1.21
Pond6*	1.91	1.58	1.56	1.37	1.46
Pond7*	1.84	1.25	2.11	0.92	1.43
Pond8*	1.89	1.05	2.22	1.13	1.31
Pond9*	1.76	1.09	1.69	0.99	1.26
Pond10	1.06	0.50	NaN	NaN	1.16
Pond11	1.03	0.56	1.01	1.04	0.73
Pond12	0.61	0.62	NaN	NaN	0.75
Pond13*	1.96	1.13	1.91	0.95	1.43
Pond14	0.59	0.76	NaN	NaN	0.18
Pond15*	1.86	1.00	2.16	0.95	1.33
Pond16*	1.83	0.94	1.91	0.94	1.35
Pond17	0.96	0.86	NaN	NaN	1.01
Pond18*	1.69	1.03	2.44	1.07	1.14
Pond19	1.03	0.39	NaN	NaN	1.11
Pond20	0.72	0.94	NaN	NaN	0.30

Table 3.3: A seasonal evaluation of YSI monthly sampling data from Aug 2007 through May 2011. Average values are in degrees Celsius.

WINTER	AVG	STDEV	MIN	MAX
Pond1	21.54	0.94	23.08	26.25
Pond2	18.33	0.51	24.05	25.01
Pond3	21.63	1.12	23.16	26.77
Pond4	18.60	0.46	24.44	25.32
Pond5	18.61	0.52	24.36	25.39
Pond6	21.86	1.58	23.22	28.06
Pond7	21.59	1.25	23.48	27.35
Pond8	21.46	1.05	23.35	26.66
Pond9	21.78	1.09	23.68	27.11
Pond10	18.81	0.50	24.73	25.66
Pond11	18.77	0.56	24.66	25.68
Pond12	18.86	0.62	24.64	25.84
Pond13	21.84	1.13	23.40	27.48
Pond14	18.93	0.76	24.37	25.69
Pond15	21.73	1.00	23.63	26.95
Pond16	21.51	0.94	23.36	26.39
Pond17	18.44	0.86	23.90	25.55
Pond18	21.45	1.03	23.56	26.42
Pond19	18.25	0.39	23.93	24.71
Pond20	19.00	0.94	24.69	26.41

SPRING	AVG	STDEV	MIN	MAX
Pond1	27.39	1.42	25.43	28.94
Pond2	25.64	NaN	25.64	25.64
Pond3	26.99	1.18	25.17	28.17
Pond4	26.78	NaN	26.78	26.78
Pond5	26.69	NaN	26.69	26.69
Pond6	27.70	1.56	25.63	29.94
Pond7	27.52	2.11	25.29	30.96
Pond8	27.92	2.22	25.36	31.47
Pond9	27.84	1.69	25.52	30.08
Pond10	27.29	NaN	27.29	27.29
Pond11	26.69	1.01	25.60	27.58
Pond12	25.98	NaN	25.98	25.98
Pond13	27.86	1.91	25.83	30.38
Pond14	25.50	NaN	25.50	25.50
Pond15	27.70	2.16	25.37	31.04
Pond16	27.84	1.91	25.62	30.75
Pond17	26.23	NaN	26.23	26.23
Pond18	27.28	2.44	24.85	31.34
Pond19	26.24	NaN	26.24	26.24
Pond20	25.90	NaN	25.90	25.90

SUMMER	AVG	STDEV	MIN	MAX
Pond1	27.07	1.00	25.56	29.76
Pond2	NaN	NaN	0.00	0.00
Pond3	26.80	0.95	25.51	28.53
Pond4	NaN	NaN	0.00	0.00
Pond5	NaN	NaN	0.00	0.00
Pond6	27.64	1.37	26.02	30.19
Pond7	26.94	0.92	25.60	29.77
Pond8	26.98	1.13	25.67	29.60
Pond9	27.23	0.99	26.05	28.90
Pond10	NaN	NaN	0.00	0.00
Pond11	26.60	1.04	25.80	27.77
Pond12	NaN	NaN	0.00	0.00
Pond13	27.24	0.95	26.16	30.46
Pond14	NaN	NaN	0.00	0.00
Pond15	27.02	0.95	25.88	29.74
Pond16	27.02	0.94	25.97	29.83
Pond17	NaN	NaN	0.00	0.00
Pond18	26.52	1.07	25.10	29.49
Pond19	NaN	NaN	0.00	0.00
Pond20	NaN	NaN	0.00	0.00

FALL	AVG	STDEV	MIN	MAX
Pond1	26.28	1.34	24.22	28.82
Pond2	25.34	1.42	24.34	26.35
Pond3	26.67	1.34	24.46	28.85
Pond4	25.81	1.20	24.96	26.66
Pond5	25.82	1.21	24.97	26.68
Pond6	26.32	1.46	24.03	28.76
Pond7	26.10	1.43	23.70	28.42
Pond8	26.23	1.31	23.94	28.44
Pond9	26.63	1.26	24.88	28.64
Pond10	25.89	1.16	25.07	26.71
Pond11	25.56	0.73	24.72	26.00
Pond12	25.34	0.75	24.81	25.87
Pond13	26.44	1.43	24.97	29.28
Pond14	25.92	0.18	25.80	26.05
Pond15	26.02	1.33	24.19	28.45
Pond16	26.17	1.35	24.37	28.54
Pond17	25.29	1.01	24.58	26.01
Pond18	26.04	1.14	24.39	27.65
Pond19	25.68	1.11	24.90	26.47
Pond20	26.11	0.30	25.89	26.32

Table 3.4: Division of stakes among four temperature zones based on 6-month He'eia Fishpond monthly sampling data (Table 3.1). Bolded sites indicate recommended sites based on the standard deviation analysis, temperature grouping, and pond site location evaluations. Site names from Young (2011).

SITE	10/14/10	11/11/10	12/2/10	1/27/11	2/17/11	4/29/11	AVERAGE
Group 1	Pond3	Pond14	Pond5	**Pond13**	**Pond6**	**Pond6**	**Pond9**
	Pond4	Pond20	Pond8	Pond14	**Pond9**	Pond8	Pond10
	Pond5		Pond10	Pond20	Pond10	**Pond9**	Pond20
	Pond10		Pond11		Pond11	Pond10	
	Pond16		**Pond13**		Pond12		
	Pond18		Pond20		Pond14		
					Pond15		
					Pond16		
Group 2	Pond2	Pond8	Pond4	**Pond1**	Pond3	Pond2	Pond3
	Pond9	**Pond9**	**Pond9**	Pond10	Pond4	Pond4	Pond4
	Pond19	Pond10	Pond12	Pond12	Pond5	Pond5	Pond5
	Pond20	Pond13			Pond17	Pond11	Pond11
					Pond18	Pond16	Pond12
							Pond13
							Pond14
Group 3	Pond7	Pond4	**Pond1**	Pond2	**Pond1**	**Pond1**	**Pond6**
	Pond8	Pond5	Pond3	Pond3	Pond2	Pond3	Pond15
	Pond11	**Pond6**	Pond7	Pond4	Pond7	Pond7	Pond16
	Pond12	Pond7	Pond14	Pond5	Pond8	Pond13	**Pond18**
	Pond13	Pond11	Pond15	**Pond9**		Pond15	
	Pond14	Pond12	Pond16	Pond11		Pond17	
	Pond15	Pond15	Pond17	Pond15		**Pond18**	
	Pond17	Pond16		Pond19		Pond19	
		Pond17					
		Pond18					
		Pond19					
Group 4	**Pond1**	**Pond1**	Pond2	**Pond6**	Pond13	Pond12	**Pond1**
		Pond2	**Pond18**	Pond7	Pond19	Pond14	Pond2
		Pond3	Pond19	Pond8	Pond20	Pond20	Pond7
				Pond16			Pond17
				Pond17			Pond19
				Pond18			

79
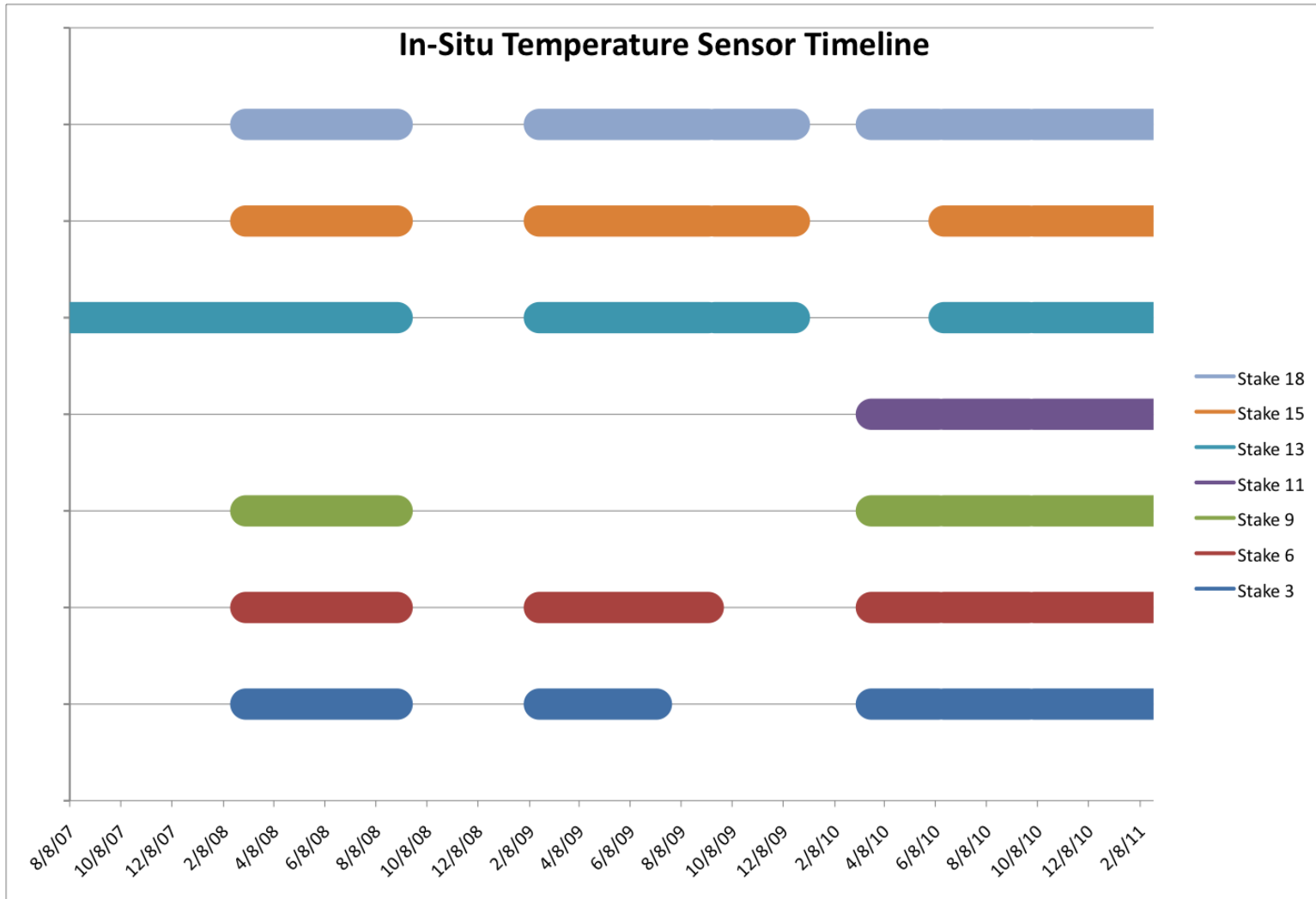
Figure 3.1: TidbiT® v2 Temperature Logger deployment history at He'eia Fishpond. Site names from Young (2011)
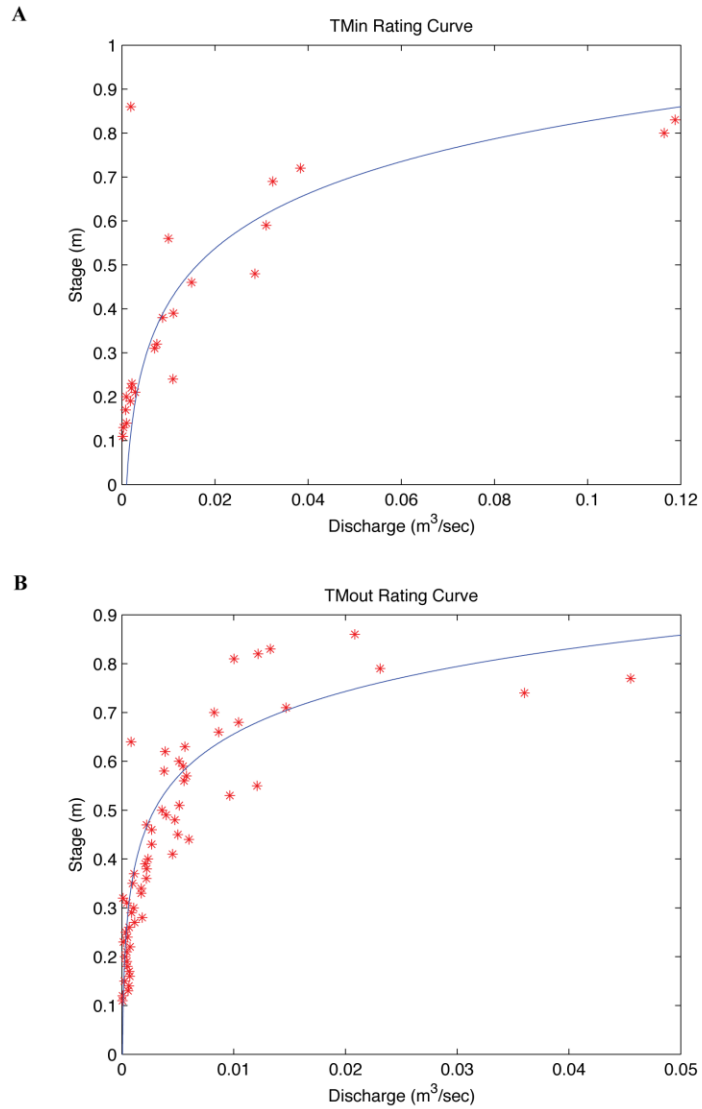
Figure 3.2: Example of rating curves for TM water flow (A) into and (B) out of He'eia Fishpond. Note the different discharge (m^3/sec) scales on the x-axes. Taken from Young (2011).
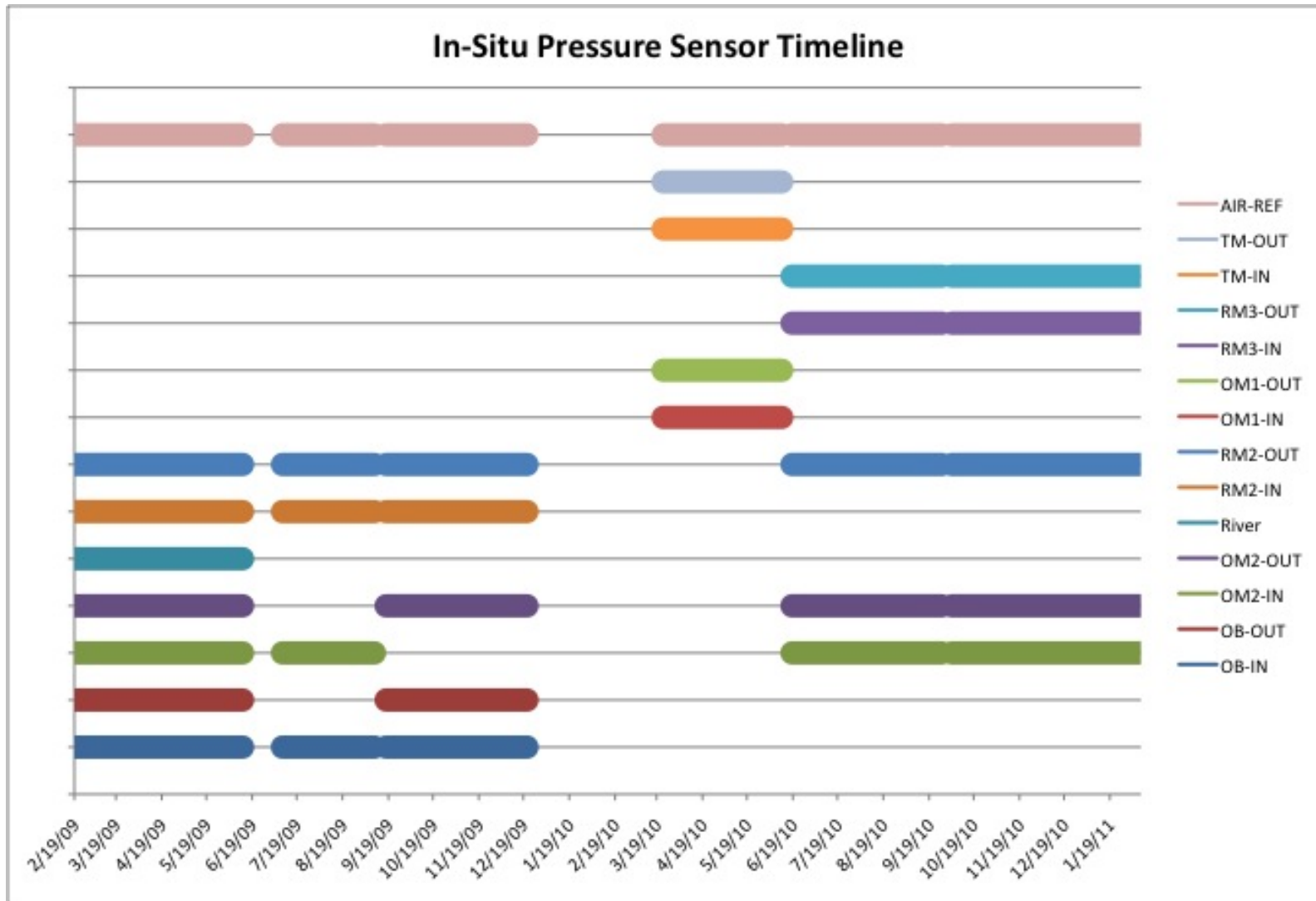
Figure 3.3: HOBO® Water Level Logger deployment history. TM = Triple *Mākāhā*, RM3 = River *Mākāhā* 3, RM2 = River *Mākāhā* 2, OM1 = Ocean *Mākāhā* 1, RM2 = River *Mākāhā* 2, OM2 = Ocean *Mākāhā* 2, OB = Ocean Break. Site names from Young (2011)

Figure 3.4. Final HOBO® Water Level Logger and ADCP (acoustic Doppler current profiler) scheme. OM = Ocean *Mākāhā* (2), OB = Ocean Break, TM = Triple *Mākāhā*, RM = River *Mākāhā* (3). Site names from Young (2011).

Figure 3.5: He'eia Fishpond (via Google Earth) plus layout of all stakes (1-20), ocean *mākāhā* (OM2, OM1, TM), river *mākāhā* (RM3, RM2, RM1), and ocean sites (OB, OCN2, OCN1). Site names from Young (2011).
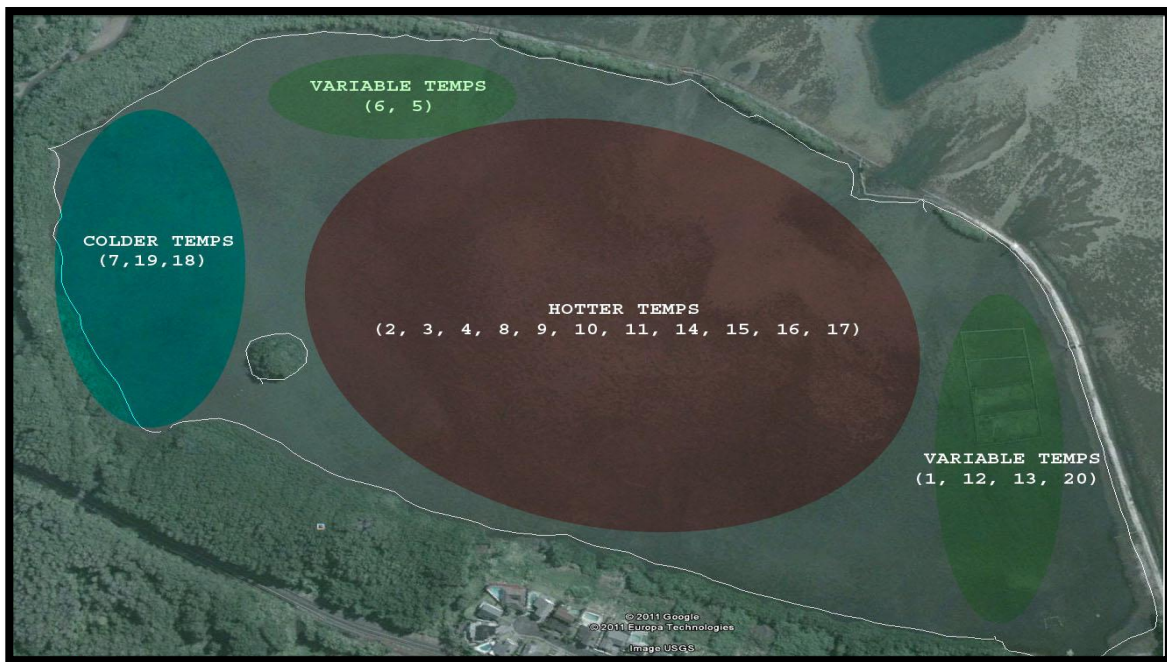
Figure 3.6: An estimation of temperature zones within He'eia Fishpond. Figure was constructed using contouring data from 2007 – 2011. Site names from Young (2011)

84

CHAPTER 4

IDENTIFYING SEASONAL TEMPERATURE CHANGES WITHIN HE'EIA

4.1 Introduction

Numerous measurements of physical oceanographic parameters have been conducted in He'eia Fishpond since 2007. Data from these studies have formed the beginning of a long-term climate record of Kane'ohe Bay, Oahu. In-situ v2 TidbiT® temperature sensors deployed along the perimeter, and within the pond were utilized to create several month long temperature time series (Fig 3.1). In addition, regular monthly sampling of water column profiles (using a YSI 6600V2 multi-parameter water quality sonde) has established a month-to-month record of oceanographic parameters (temperature, salinity, dissolved oxygen, turbidity, chlorophyll content) in the fishpond. Evaluating both of these data sets, with wind speed and direction, as well as air temperature data sets from KBMCB (Kane'ohe Bay Marine Corps Base), will give a picture of the environmental climate of the fishpond within the past few years.

These time series capture La Niña (September 2007 – May 2008, and July 2010 – November 2011), El Niño (June 2009 – April 2010) and background conditions (June 2008 – May 2009 and May 2010 – June 2010). Before this contribution, ENSO (El Niño/Southern Oscillation) cycling effects within Kane'ohe Bay and the fishpond were not well described. The onset of El Niño can result in extreme weather events throughout the islands. Identifying and forecasting specific time periods during which extreme conditions may exist for He'eia Fishpond may aid

Paepae O He'eia in reducing fish losses, such as the fish kills of May 2009 (explored in depth later), which is hypothesized to be a result of extreme temperature spikes due to El Niño conditions.

Before exploring the data sets, it's prudent to examine the background climate (as well as ENSO effects) of Kane'ohe Bay itself. With a base knowledge of atmosphere and oceanic conditions, finding anomalies associated with seasonal changes and ENSO cycles will be facilitated.

Climate of Kane'ohe Bay, Oahu

Air and Sea Surface Temperature: The Hawaiian Islands lie in the sub-tropic climate zone, resulting in a roughly equal day length and small seasonal variation in incoming solar radiation over the year. A clear winter day in Hawaii receives 67% of maximum solar radiation compared to a clear summer day, while a clear winter day at a locations 40º N and 50º N latitude receive 33% and 20% of maximum solar radiation compared to a clear summer day (Price 1983). In Hawaii, this results in a narrow range of air temperature, from 20ºC to 28ºC annually (Jokiel 2011). Being surrounded by a tropical ocean has an enormous effect on the climate of Hawaii. The ocean acts as a natural buffer to curb significant temperature changes. Weather fronts from any continental land masses have at least 2,000 miles to travel before interacting with the geography of Hawaii, allowing the ocean to regulate any extreme fluctuations in temperature (Price 1983).

Sea surface temperatures are similarly affected by these air masses. The range of sea surface temperatures year-round is 22.7 to 26.6ºC (Price 1983), with colder

temperatures in the winter months and warmer temperatures in the summer months. A small lag is observed between air and sea temperatures due to the amount of time it takes these air masses to deliver the thermal energy required to heat the sea surface surrounding the islands. Thus, months with cooler air temperatures are February and March rather than December and January, for example, with August and September exhibiting hotter temperatures than June and July (Price 1983).

Trade Wind Effect: The Hawaiian Island chain lies in the northeast trade wind belt, a nearly consistent wind phenomenon that results in NE and E trade winds averaging 10-11 knots that blow 70% of the year (Jokiel 2011). This wind is generally more consistent in the summer months (May – October), and stronger, more sporadic events are associated with the winter months (October – April). Interruptions of the trade winds occur more often in the winter, when migratory cyclones or Kona storms (the source of Kona winds) are more common (Price 1983). Trade winds strongly influence the climate of windward facing areas of Oahu, including Kane'ohe Bay. With the Ko'olau mountain chain (Fig 4.1) forming a steep cliff rise, prevailing trade winds bring moisture to the end of the ahu'pua'a (Hawaiian land division). The rapidly rising air causes stiff winds near the Nu'uanu Pali, causing an orographic effect that induces rainfall (Jokiel 2011).

Rainfall: The orographic effect dominates the geographic rainfall patterns of Kane'ohe Bay. The ridge crest of the Ko'olau (Fig 4.1) receives on average 15-20 inches of rain throughout the year, while the edge of Kane'ohe Bay experiences

significantly lower rainfall values, down to 3-4 inches. This information is important

when considering fresh water sources to Kane'ohe Bay. Ostrander et al. (2008) found

that Kane'ohe Bay freshwater plumes were strongly correlated with stream discharge.

This results in large volumes of sediment runoff, with larger amounts expected in the

rainier winter months than in the typically dryer summer months. Total rainfall values

for the entire watershed (including Ko'olau ridge) measure 94 inches per year on

average, while the inner bay receives up to 55 inches per year (Smith et al. 1981). The

bay and watershed receive up to 31 billion gallons of fresh water from runoff and

rainfall each year, which must have a significant effect on water and air temperature

(Smith et al. 1981).

ENSO Effects on Hawaii

ENSO Description: The El Niño/Southern Oscillation (ENSO) is a climate

pattern phenomenon that largely affects the tropical Pacific but has worldwide

consequences. It is the largest year-to-year variation of Earth's climate, with an El

Niño phase and a La Niña phase that result from ocean and atmospheric interactions

(McPhaden et al, 2011). The phases are generally characterized by the "warm oceanic

phase" (El Niño), where high air surface pressure exists in the western Pacific ocean,

and the "cold oceanic phase" (La Niña), with lower air surface pressure in the western

Pacific (McPhaden et al, 2011).

El Nino is characterized by unusually warm ocean temperatures in the

Equatorial Pacific and drought in the West Pacific. Normally, non-El Nino conditions

allow for trade winds to blow west across the tropical Pacific. El Nino causes these

trade winds to relax, allowing a warm pool to make its way east towards the American west coast. Heavy rainfall follows the warm pool, with associative flooding across the southern U.S. and Peru. La Niña follows El Niño, and influences the climate system in the opposite manner, returning warmer water back to the western Pacific (McPhaden et al, 2011). Colder surface waters again form in the eastern Pacific with the return of the trade winds. The pressure gradient is restored as low pressure follows the warm pool back towards the western Pacific, and higher pressure builds over the eastern Pacific (Fig 4.3).

   Hawaii ENSO Response: October through May of an El Niño year in Hawaii typically exhibits less rainfall than in background conditions. Warm pools of seawater associated with El Niño cause an enhanced tropic convection, which leads to strong air circulation in the north Pacific. Descending air associated with upper atmospheric circulation sinks onto Hawaii, limiting rising air from forming clouds, thus inhibiting rainfall (Chu 1995). A phenomenon known as the Madden-Julian Oscillation, however, is thought to cause the wet winter pattern known as the "Pineapple Express", which can temporarily cause rainfall for the islands. El Niño typically pushes this system northeast, resulting in drought, but the early arrival of the Pineapple Express is a known indicator of a potential El Niño the following year.

   Hawaii is also known to experience more tropical storms during El Niño than in other climate conditions. The warmer waters to the south of Hawaii (due to the moving warm pool) can create tropical cyclones, causing El Niño years to have a

higher chance of strong storm events. Due to weakening trade winds associated with the onset of El Nino, wind direction is more sporadic during El Nino.

The association between La Niña and Hawaiian weather has not yet been well documented, apart from increased wind velocities, sometimes slightly colder temperatures, and increased rainfall (Chu 1995).

4.2 Methods

In order to identify seasonal changes within He'eia Fishpond, several steps were taken to characterize different climate patterns during El Niño and La Niña:

1) Construction of a wind, temperature (pond and air), rainfall, and tidal time series. This evaluation will display any seasonal trends as well as help isolate the different ENSO climate stages and their effects on local weather.

2) Analysis of temperature measurements from in-situ TidbiT® v2 sensors over a four year period.

3) Evaluation of monthly sampling contours. YSI profiles taken each month were used to form temperature contour maps of He'eia Fishpond. Coupled with tide, rain, and air temperature over the given sampling period, these maps will give insight into how the pond responds to seasonal and daily fluctuations in the environment.

4) Statistical analysis of oceanic and atmospheric parameters. Using Microsoft Excel, raw data were organized to represent seasonal, yearly, and monthly averages for May 2009, when a large fish kill

occurred. Standard deviation, minimum values, and maximum values were also calculated to determine range as well as typical divergence from averages. These data are compared with values from the literature to help determine if He'eia Fishpond instruments can be viable indicators of Kane'ohe Bay climate (such as El Niño).

He'eia Environmental Time Series: Air temperature, wind direction and magnitude, precipitation, and tide data were obtained through Mesowest (2011), and organized into MATLAB® to create time series plots (Fig 4.5). In-situ data from TidbiT® v2 temperature sensors located at stakes 6, 13, and 18 (Fig 4.4) were available as far back as March 5, 2008 and extend into February 22, 2011. Stakes 6, 13, and 18 were chosen due to these stakes having the most consistent deployment record (Fig 3.1) and for the spatial grid they form (Fig 4.4). For the purpose of this study, the time series was limited to June 1, 2008 through February 22, 2011 in order to capture each of the main climate events: La Niña (September 2007 – May 2008), normal (June 2008 – May 2009), El Niño (June 2009 – April 2010), normal (May 2010 – June 2010), and La Nina (July 2010 – November 2011 (present)).

Data from both He'eia Fishpond and KBMCB (Mesowest 2011) were combined into one data set since the two stations are in relatively close proximity to each other (Fig 1.3). Wind plots were created by evaluating the magnitude of the wind with its direction and creating a "feather" plot. Tide data were obtained through KBMCB rather than pond tide sensors due to KBMCB having more complete data sets. In order to accommodate for the He'eia tide lag time observed by Young (2011),

these tide data sets were compared with HOBO® pressure sensors deployed in the

pond, which also produce reliable tide records.

TidbiT® time series charts (Fig 4.6) were created by compiling raw data into

excel and further organizing the data using various techniques. Special attention was

given to May 2009 data in order to characterize the temperature of He'eia during the

fish kill that occurred in this month. Excel charts (Tables 4.1 - 4.3) represent these

various ways of organizing the data.

Evaluation of Monthly Sampling Contours: Contours were created from YSI®

6600V2 Multi-parameter water quality sonde data using Matlab® visualization

software (Fig 3.5). Water column profiles created a divided record of data between

surface and deep water, with surface water being the only parameter contoured in this

study. Monthly sampling began between 9 and 11 AM, on differing tides, and usually

finished by 1 -3 PM. Data were offloaded and organized according to site and

surface/deep profiles. Only pond and *mākāhā* sites were used to form contour plots,

since the ocean sites (OCN1, OB, OCN2) tend to distort the true value of temperature

due to the barrier of the pond wall separating the two water masses. Each contour

map has an accompanying tide, air temperature, and rainfall chart obtained from

Mesowest (2011) data (Fig 4.13).

4.3 Results

He'eia Environmental Time Series

Air Temperature: Air temperature in Kane'ohe Bay, Oahu fluctuated

throughout the year (between 14.00 and 30.00 C°), with averages of 24.32 C°.

Average winter temperatures are 22.75 with a standard deviation of ±1.91 and a range

of 14.39°C – 29.39°C. Average spring temperatures are 23.62 °C with a standard

deviation of ±1.89 and a range of 15.61°C - 30.00°C. Average summer temperatures

are 25.75 C° with a standard deviation of ±1.39 and a range of 21.00 – 29.39°C.

Average fall temperatures are 24.99°C with a standard deviation of ±1.79°C and a

range of 16.72°C – 30.00°C (Table 4.1).

Background (June 2008 – May 2009 and May 2010 – June 2010) conditions

exhibit slightly lower average temperatures (24.05 C°) than El Niño (June 2009 –

April 2010) (24.49 C°) and La Niña (September 2007 – May 2008 and July 2010 –

present)(24.52 C°). The variability in temperature was characterized by documenting

the standard deviation from mean temperatures over each ENSO event. The highest

variability occurred in the background conditions (±2.17°C), lowest in La Niña

conditions (±1.93°C), and El Niño was in the middle at ±2.11°C. Background

conditions displayed a higher range of temperature (15.61°C – 29.39°C) than El Niño

(15.61°C – 30.00°C) and La Niña (14.39°C – 30.00°C).

Wind Speed and Direction: Winds remain light and variable throughout most

of the year. Kane'ohe Bay experiences an average of 7.97 mph winds from a compass

bearing of 88.71° (easterly winds) annually. Winter months observed an average

speed of 7.46 mph with a standard deviation of ±4.97 mph. The average compass

bearing was 114.38º, with a high standard deviation of ±88.15º. Spring saw higher

average wind speed (8.45 mph) while exhibiting a lower standard deviation (±4.10

mph) than winter. The Spring wind direction was also very different, at an average

compass bearing of 86.28º, with a much lower ±62.88º standard deviation. During the

summer, wind speed averaged the highest, at 8.47 mph, saw the least variability from

that average, at ±3.13 mph, and averaged the most northerly (72.07º) and least

variable (±29.29º) winds. Finally, fall observed average wind speeds of 7.49 mph;

with a standard deviation of ±4.14 mph. Average compass direction was an easterly

87.94º with a standard deviation of ±59.10º.

As for ENSO events, background conditions observed average wind speeds of

7.95 mph. with a standard deviation of ±4.22 mph. Wind direction averaged 92.45º

with a high standard deviation of ±67.53º. El Niño saw a much higher average wind

speed of 8.43 mph, with a standard deviation of ±4.24. The wind direction averaged

84.28º and was variable by ±63.21º. La Niña exhibited the lowest average wind speed

(7.56 mph) and lowest variability (±3.89 mph). Average wind direction was 88.07º, ±

56.69º (Table 4.2).

Rainfall: Seasonal rainfall in Hawaii was heaviest in the fall months and

lightest in the summer months (Table 4.1). Winter averaged 0.03 inches of rain per

hour, with a maximum rainfall event of 1.71 inches in an hour, and observed a high

standard deviation of ±0.10 inches per hour. Spring was nearly identical, except for a

slightly higher standard deviation of ±0.11 inches per hour and a maximum rainfall

event of 1.89 inches of rain in an hour. Summer had the lowest average rainfall per hour, at 0.01 (±0.04 inches per hour) and the smallest maximum rainfall event (0.45 inches over an hour). Fall had a high average rainfall (0.05 inches per hour) and equally high standard deviation (±0.14 inches per hour) while exhibiting a maximum heavy rainfall event of 1.40 inches of rain in an hour (Table 4.1).

Background conditions averaged 0.04 inches of rain per hour, with a high standard deviation of ±0.12 inches per hour and a maximum rainfall event of 1.40 inches. El Niño observed an average of 0.03 inches of rain per hour (±0.09 inches per hour) and had a maximum rainfall of 1.64 inches. Finally, La Niña had the lowest average rainfall at 0.02 inches per hour, with a standard deviation of ±0.10. The highest maximum rainfall over an hour occurred during La Niña, at 1.89 inches.

Pond Temperatures: Pond (stake 6, 13, 18) temperature averages over the entire year did not vary significantly (±0.2ºC) from each other, yet exhibited noteworthy differences seasonally. Winter temperature averages for stakes 6, 13, and 18 (23.68º, 24.48º, and 23.80ºC respectively) were the lowest temperatures observed. Spring temperature averages were slightly higher (26.27º, 26.10º, and 26.35ºC respectively) than fall temperature averages (25.77º, 26.40º, and 26.92ºC respectively). Summer exhibited the highest average temperatures for stakes 6, 13, and 18 (27.94º, 27.38º, and 27.77ºC respectively).

Temperature averages between stakes were similar for spring and summer, yet differed more for the winter and fall months. The standard deviation between the three averages yielded ±0.13ºC for spring and ±0.28ºC for summer. The standard

deviation for winter yielded a greater value ±0.42ºC and ±0.57ºC for fall, suggesting greater spatial temperature variability.

May 2008, 2009, 2010: Pond temperatures for the months of May 2008, 2009, and 2010 varied significantly (Table 4.3). "Stake 6" temperatures were averaged to be 27.73ºC for 2008, 29.34ºC for 2009, and 26.87ºC for 2010. "Stake 18" temperatures were averaged to be 27.71ºC for 2008, 30.26ºC for 2009, and 26.34ºC for 2010. "Stake 13" had no record for May 2010, but average temperatures were 27.09ºC in 2008 and 29.11ºC for 2009. In all cases (except the missing data for stake 13 in 2010), May 2009 (El Niño) exhibited the hottest pond temperatures followed by May 2008 and May 2010 respectively. While air temperatures in Kane'ohe didn't deviate significantly (±0.29ºC) between the three years, wind direction varied greatly. May 2008 wind averaged a compass bearing of 91.33º (±56.25º), May 2009 (El Niño year) averaged a compass bearing of 127.94º and exhibited the highest standard deviation from that compass direction (109.97º), whereas May 2010 averaged 75.66º (±18.96º). (Table 4.3).

Monthly Sampling Contours Charts (Figures 4.7 – 4.31)

Spatial Variation: Pond contours showed similar characteristics throughout the entire 25-month sampling period (January 2008 – February 2011, some months excluded). Temperatures near the river mouth at RM3 (Fig 3.6)(stakes 7, 18, 19) were always colder than the rest of the pond (referred to as Northwest He'eia Fishpond)

96

with a cold pool usually stretching out to stake 9. Central He'eia Fishpond (stakes 2, 3, 4, 8, 9, 10, 11, 14, 15, 16, 17) generally exhibits warmer temperatures than near the ocean *mākāhā*. The region of the pond near stakes 5 and 6 (North He'eia Fishpond) (Fig 3.6) differs significantly month-to-month, sometimes being the hottest region and sometimes exhibiting colder temperatures, thus exhibiting the greatest variability. Stakes 1, 12, 13, and 20 form another variable temperature region (South He'eia Fishpond) near the dock of He'eia Fishpond, where temperatures are less predictable. While temperatures there vary from month to month, a visual analysis of all monthly contours suggests that the North He'eia Fishpond region is consistently warmer than the South He'eia Fishpond region. Ocean *mākāhā* sites were variable in temperature from month to month. A summary of these findings is shown in Figure 4.8.

Normal (Background) ENSO: Visual evaluation of the contour plots revealed some interesting results. In 2008, data were available from January to August, and showed conditions typical to Hawaii in a normal year (ENSO cycle – Normal). Air temperatures were colder in January (~25ºC), typically increasing by 1ºC each month up until May (~28ºC), excluding March (which wasn't sampled). June and July still exhibited higher air and pond temperatures (~27ºC), yet slightly lower than May's overall air and pond temperatures. August displayed high pond and air temperatures, similar to May (~28ºC). The only sampling that exhibited significant rainfall was January, with less than 0.3 inches of rainfall in the 24-hour period leading up to sampling.

El Niño: Monthly sampling data from the El Niño of 2009 existed between

July and December. Monthly temperatures were sporadic. July noted hot (30ºC) pond

and air temperatures, while the following August sampling was cooler, down to

~26ºC. A large amount of rainfall in the 24hr period leading up to sampling, with

rainfall exceeding 0.21 inches per hour, was recorded in the August sampling.

October (~28º) was warmer than September (~26ºC), with no rainfall on either days.

November was the coldest month, with pond temperatures down to ~24ºC, while the

following December sampling experienced the widest range of temperatures

throughout the pond (20ºC – 27ºC). No significant rainfall, apart from August, was

recorded.

La Niña: The 2010-2011 La Niña existed between May 2010 and March

2011. All months except March (2010 and 2011) were sampled. January was very

cold, down to ~23ºC air temperature averages and ~22ºC pond temperature averages.

Significant rainfall was experienced in the hours before the sampling. February was

slightly warmer in both air and pond temperature, but still on the lower spectrum of

temperatures. The April sampling saw ~25ºC temperatures, but sampling took place

during a rainstorm, which is apparent in the air temperature plot. May sampling

experienced higher in air temperatures (~27ºC) despite heavy rainfall (0.09 inches per

hour) before sampling was conducted. June was similar to May in all aspects, despite

no rainfall. July, August, September, and October samplings experienced around

26ºC for pond temperature averages, while exhibiting significantly higher (~29ºC) air

temperature averages, with no significant rainfall. November, December, and January

2011 exhibited colder pond temperatures (~24ºC), while air temperature slowly

dropped from 28ºC in November to 26ºC in January, with rain falling in the

December sampling.

4.5 Discussion

Environmental Time Series: He'eia Fishpond temperature averages were

similar to Kane'ohe Bay climate data. He'eia Fishpond temperatures had a larger

range (14.39ºC – 30.00ºC)(Table 4.1) of temperatures than in the published literature

(20º - 28ºC) (Jokiel 2011), but air temperature averages were in agreement (both

averaged ~24ºC). The weakening trade winds associated with El Niño cycles was not

well represented in the overall El Niño table (Table 4.2), since wind velocity was

actually highest during El Nino, yet the lack of a consistent trade wind was more

apparent in the May 2008-2010 analysis (Table 4.3). The 30-50º difference in wind

compass direction coupled with the large standard deviation associated with the El

Niño wind direction average (109.97º) helps confirm that trade winds were sporadic

during the month of May 2009, a result that would agree with ENSO theory (Jokiel

2011).

The May 2009 study strongly suggests that pond temperature was the cause of

the fish kills during the month. Temperature *averaged* nearly 30ºC, very unusual to

He'eia Fishpond, for the entire month of May. The lack of wind speed strength could

have led to less wind-driven mixing and circulation in the pond, allowing waters to

become stagnant and hypoxic.

Apart from the May 2009 study, the climate time series exhibited very typical seasonal results for Kane'ohe Bay. Winter months were colder, summer months were warmer, and the fall and spring months fell somewhere in the middle (Table 4.1). The difference in wind direction for the winter months suggests that more sporadic atmospheric effects are occurring during this season, which would agree with past observations that Oahu experiences more storms in the winter. He'eia Fishpond in-situ temperature sensors are thus capable of recording the sensitive temperature changes between seasons.

La Niña exhibited the warmest temperatures in comparison to the other two climate events (El Niño and Background) (Table 4.2). With the lack of trade winds, El Niño was hypothesized to experience the warmest weather, yet was placed in between La Niña and Background conditions. While El Niño did experience less rainfall than in Normal conditions (0.03 inches per hour vs. 0.04 inches per hour, respectively), La Niña had the lowest recorded rainfall per hour at 0.02 inches, an unexpected result.

Contour Map: The contour maps revealed a very typical picture of Oahu climate. Temperatures are colder in the winter months, and tend to heat up as the year turns to summer. El Niño brings an assortment of climate anomalies to the Hawaiian Islands, and while not completely obvious, the sporadic month-to-month differences in contour maps and air temperature from 2009 into 2010 might be attributed to El Niño effects. Regardless, the complete picture of contour maps allows confidence in using monthly sampling data as reliable climate indicators for the given period, as long as rainfall, air temperature, and tide are accounted for.

Spatially, pond regions can be accounted for based on how the *mākāhā* control pond temperature. River *mākāhā* near stakes 7, 18, and 19 transport colder, riverine water bodies to the pond, resulting in the cold pool observed in Figure 4.8. The hot region of the pond (stakes 2, 3, 4, 8, 9, 10, 11, 14, 15, 16, 17) could possibly be explained by the solar radiation that affects this region with little or no exterior water bodies interacting with the warm pool. The variable temperatures at stake 1, 12, 13, and 20 could be accounted for due to the presence of the ocean *mākāhā* in the region, resulting in a largely tide-influenced region. The extremely limited water depth of that region would also help account for extreme temperature swings based on tide. Finally, the variable temperatures in the region of stake 5 and 6 are likely due to the lack of a water current influence. With river *mākāhā* and ocean *mākāhā* oriented towards the center pond, stakes 5 and 6 are cutoff from exterior water bodies, resulting in a stagnant area of He'eia Fishpond that is influenced greatly by solar radiation.

4.6 Conclusion

The monitoring of pond temperature at He'eia Fishpond from 2007 – 2011 has established a seasonal climate observation system. The time-series data available from in-situ temperature deployments compared favorably to temperature ranges predicted by Jokiel (2011). The continued efforts to equip He'eia Fishpond with temperature sensors will help form conclusions on the seasonal changes that occur in Kane'ohe Bay, O'ahu. Additionally, since temperature is often a marker of water

mass type, and thus a proxy for other water column parameters, nutrient studies that focus on tidal inputs to He'eia Fishpond will benefit from a long term time-series that characterizes the temperature of the pond. While the studies concerning El Niño/Southern Oscillation climate patterns didn't produce clear results, the May 2008, 2009, and 2010 study provided concrete data that supports the theory of the temperature derived May 2009 fish kill. Workers at Paepae o He'eia will benefit from the knowledge that their fish crops suffered from heat spikes over the month of May, but the contour maps (Figures 4.7 – 4. 31) created for this thesis may suggest a region of the fishpond that is consistently cooler, and thus more resistant to the effects of an El Niño summer.

Table 4.1: Seasonal Evaluation of physical parameters of He'eia Fishpond (2007 – 2011). Air temp, rain, and wind data are from Mesowest.utah.edu (2011). Pond data are from in-situ instruments.

WINTER	AIR TEMP (Cº)	WIND SPD (mph)	WIND DIRECT (º)	RAIN (in/hr)	Pond 6 (Cº)	Pond 13 (Cº)	Pond 18 (Cº)
AVG	22.75	7.46	114.38	0.03	23.68	24.48	23.80
STDEV	1.91	4.97	88.15	0.10	2.51	2.29	2.56
MIN	14.39	0.00	0.00	0.00	17.81	17.76	17.85
MAX	29.39	34.50	360.00	1.71	29.52	29.93	28.50
DIFF	15.00	34.50	360.00	1.71	11.71	12.17	10.65

SPRING	AIR TEMP (Cº)	WIND SPD (mph)	WIND DIRECT (º)	RAIN (in/hr)	Pond 6 (Cº)	Pond 13 (Cº)	Pond 18 (Cº)
AVG	23.62	8.45	86.28	0.03	26.27	26.10	26.35
STDEV	1.89	4.10	62.88	0.11	2.98	3.06	3.05
MIN	15.61	0.00	10.00	0.00	17.95	18.08	18.09
MAX	30.00	26.50	360.00	1.89	38.39	36.62	37.06
DIFF	14.39	26.50	350.00	1.89	20.44	18.54	18.97

SUMMER	AIR TEMP (Cº)	WIND SPD (mph)	WIND DIRECT (º)	RAIN (in/hr)	Pond 6 (Cº)	Pond 13 (Cº)	Pond 18 (Cº)
AVG	25.75	8.47	72.07	0.01	27.94	27.38	27.77
STDEV	1.39	3.13	29.29	0.04	1.93	1.89	1.80
MIN	21.00	0.00	7.00	0.00	23.81	23.22	23.48
MAX	29.39	21.90	360.00	0.45	37.65	35.08	37.03
DIFF	8.39	21.90	353.00	0.45	13.83	11.86	13.55

FALL	AIR TEMP (Cº)	WIND SPD (mph)	WIND DIRECT (º)	RAIN (in/hr)	Pond 6 (Cº)	Pond 13 (Cº)	Pond 18 (Cº)
AVG	24.99	7.49	87.94	0.05	25.77	26.40	26.92
STDEV	1.79	4.14	59.10	0.14	2.27	2.25	2.21
MIN	16.72	0.00	10.00	0.00	20.29	20.95	21.16
MAX	30.00	32.20	360.00	1.40	30.91	33.22	32.64
DIFF	13.28	32.20	350.00	1.40	10.62	12.28	11.48

ALL	AIR TEMP (Cº)	WIND SPD (mph)	WIND DIRECT (º)	RAIN (in/hr)	Pond 6 (Cº)	Pond 13 (Cº)	Pond 18 (Cº)
AVG	24.32	7.97	88.71	0.03	26.75	26.47	26.88
STDEV	2.10	4.14	63.27	0.11	2.78	2.60	2.62
MIN	14.39	0.00	0.00	0.00	17.81	17.76	17.85
MAX	30.00	34.50	360.00	1.89	38.39	36.62	37.06
DIFF	15.61	34.50	360.00	1.89	20.58	18.87	19.22

Table 4.2: Evaluation of He'eia Fishpond in-situ temperature data and Kane'ohe Bay oceanographic (air temperature, rainfall, wind speed/direction) with respect to ENSO conditions (La Niña, El Niño, Normal). Data covers March 2008 – February 2011. Air temp, wind, and rain data are from Mesowest.utah.edu (2011). Pond data are from in-situ instruments.

Normal	AIR TEMP (C°)	WIND SPD (MPH)	WIND DIRECT (°)	RAIN (in/hr)	Pond 6 (C°)	Pond 13 (C°)	Pond 18 (C°)
AVG	24.05	7.95	92.45	0.04	26.59	26.51	26.76
STDev	2.17	4.22	67.53	0.12	3.42	3.21	3.07
MIN	15.61	0.00	7.00	0.00	17.81	17.76	17.85
MAX	29.39	32.20	360.00	1.40	38.39	36.62	37.06
DIFF	13.78	32.20	353.00	1.40	20.58	18.87	19.22

El Niño	AIR TEMP (C°)	WIND SPD (MPH)	WIND DIRECT (°)	RAIN (in/hr)	Pond 6 (C°)	Pond 13 (C°)	Pond 18 (C°)
AVG	24.49	8.43	84.28	0.03	26.63	26.89	26.97
STDev	2.11	4.24	63.21	0.09	2.43	2.31	2.47
MIN	15.61	0.00	10.00	0.00	18.76	20.80	18.25
MAX	30.00	23.00	360.00	1.64	36.96	34.93	37.03
DIFF	14.39	23.00	350.00	1.64	18.20	14.13	18.78

La Niña	AIR TEMP (C°)	WIND SPD (MPH)	WIND DIRECT (°)	RAIN (in/hr)	Pond 6 (C°)	Pond 13 (C°)	Pond 18 (C°)
AVG	24.52	7.56	88.07	0.02	27.10	26.03	26.96
STDev	1.93	3.89	56.69	0.10	2.04	2.06	1.96
MIN	14.39	0.00	0.00	0.00	20.29	18.84	20.58
MAX	30.00	34.50	360.00	1.89	36.00	34.75	33.48
DIFF	15.61	34.50	360.00	1.89	15.72	15.90	12.90

Table 4.3: Evaluation of May He'eia Fishpond in-situ temperature data and Kane'ohe Bay oceanographic (air temp, rainfall, wind direction/magnitude, from mesowest.utah.edu (2011)) data over three years (2008, 2009, 2010). Pond data are from in-situ instruments.

May-08	AIR TEMP (C°)	WIND SPD (MPH)	WIND DIRECT (°)	RAIN (in/hr)	Pond 6 (C°)	Pond 13 (C°)	Pond 18 (C°)
AVG	24.85	7.05	91.33	0.11	27.73	27.09	27.71
STDev	1.55	3.49	56.25	0.41	2.26	2.35	2.26
MIN	20.00	0.00	10.00	0.00	23.02	22.34	22.86
MAX	30.00	17.30	360.00	1.70	35.33	32.96	33.48
DIFF	10.00	17.30	350.00	1.70	12.31	10.62	10.62

May-09	AIR TEMP (C°)	WIND SPD (MPH)	WIND DIRECT (°)	RAIN (in/hr)	Pond 6 (C°)	Pond 13 (C°)	Pond 18 (C°)
AVG	24.44	5.50	127.94	0.02	29.34	29.11	30.26
STDev	1.84	4.16	109.97	0.05	2.38	2.15	1.89
MIN	18.28	0.00	10.00	0.00	24.32	24.78	26.47
MAX	28.89	21.90	360.00	0.34	38.39	36.62	37.06
DIFF	10.61	21.90	350.00	0.34	14.07	11.84	10.60

May-10	AIR TEMP (C°)	WIND SPD (MPH)	WIND DIRECT (°)	RAIN (in/hr)	Pond 6 (C°)	Pond 13 (C°)	Pond 18 (C°)
AVG	25.00	9.78	75.66	0.01	26.87	NaN	26.34
STDev	1.28	2.90	18.96	0.01	1.78	NaN	1.64
MIN	21.11	0.00	20.00	0.00	23.00	NaN	22.69
MAX	28.28	21.90	350.00	0.08	32.65	NaN	30.78
DIFF	7.17	21.90	330.00	0.08	9.64	NaN	8.09

Figure 4.1: Map of Oahu showing the Ko'olau mountain range. He'eia Fishpond and Kane'ohe Bay border the Ko'olau range.

WARM EPISODE RELATIONSHIPS   JUNE - AUGUST
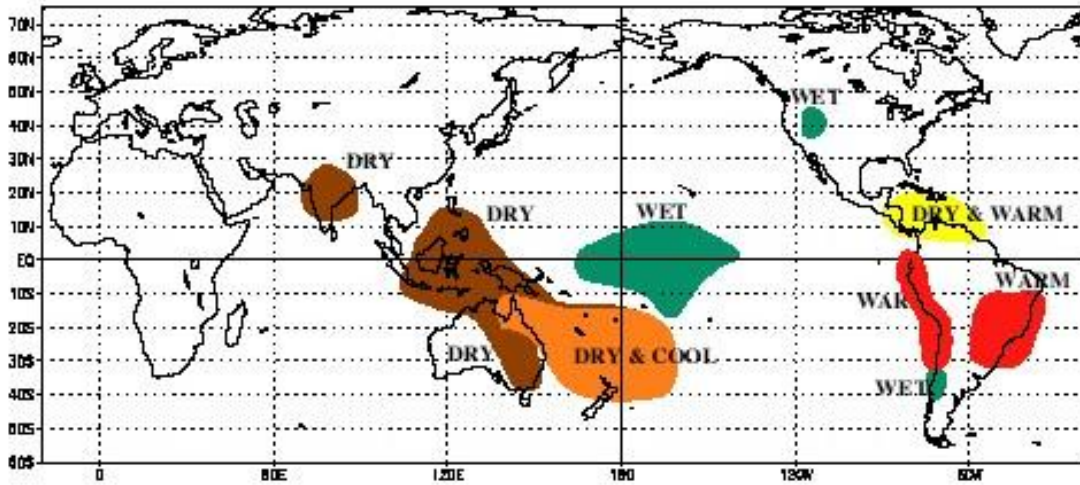
Figure 4.2: Warm episode (El Niño) effects on the climate of the world.

COLD EPISODE RELATIONSHIPS   JUNE - AUGUST
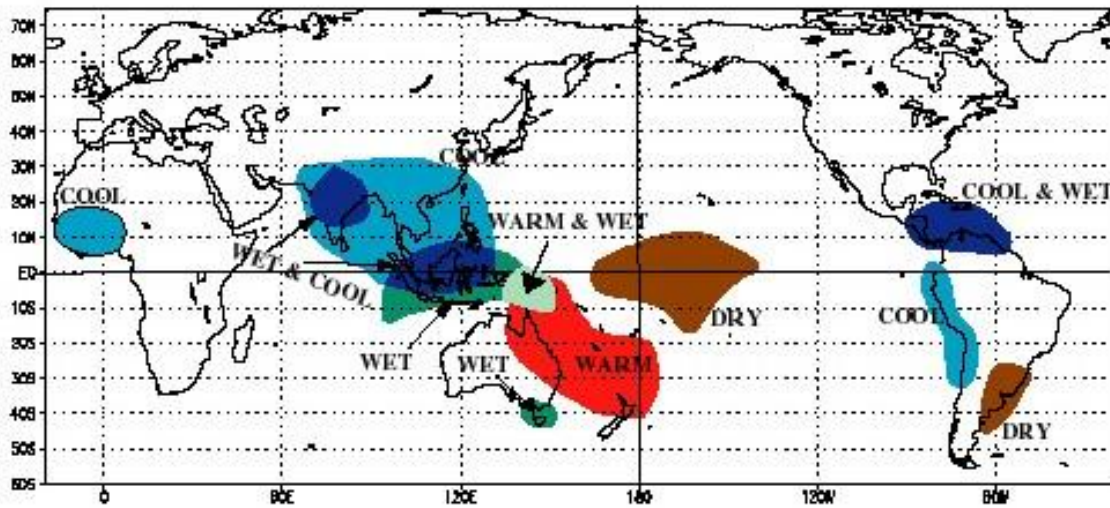
Figure 4.3: Cold episode (La Niña) effects on the climate of the world.

Figure 4.4: Location of stakes 6, 13, and 18. These three stakes were chosen to represent the pond spatially and temporally for the contour and climate analysis based on their consistent deployments and locations throughout the pond. Site names from Young (2011).
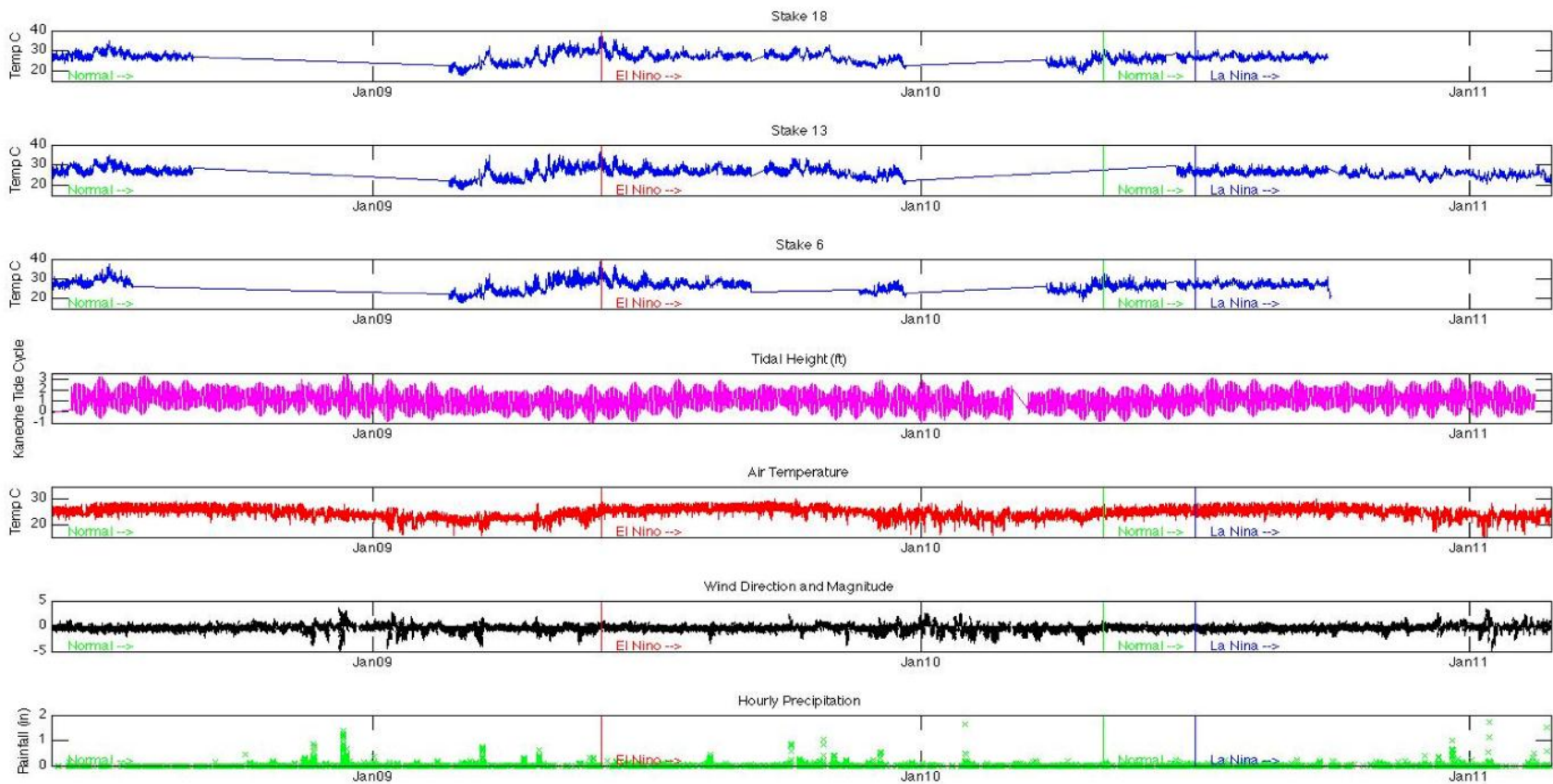
Figure 4.5: Climate time series of He'eia Fishpond and Kane'ohe Bay, Oahu. Time series starts March 5, 2008 and was completed February 22, 2011. El Niño, La Niña, and normal climate patterns are marked.
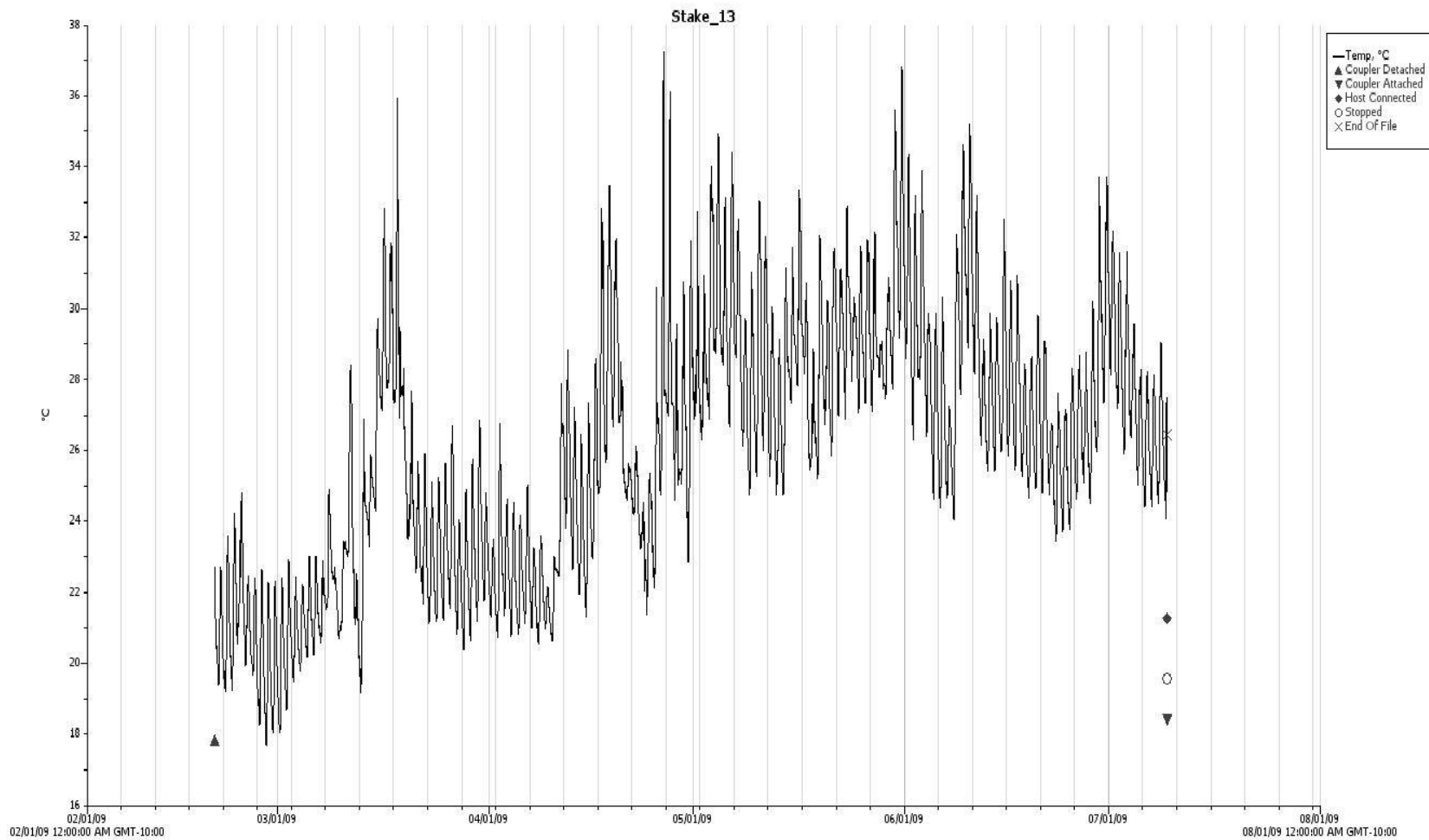
Figure 4.6: Example of TidbiT® temperature sensor time series chart. This particular chart represents May 2009, when it is hypothesized that a large fishkill occurred in He'eia Fishpond due to large spikes in pond temperature.
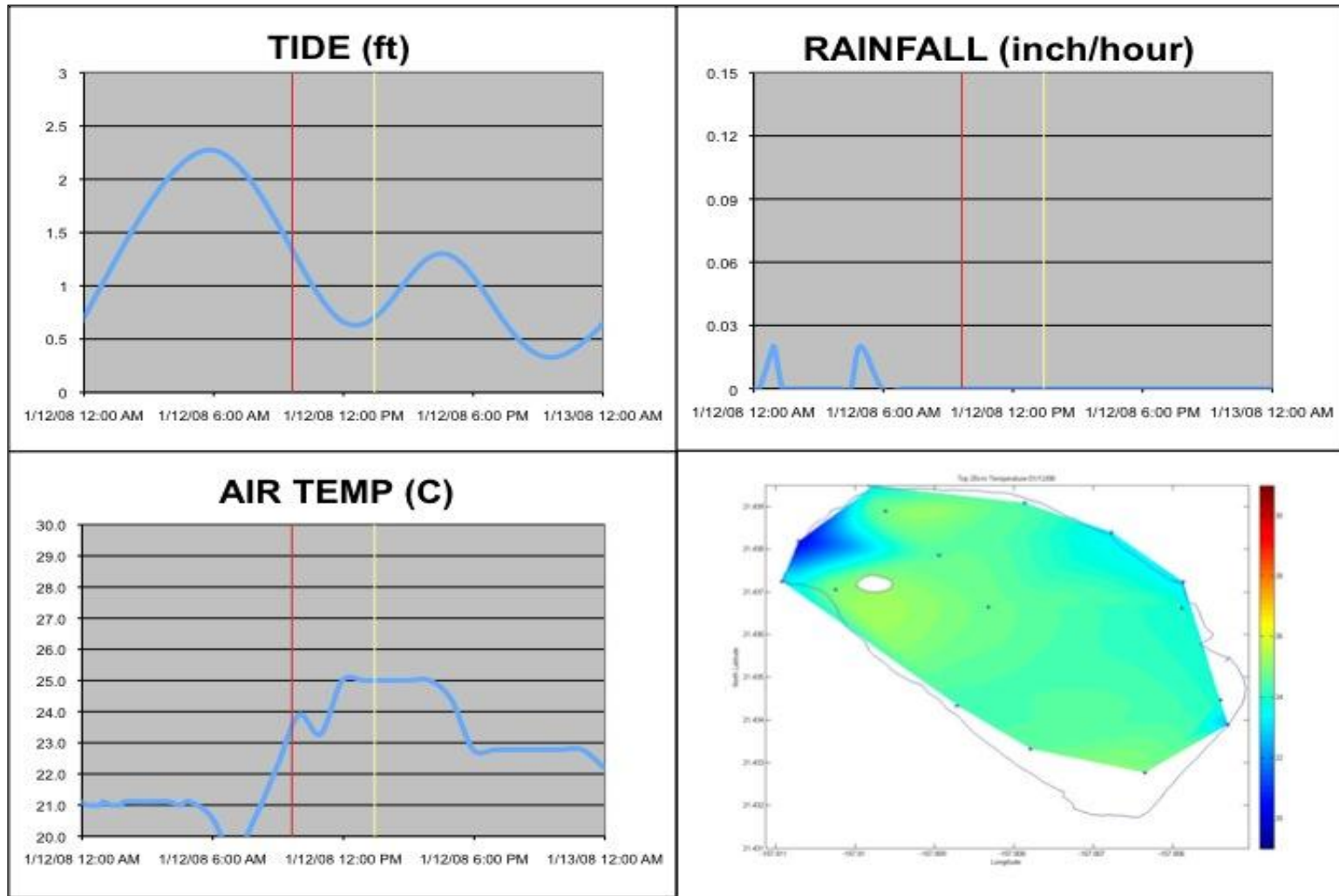
Figure 4.7: Tide, rainfall, and air temperature plots for the 1/12/2008 sampling (data from Mesowest.utah.edu), as well as the surface temperature contour plot from the YSI data. Red line indicates start of sampling, yellow line indicates end of sampling.
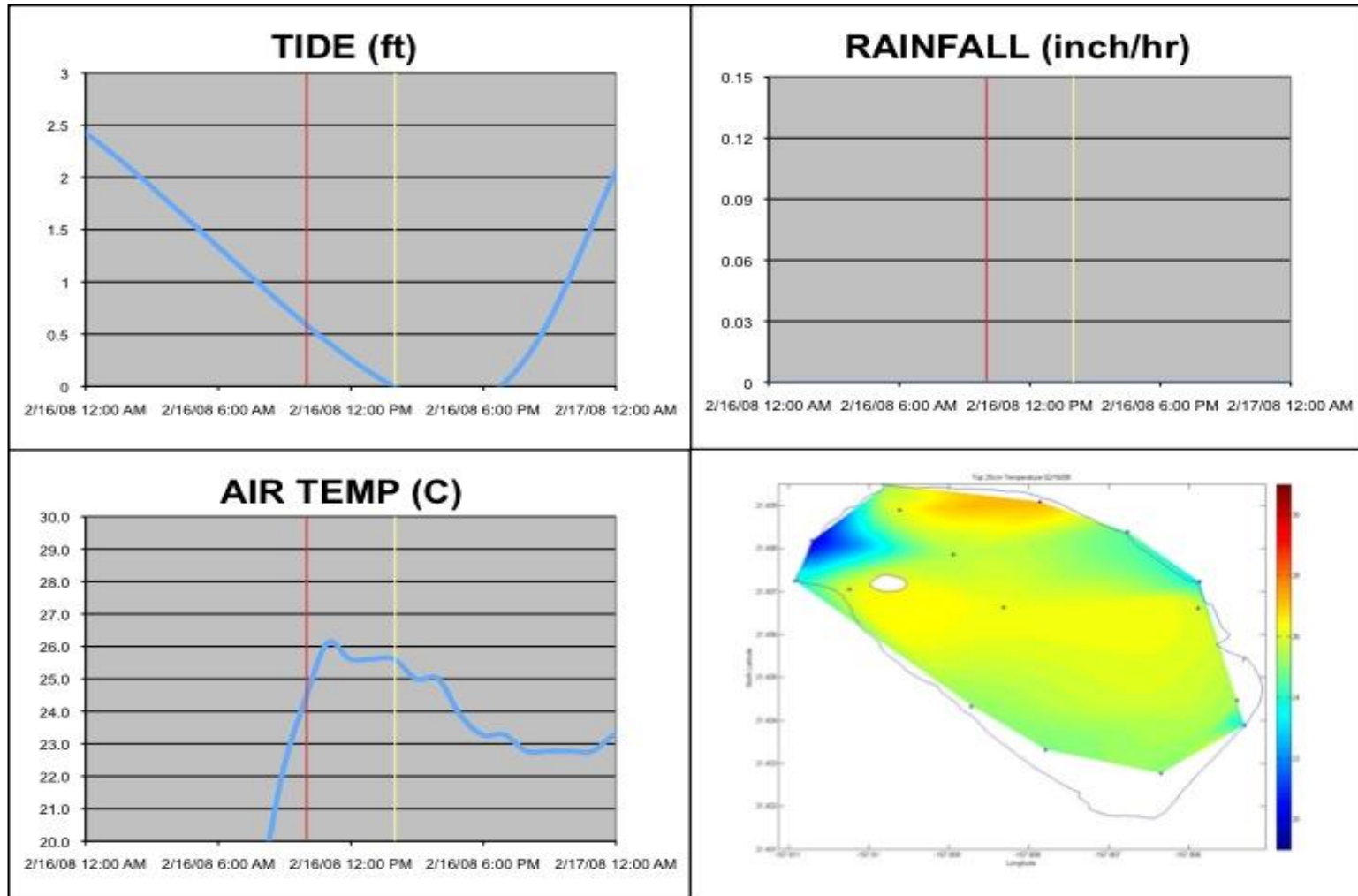
Figure 4.8: Tide, rainfall, and air temperature plots for the 2/16/2008 sampling (data from Mesowest.utah.edu), as well as the surface temperature contour plot from the YSI data. Red line indicates start of sampling, yellow line indicates end of sampling.
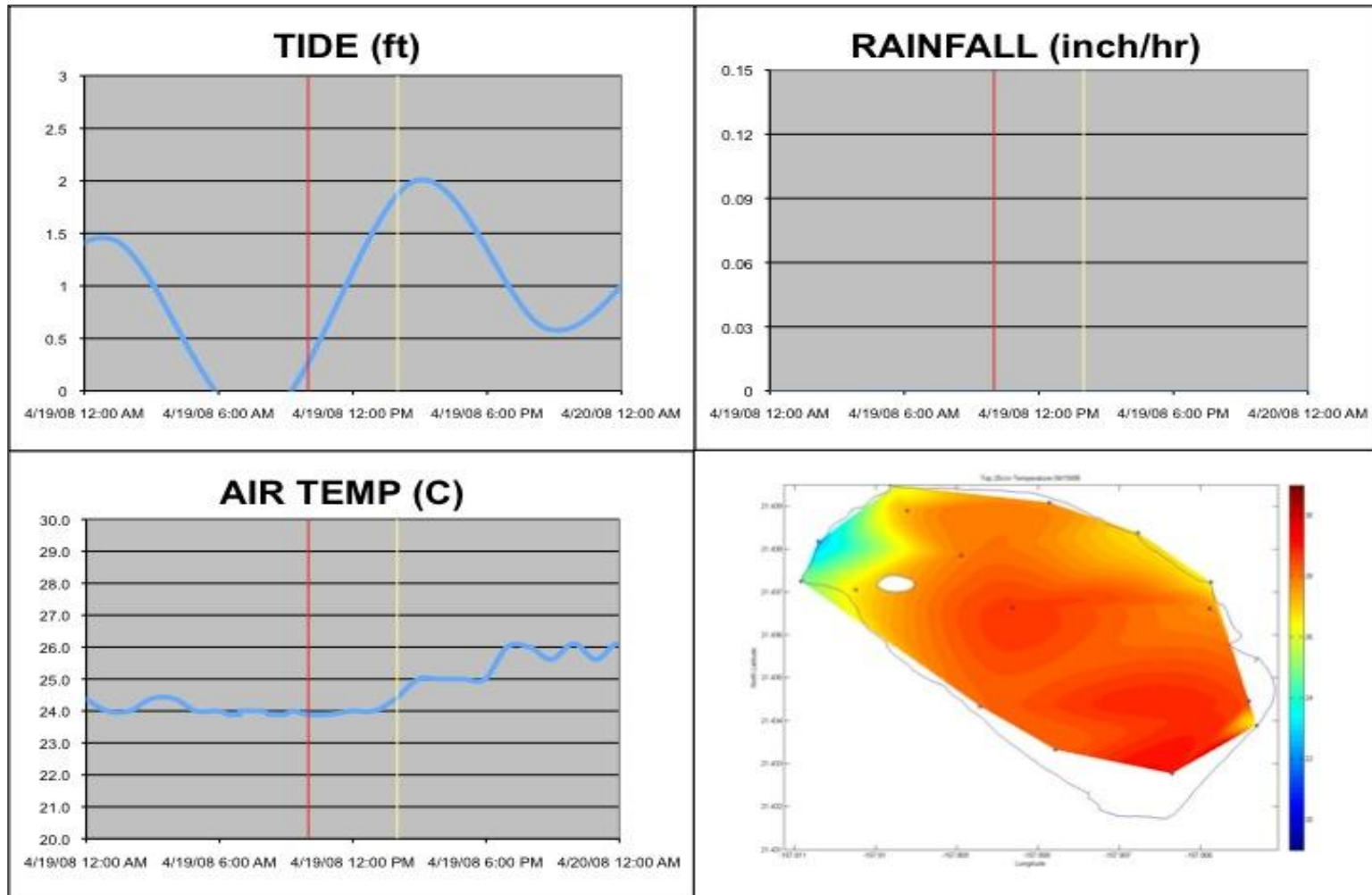
Figure 4.9: Tide, rainfall, and air temperature plots for the 4/19/2008 sampling (data from Mesowest.utah.edu), as well as the surface temperature contour plot from the YSI data. Red line indicates start of sampling, yellow line indicates end of sampling.
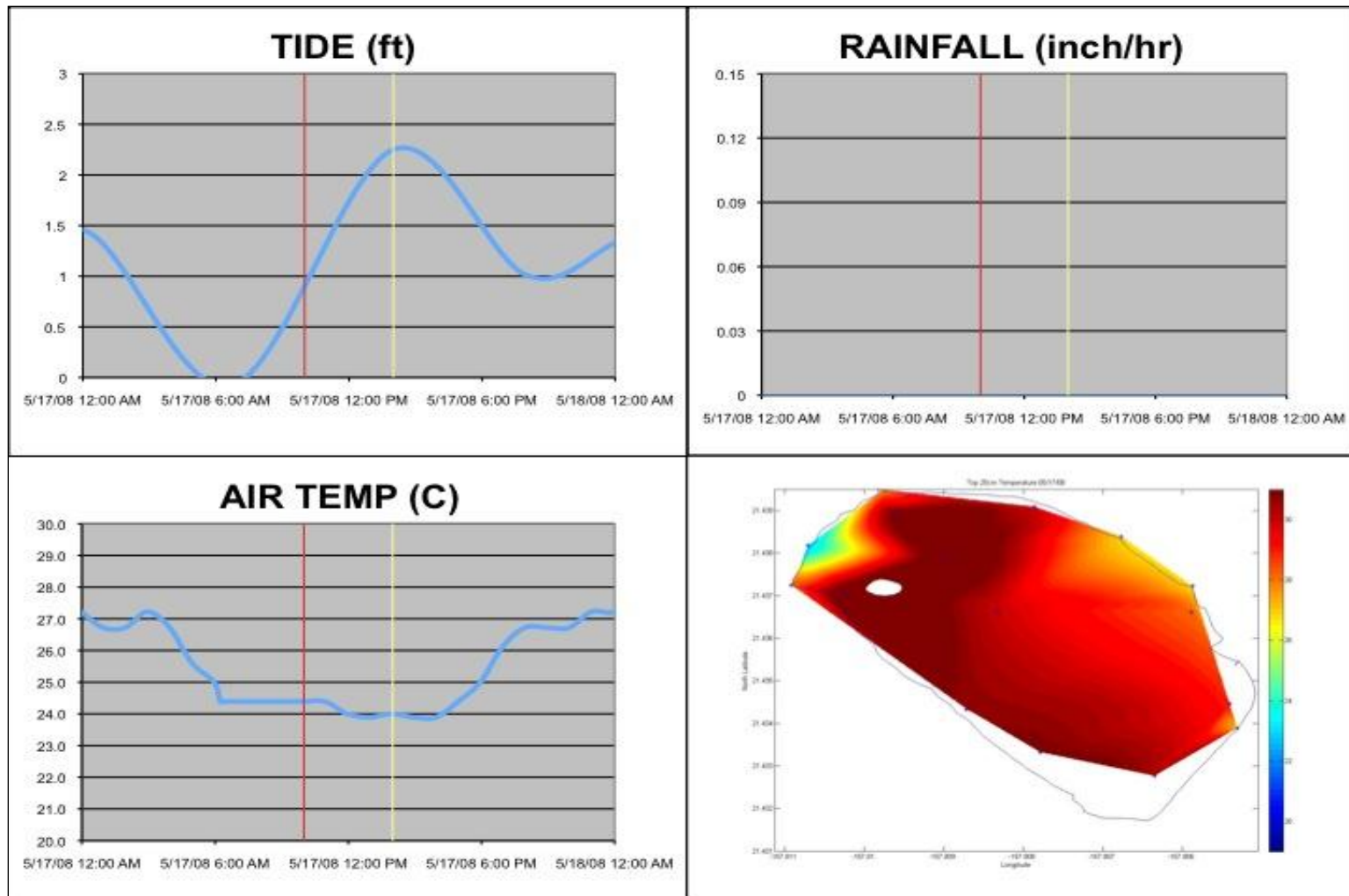
Figure 4.10: Tide, rainfall, and air temperature plots for the 5/17/2008 sampling (data from Mesowest.utah.edu), as well as the surface temperature contour plot from the YSI data. Red line indicates start of sampling, yellow line indicates end of sampling.
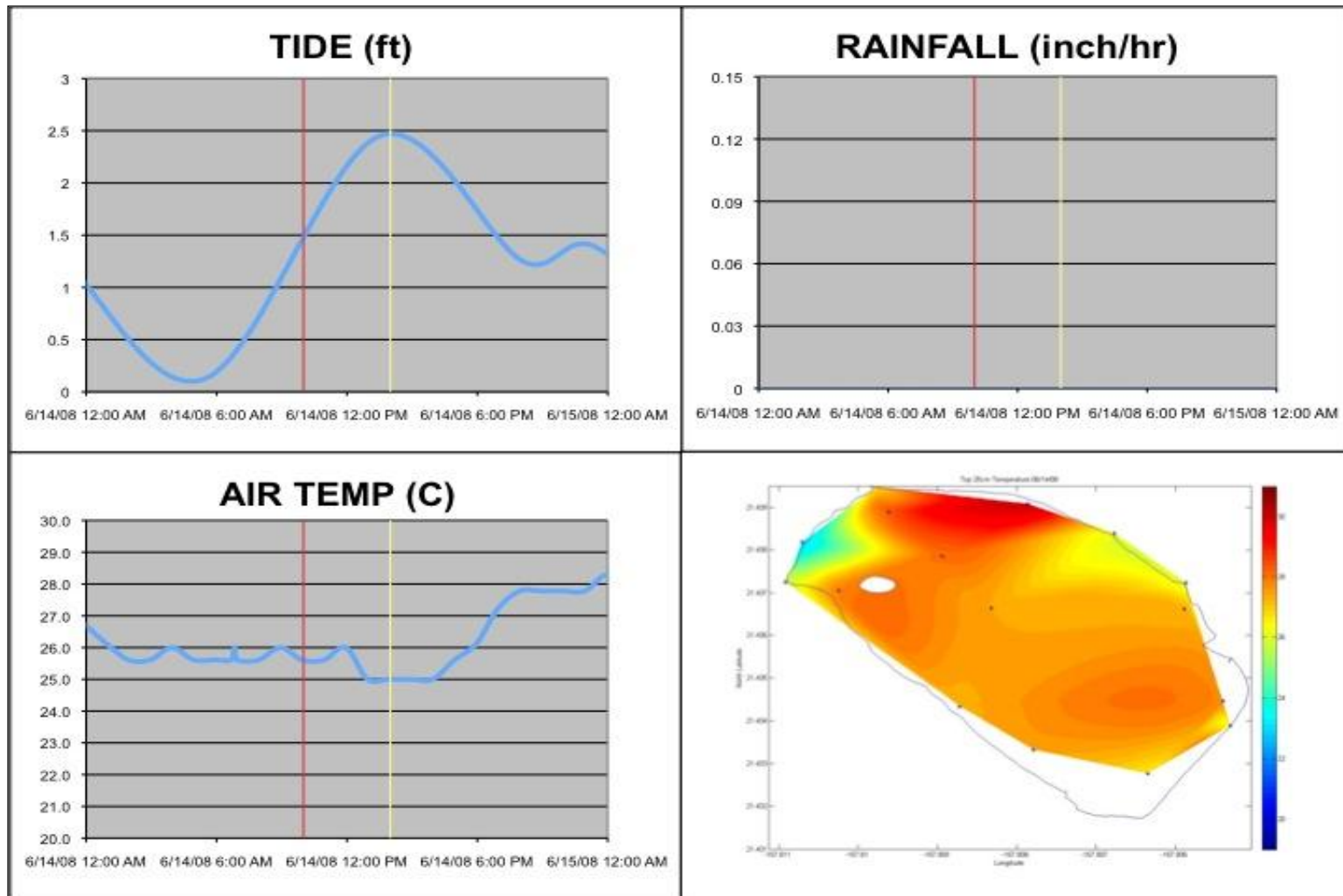
Figure 4.11: Tide, rainfall, and air temperature plots for the 6/14/2008 sampling (data from Mesowest.utah.edu), as well as the surface temperature contour plot from the YSI data. Red line indicates start of sampling, yellow line indicates end of sampling.
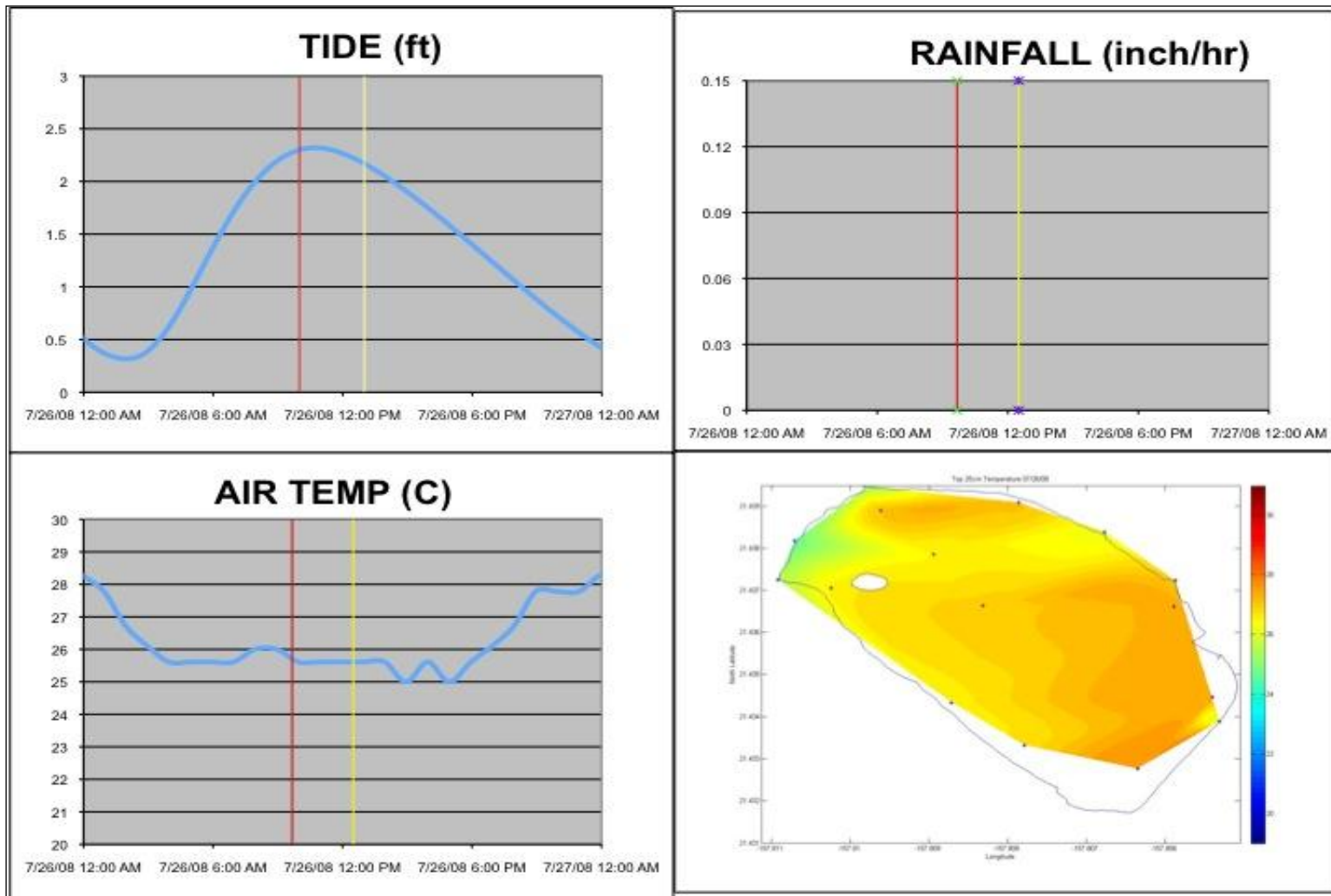
Figure 4.12: Tide, rainfall, and air temperature plots for the 7/26/2008 sampling (data from Mesowest.utah.edu), as well as the surface temperature contour plot from the YSI data. Red line indicates start of sampling, yellow line indicates end of sampling.
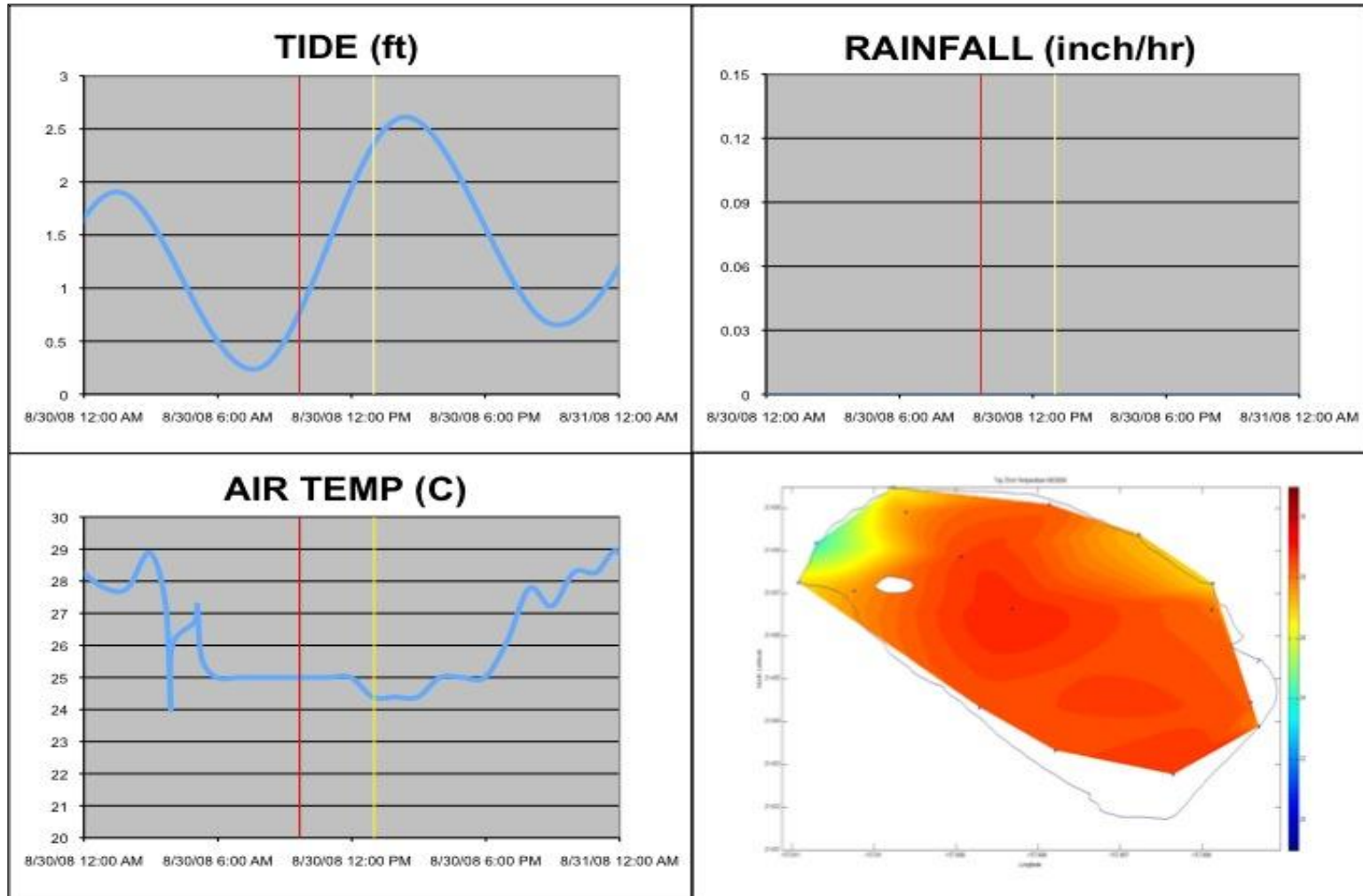
Figure 4.13 Tide, rainfall, and air temperature plots for the 8/30/2008 sampling (data from Mesowest.utah.edu), as well as the surface temperature contour plot from the YSI data. Red line indicates start of sampling, yellow line indicates end of sampling.
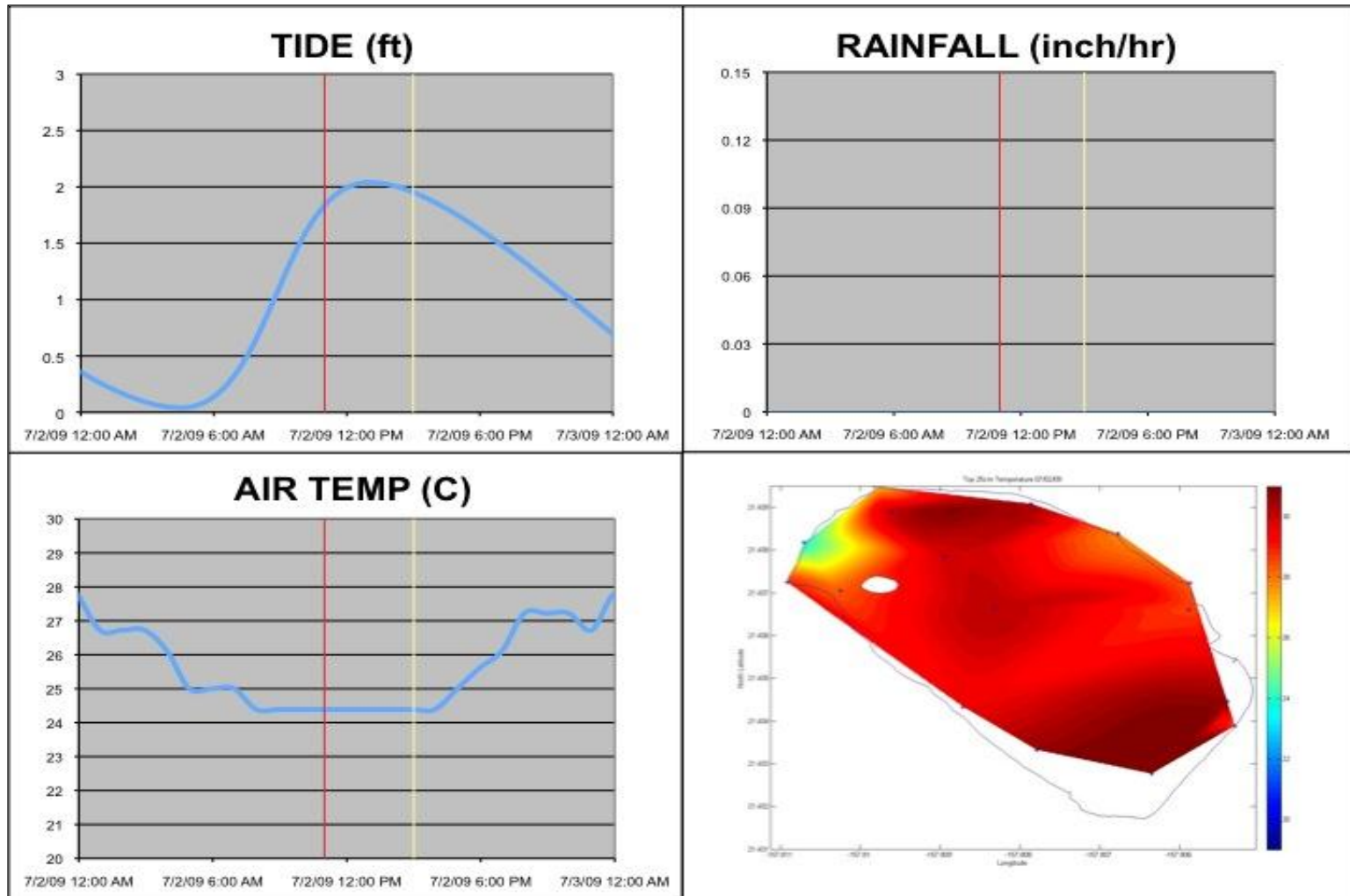
Figure 4.14: Tide, rainfall, and air temperature plots for the 7/02/2009 sampling (data from Mesowest.utah.edu), as well as the surface temperature contour plot from the YSI data. Red line indicates start of sampling, yellow line indicates end of sampling.
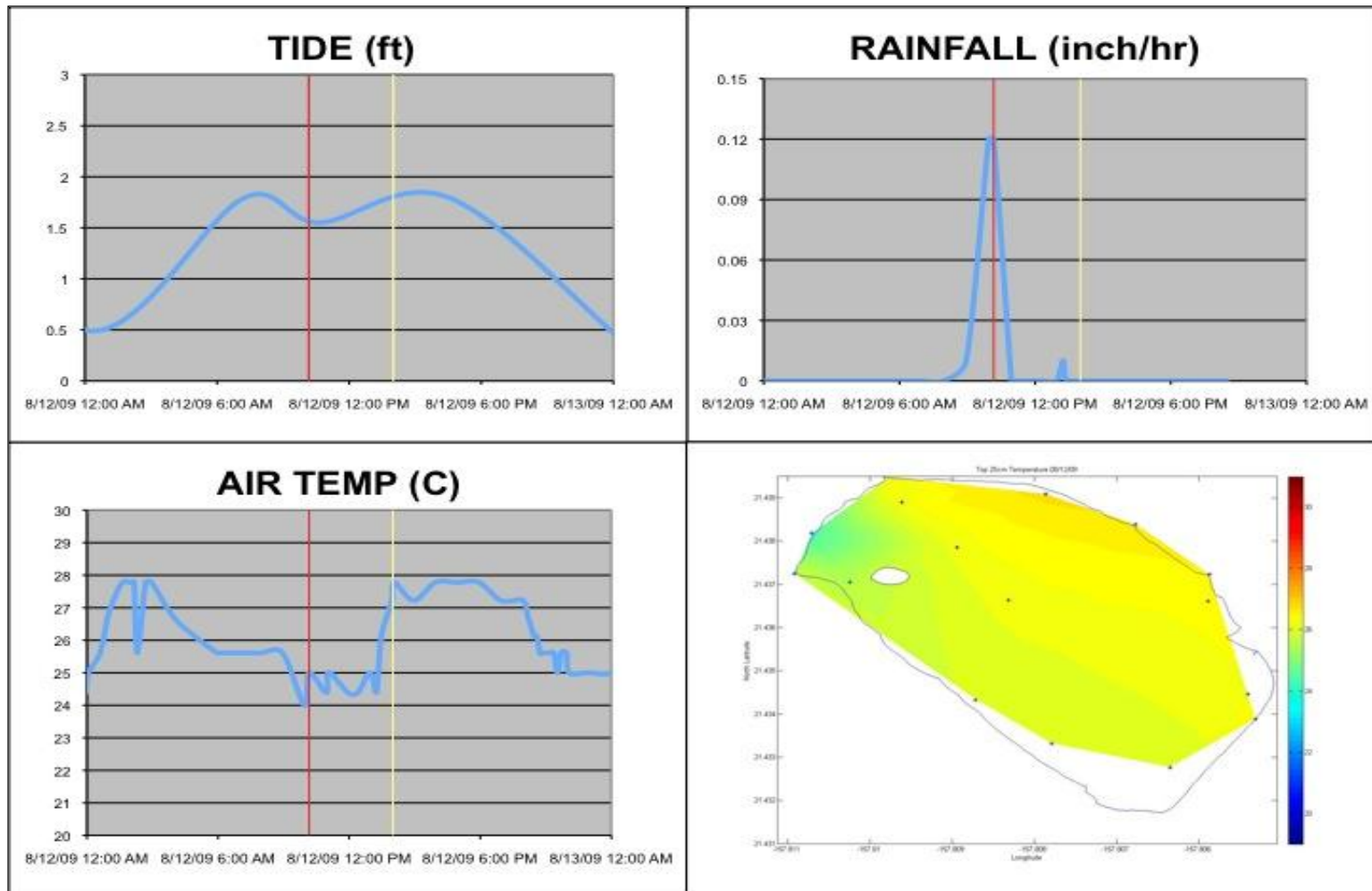
Figure 4.15: Tide, rainfall, and air temperature plots for the 8/12/2009 sampling (data from Mesowest.utah.edu), as well as the surface temperature contour plot from the YSI data. Red line indicates start of sampling, yellow line indicates end of sampling.
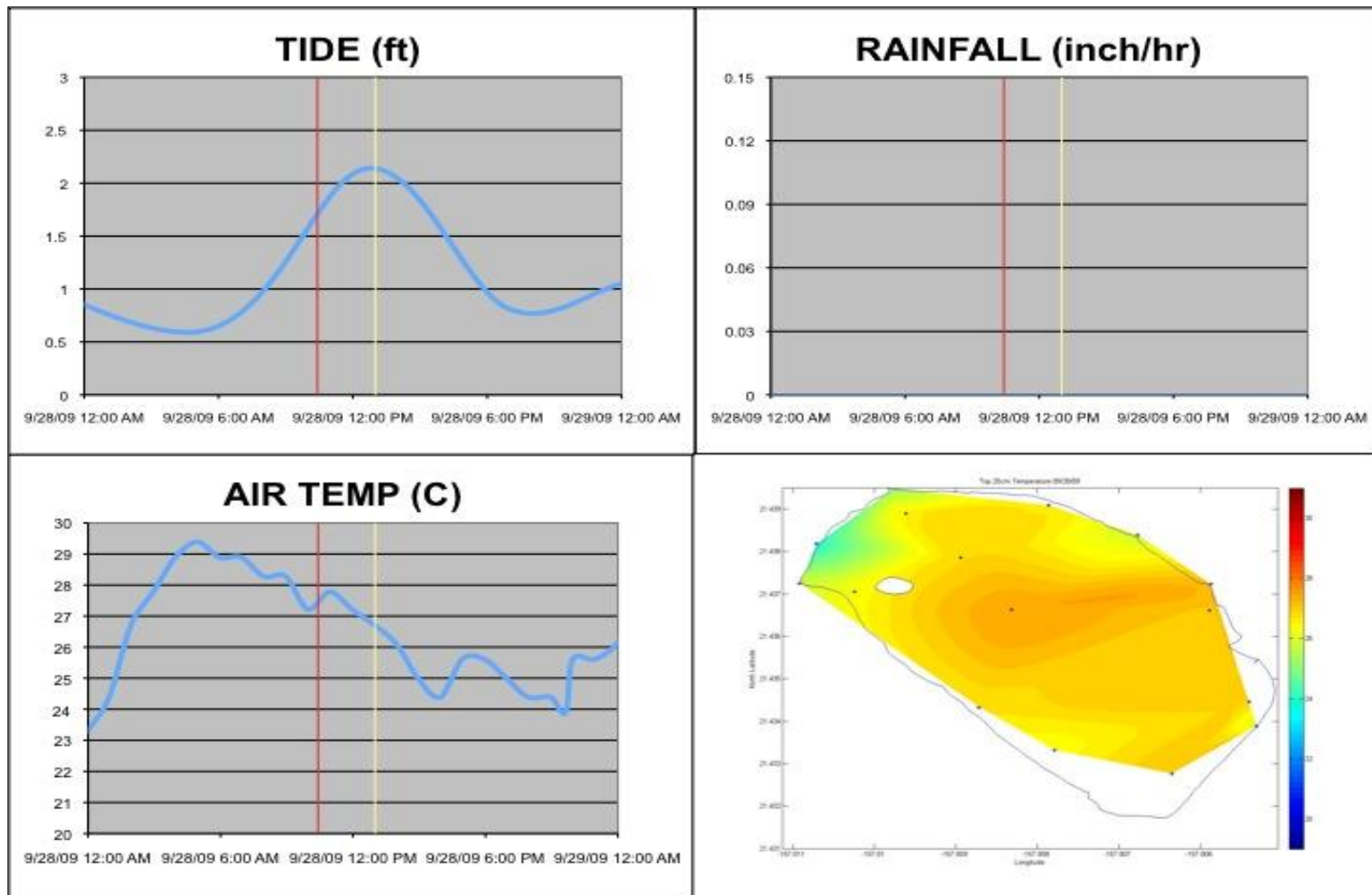
Figure 4.16: Tide, rainfall, and air temperature plots for the 9/28/2009 sampling (data from Mesowest.utah.edu), as well as the surface temperature contour plot from the YSI data. Red line indicates start of sampling, yellow line indicates end of sampling.
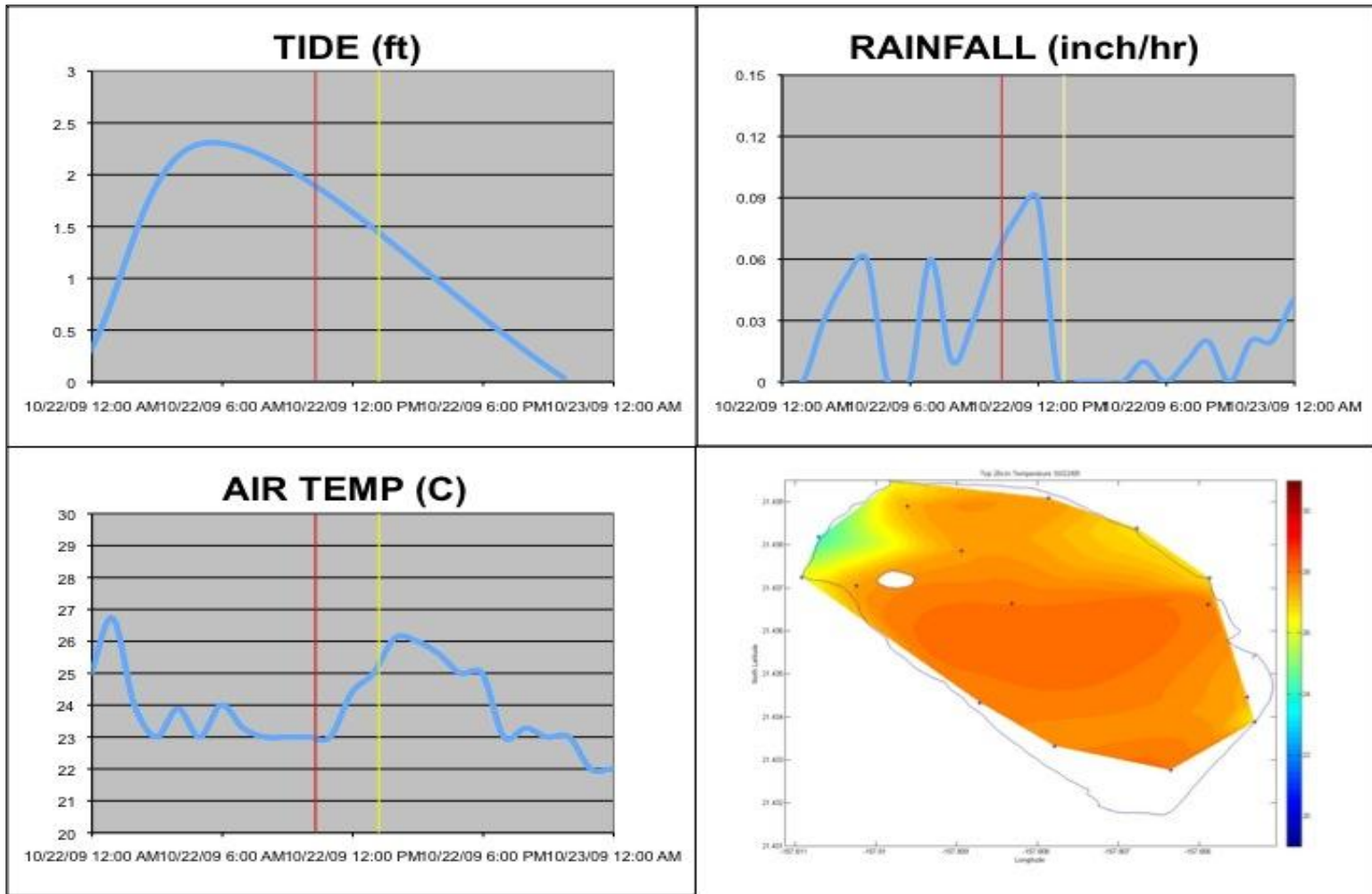
Figure 4.17: Tide, rainfall, and air temperature plots for the 10/22/2009 sampling (data from Mesowest.utah.edu), as well as the surface temperature contour plot from the YSI data. Red line indicates start of sampling, yellow line indicates end of sampling.
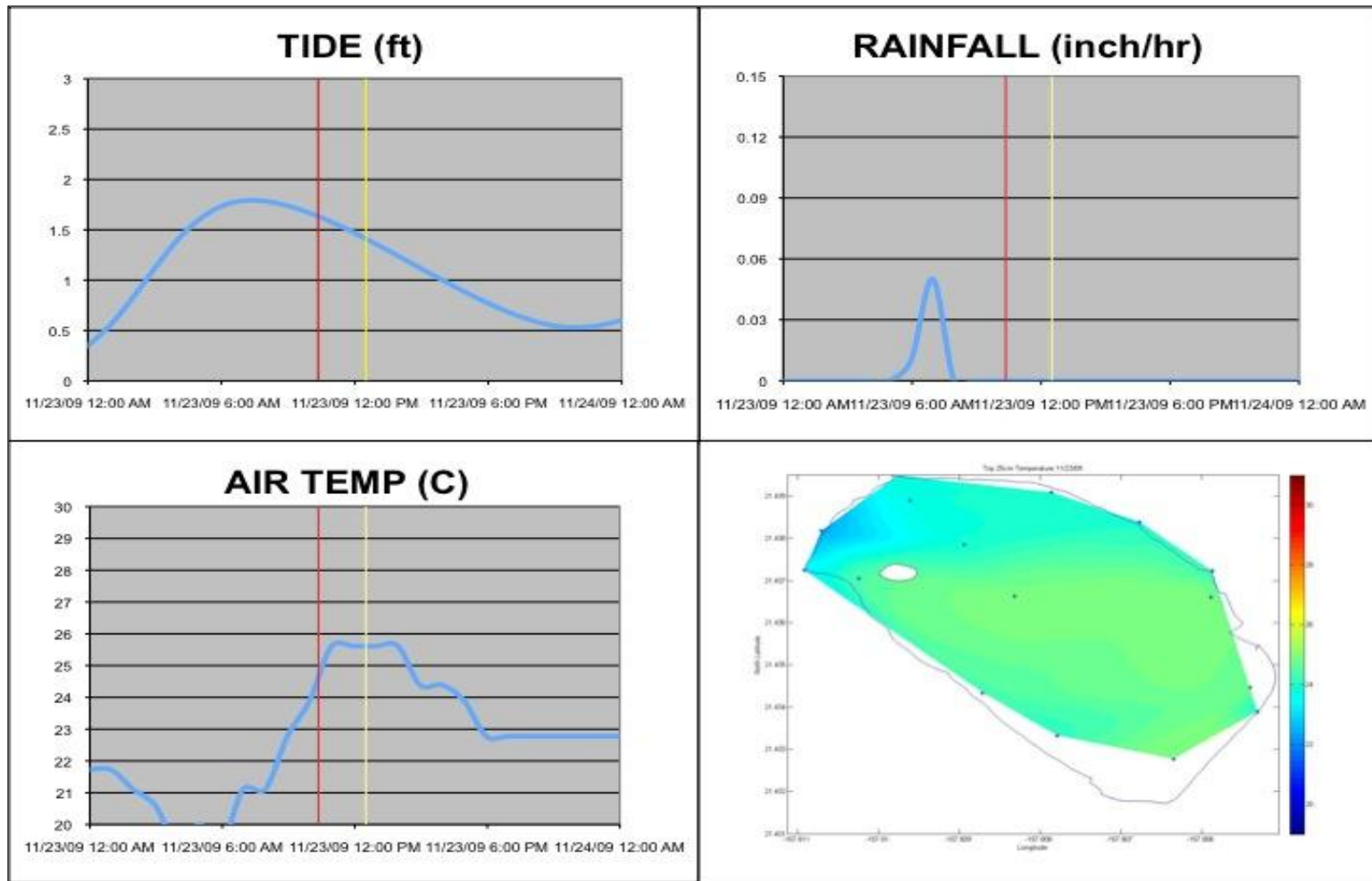
Figure 4.18: Tide, rainfall, and air temperature plots for the 11/23/2009 sampling (data from Mesowest.utah.edu), as well as the surface temperature contour plot from the YSI data. Red line indicates start of sampling, yellow line indicates end of sampling.

122
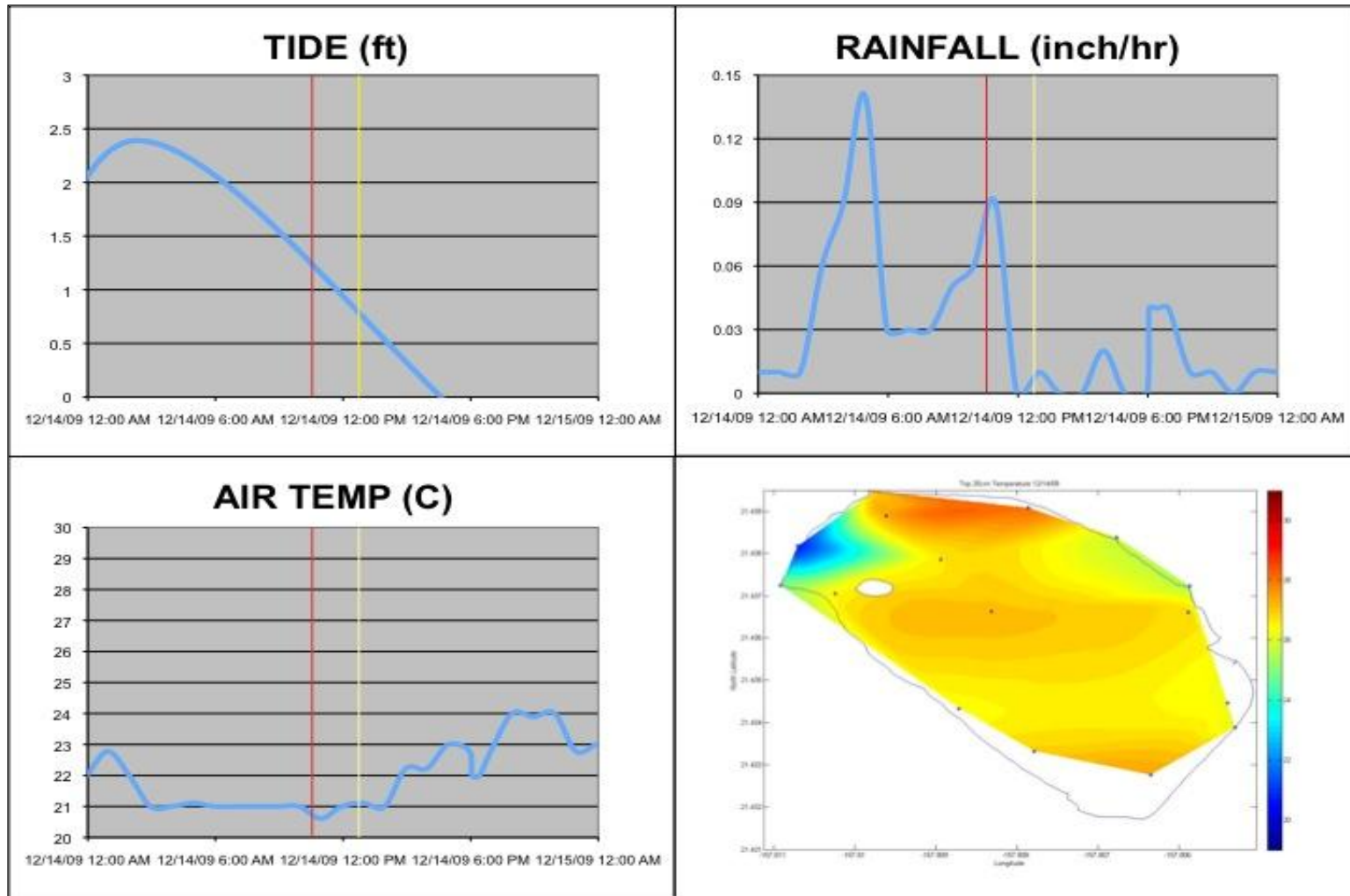
Figure 4.19: Tide, rainfall, and air temperature plots for the 12/14/2009 sampling (data from Mesowest.utah.edu), as well as the surface temperature contour plot from the YSI data. Red line indicates start of sampling, yellow line indicates end of sampling.
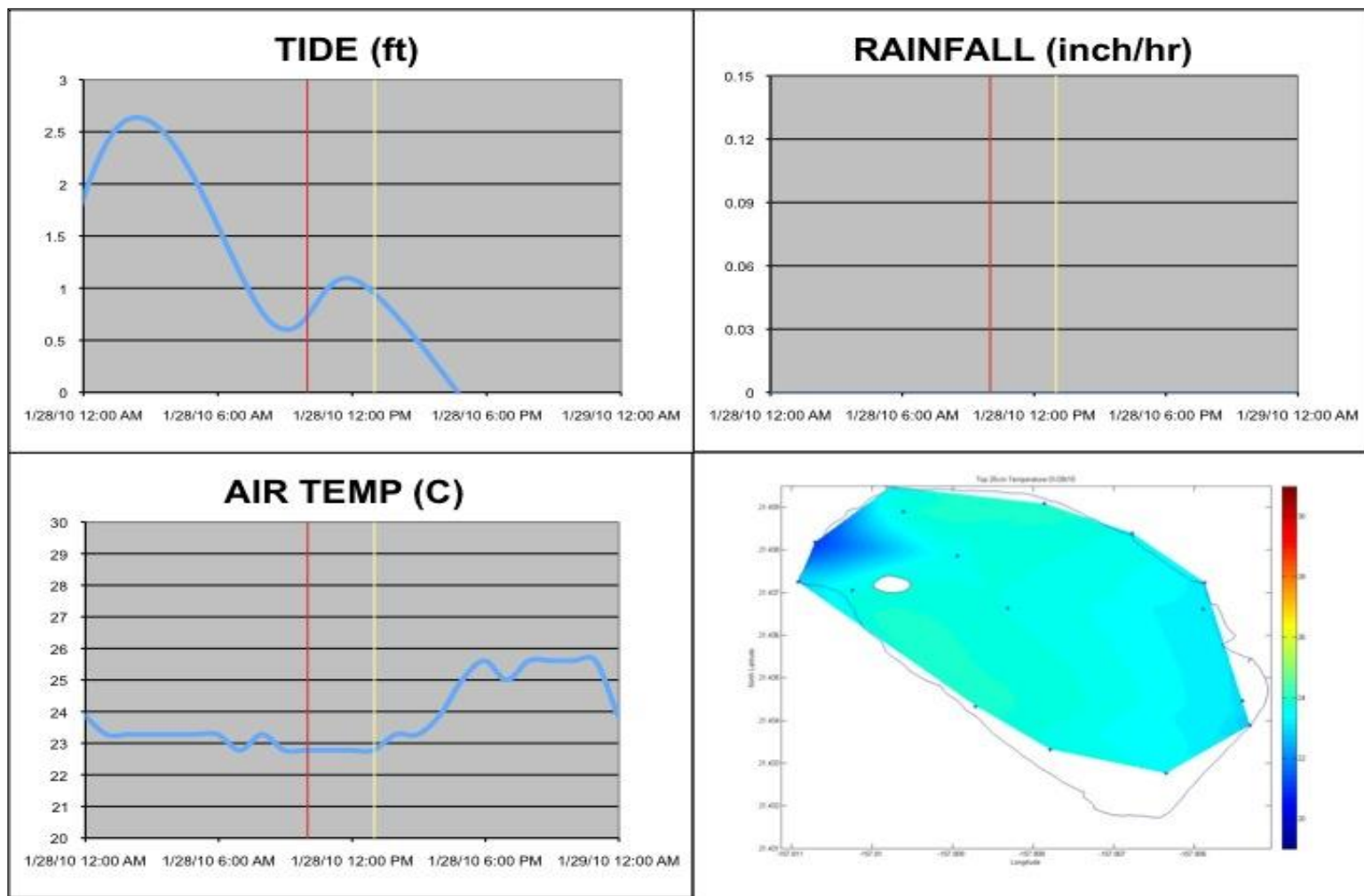
Figure 4.20: Tide, rainfall, and air temperature plots for the 1/28/2010 sampling (data from Mesowest.utah.edu), as well as the surface temperature contour plot from the YSI data. Red line indicates start of sampling, yellow line indicates end of sampling.

124
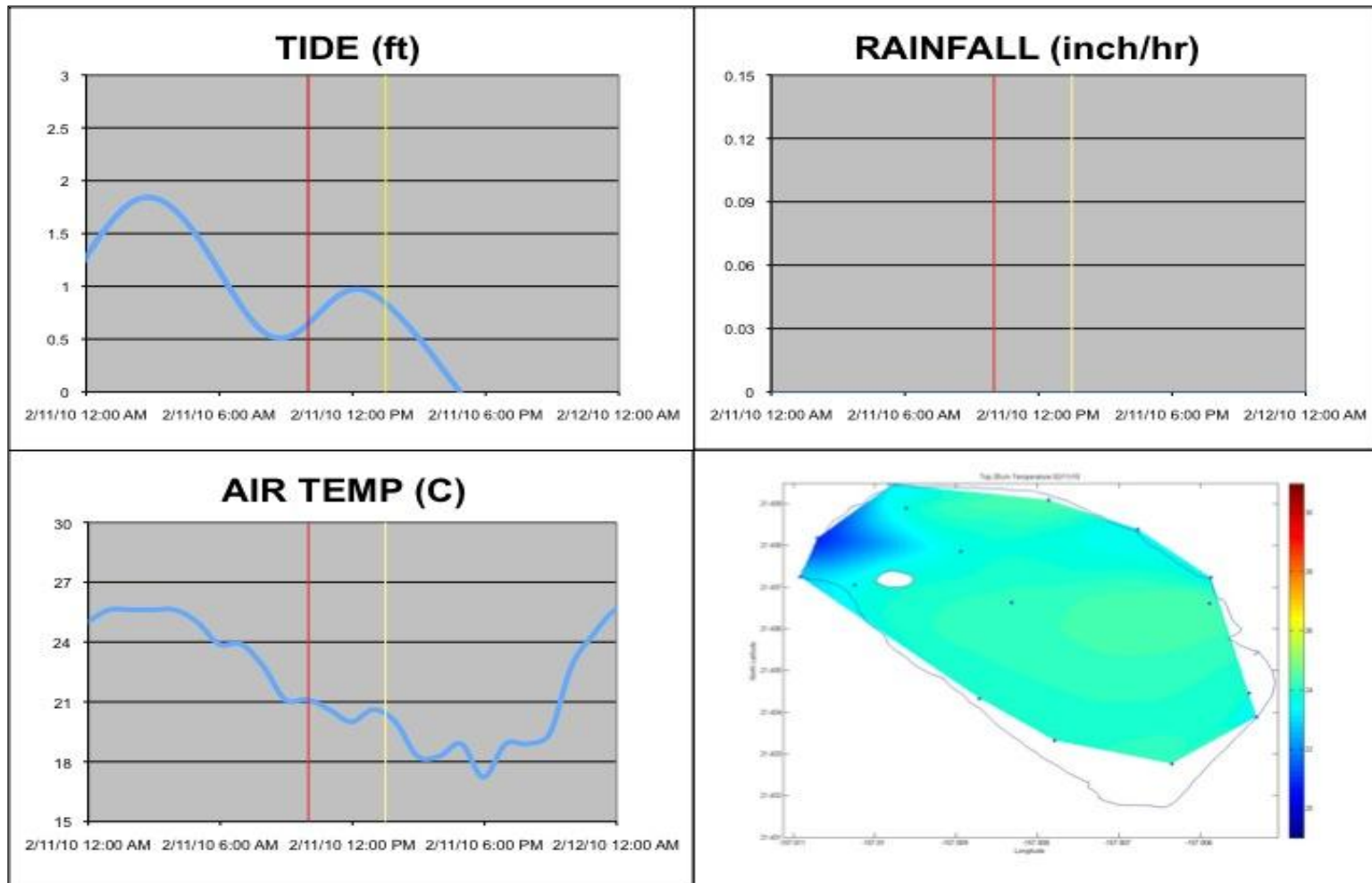
Figure 4.21: Tide, rainfall, and air temperature plots for the 2/11/2010 sampling (data from Mesowest.utah.edu), as well as the surface temperature contour plot from the YSI data. Red line indicates start of sampling, yellow line indicates end of sampling.
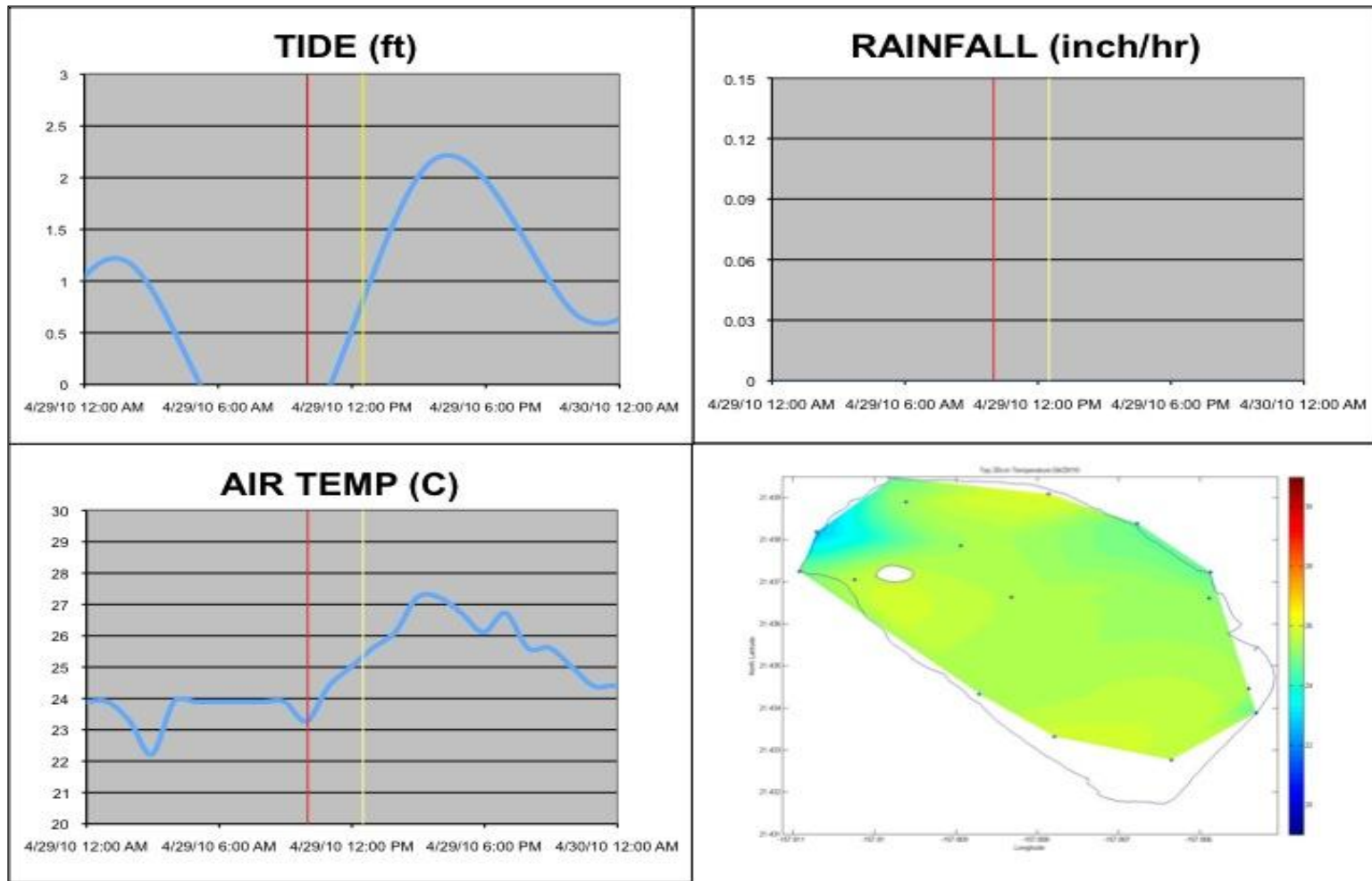
Figure 4.22: Tide, rainfall, and air temperature plots for the 4/29/2010 sampling (data from Mesowest.utah.edu), as well as the surface temperature contour plot from the YSI data. Red line indicates start of sampling, yellow line indicates end of sampling.

126
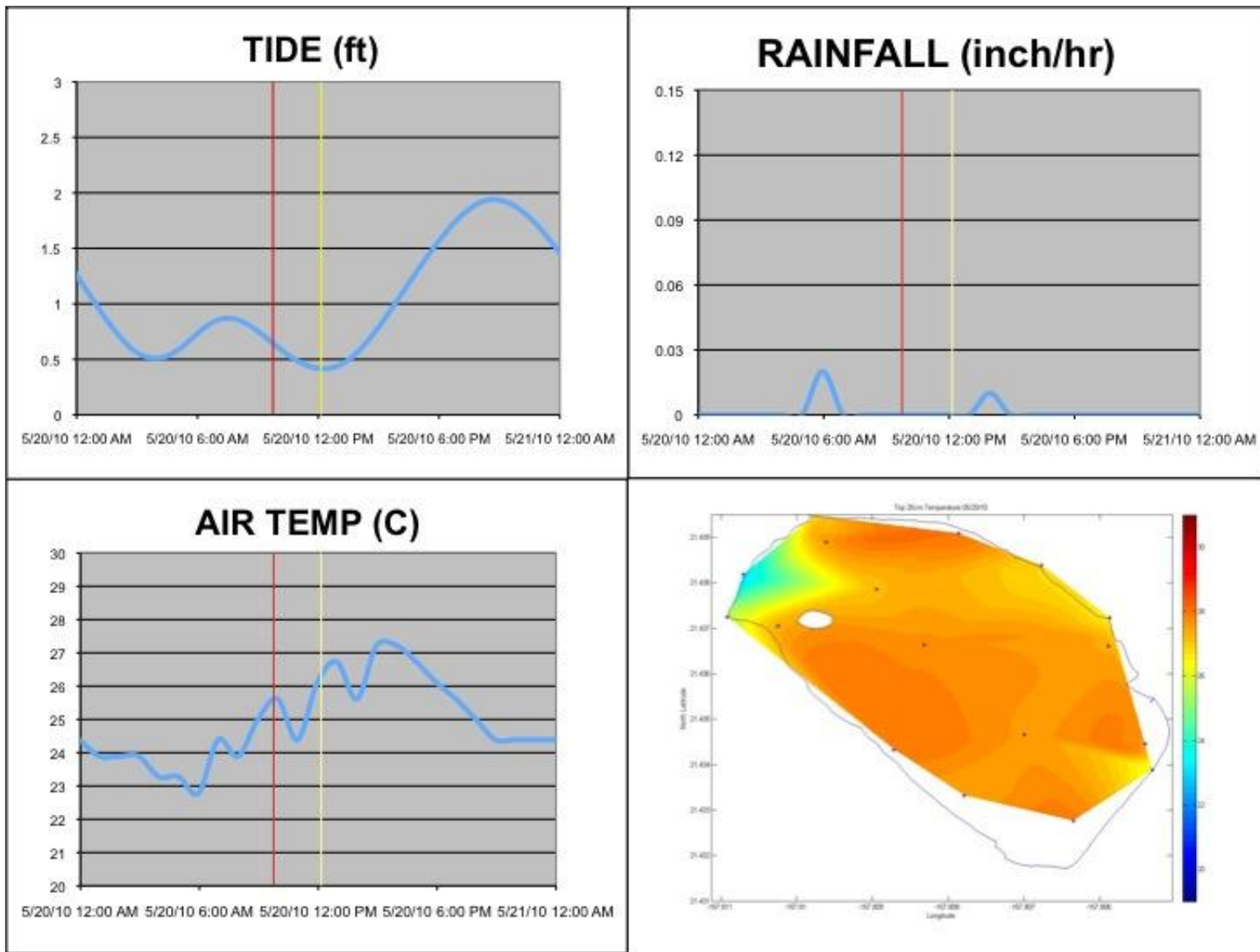
Figure 4.23: Tide, rainfall, and air temperature plots for the 5/21/2010 sampling (data from Mesowest.utah.edu), as well as the surface temperature contour plot from the YSI data. Red line indicates start of sampling, yellow line indicates end of sampling.
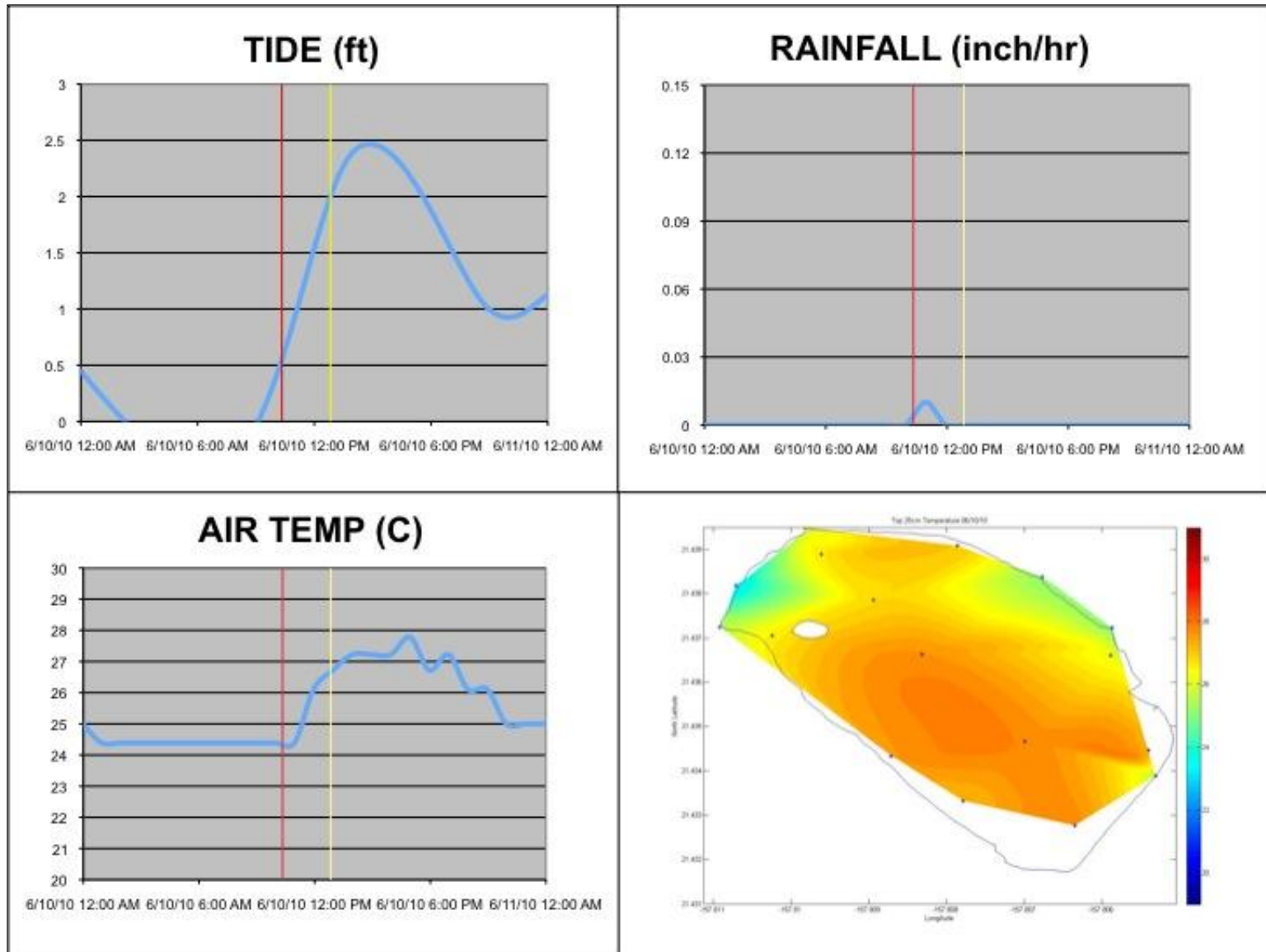
Figure 4.24: Tide, rainfall, and air temperature plots for the 6/10/2010 sampling (data from Mesowest.utah.edu), as well as the surface temperature contour plot from the YSI data. Red line indicates start of sampling, yellow line indicates end of sampling.
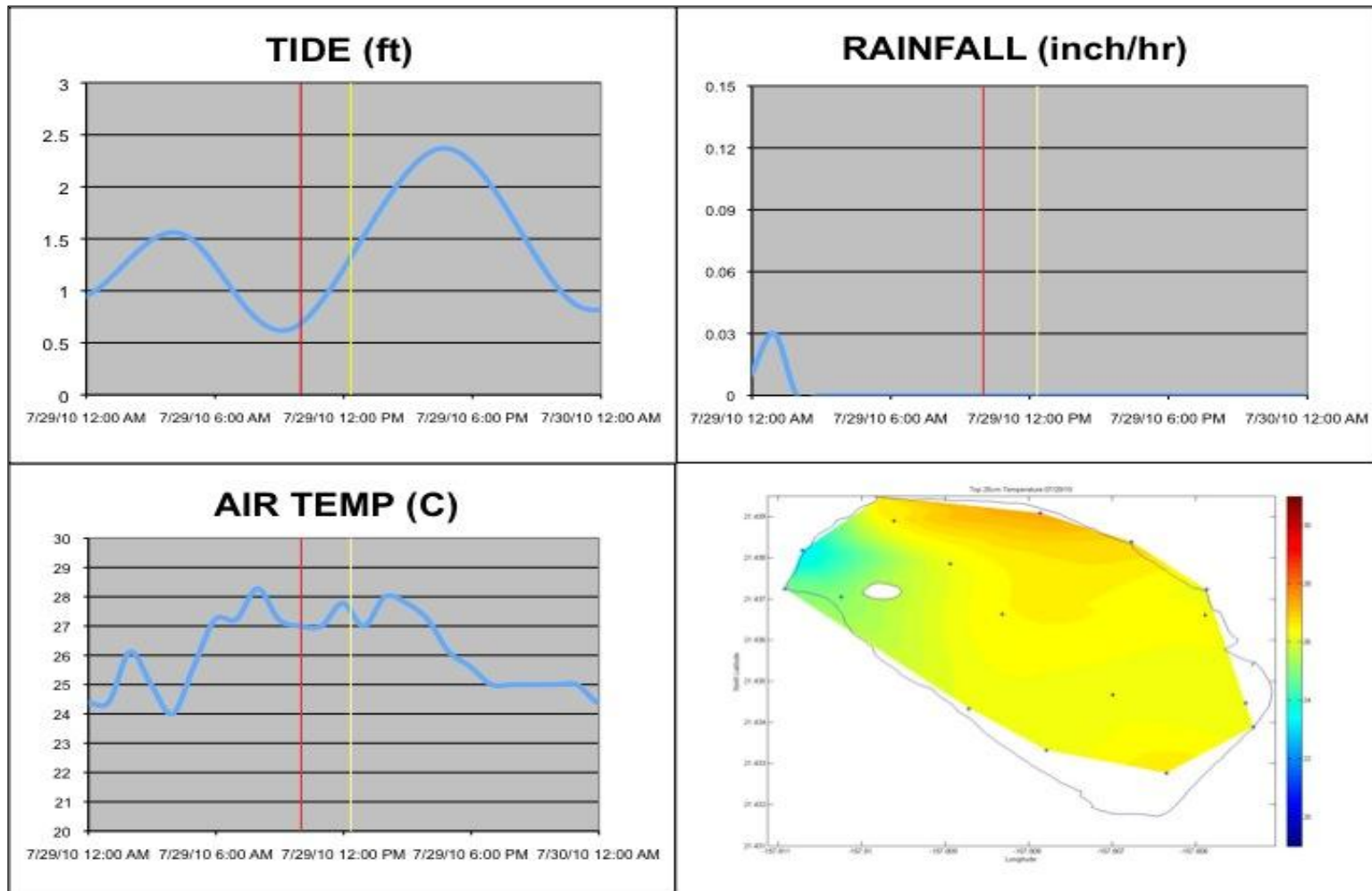
Figure 4.25: Tide, rainfall, and air temperature plots for the 7/29/2010 sampling (data from Mesowest.utah.edu), as well as the surface temperature contour plot from the YSI data. Red line indicates start of sampling, yellow line indicates end of sampling.
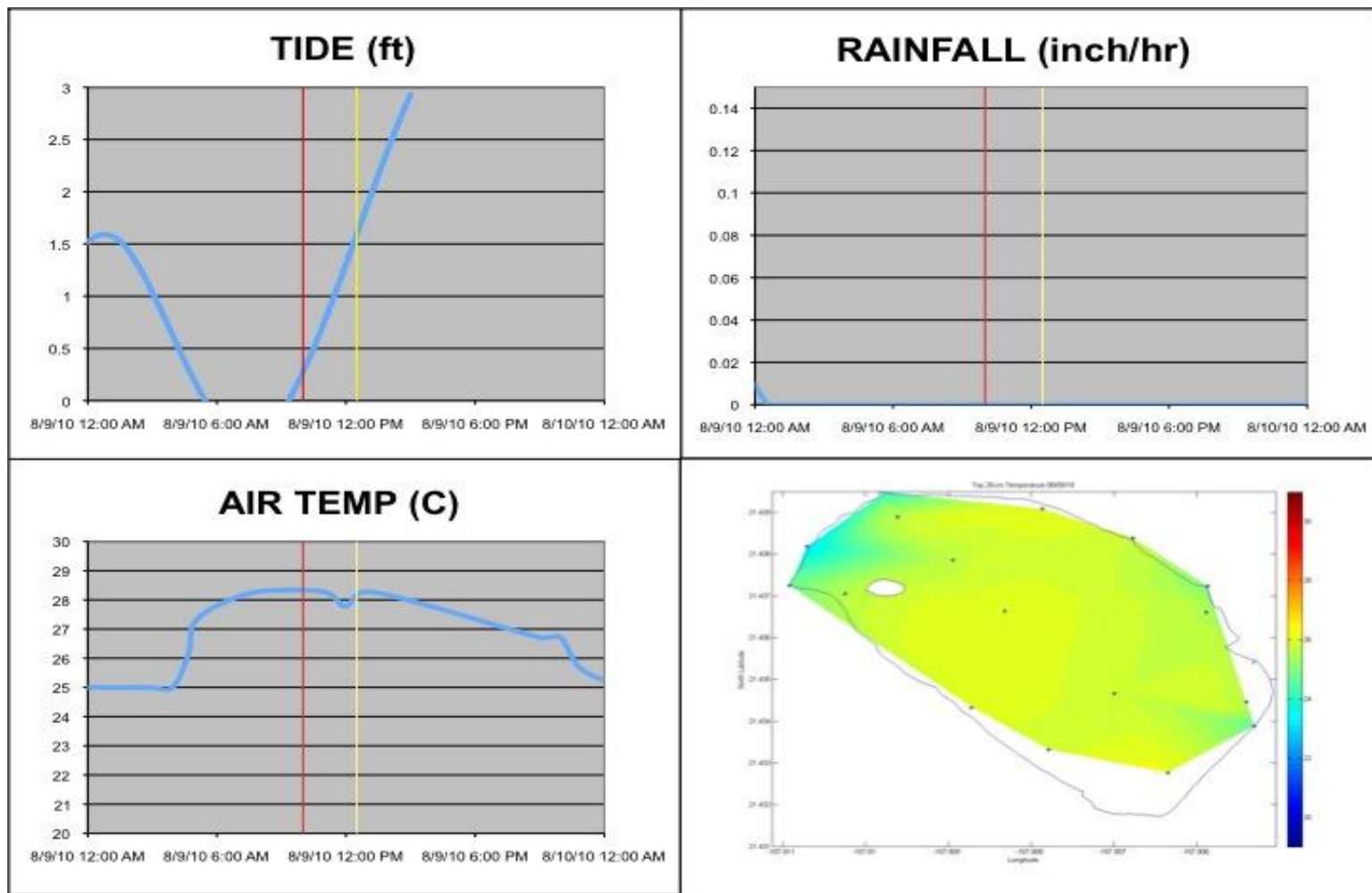
Figure 4.26: Tide, rainfall, and air temperature plots for the 8/09/2010 sampling (data from Mesowest.utah.edu), as well as the surface temperature contour plot from the YSI data. Red line indicates start of sampling, yellow line indicates end of sampling.
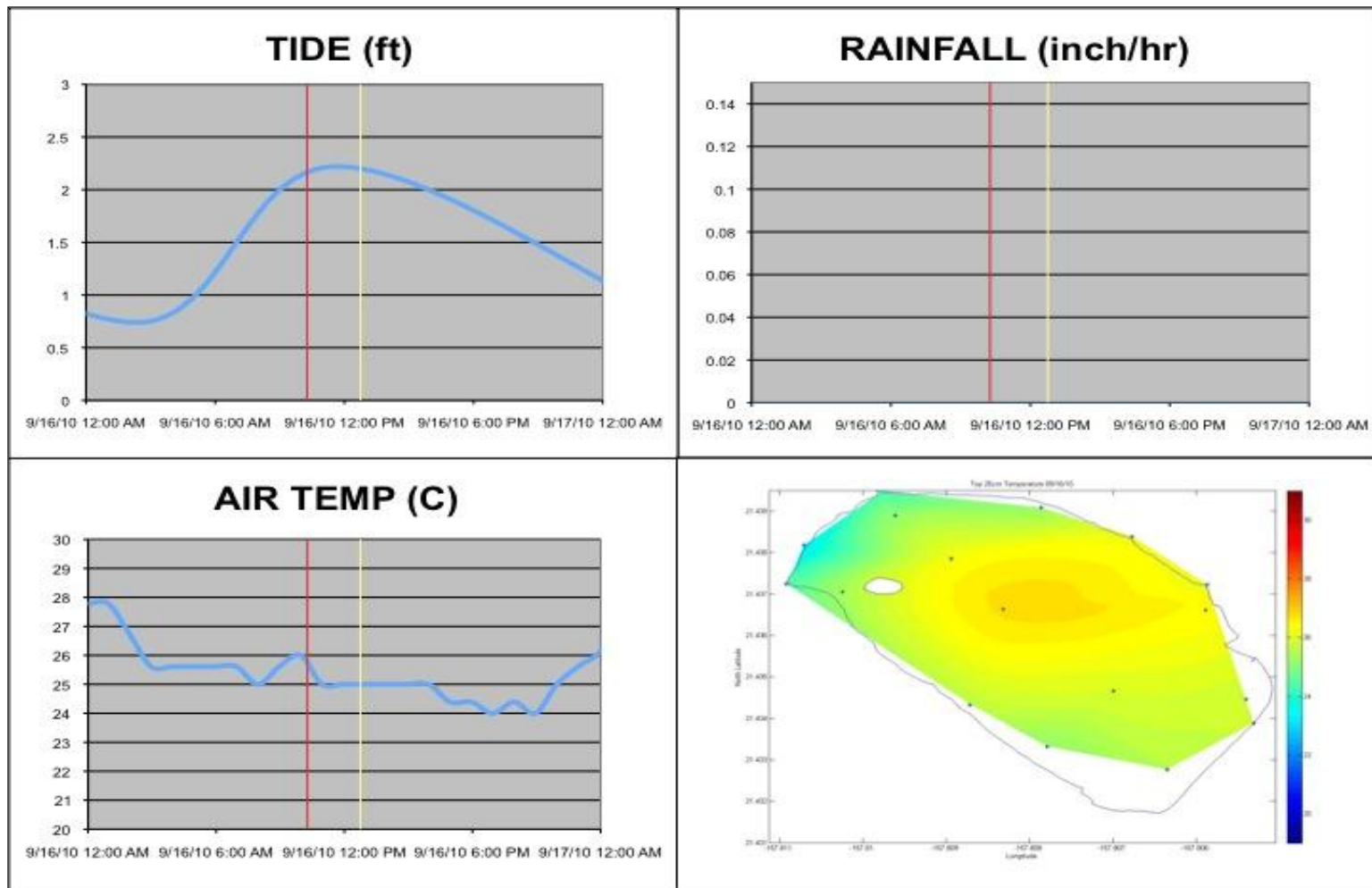
Figure 4.27: Tide, rainfall, and air temperature plots for the 9/17/2010 sampling (data from Mesowest.utah.edu), as well as the surface temperature contour plot from the YSI data. Red line indicates start of sampling, yellow line indicates end of sampling.
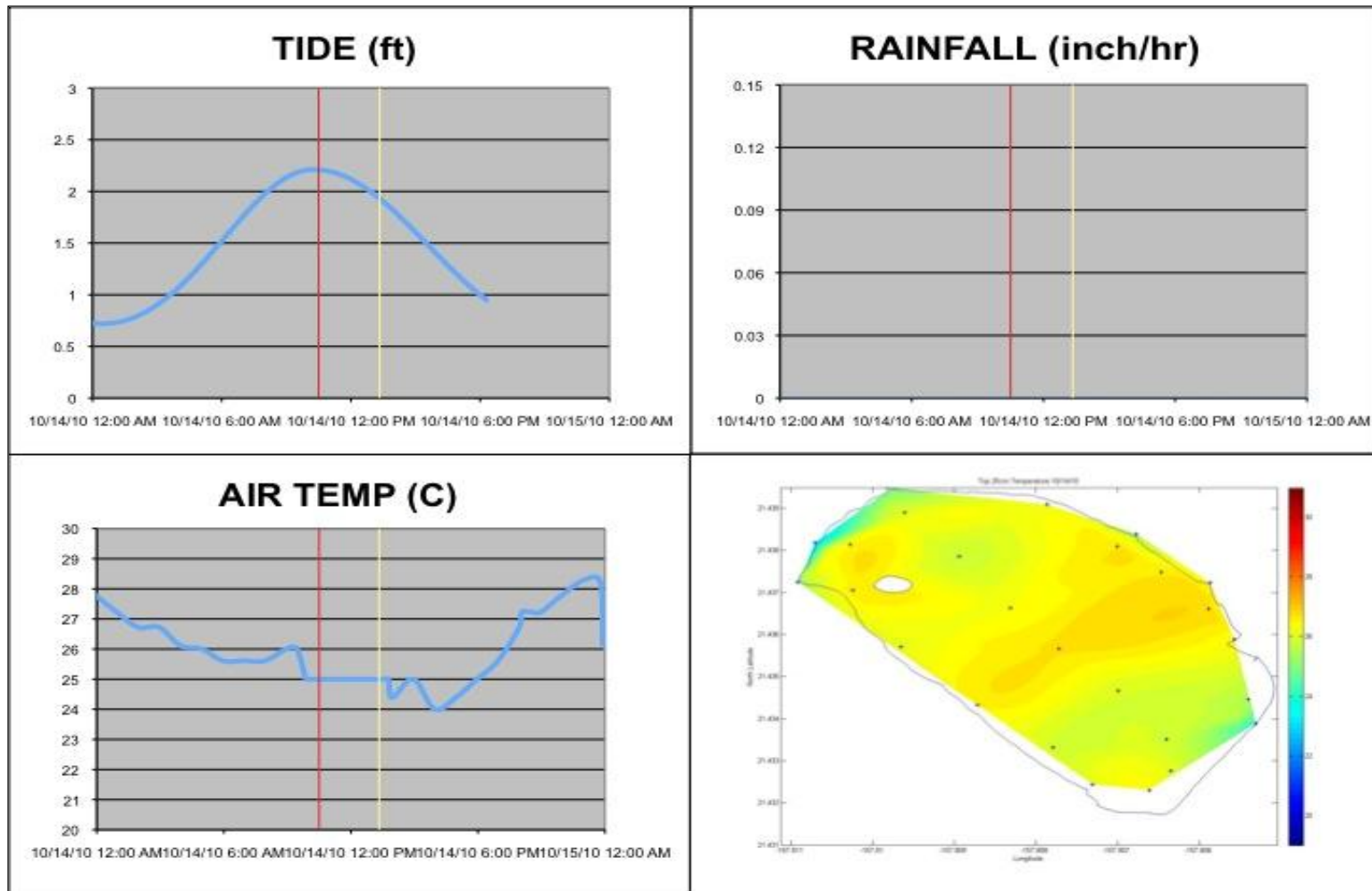
Figure 4.28: Tide, rainfall, and air temperature plots for the 10/14/2010 sampling (data from Mesowest.utah.edu), as well as the surface temperature contour plot from the YSI data. Red line indicates start of sampling, yellow line indicates end of sampling.

132
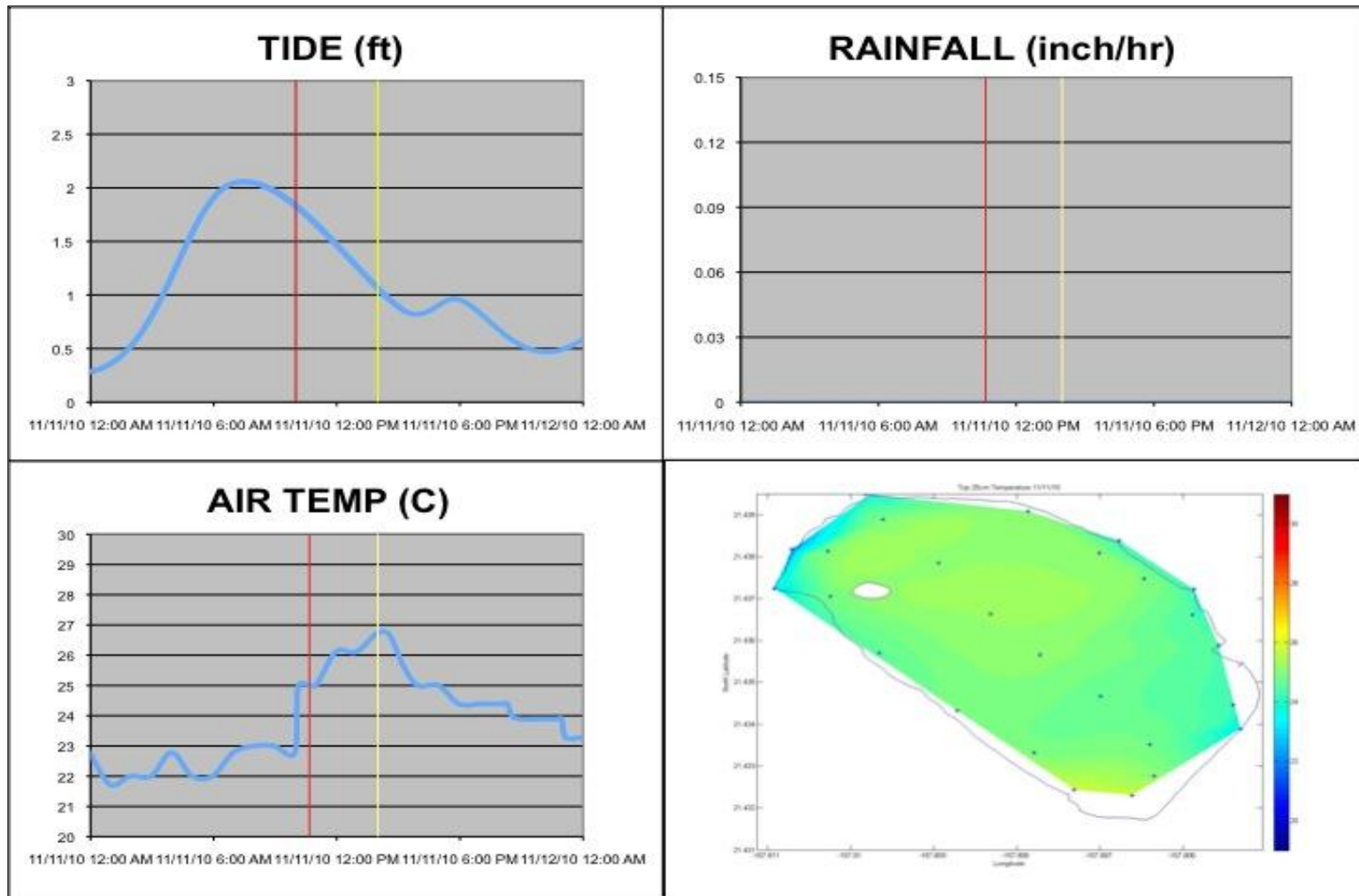
Figure 4.29: Tide, rainfall, and air temperature plots for the 11/11/2010 sampling (data from Mesowest.utah.edu), as well as the surface temperature contour plot from the YSI data. Red line indicates start of sampling, yellow line indicates end of sampling.
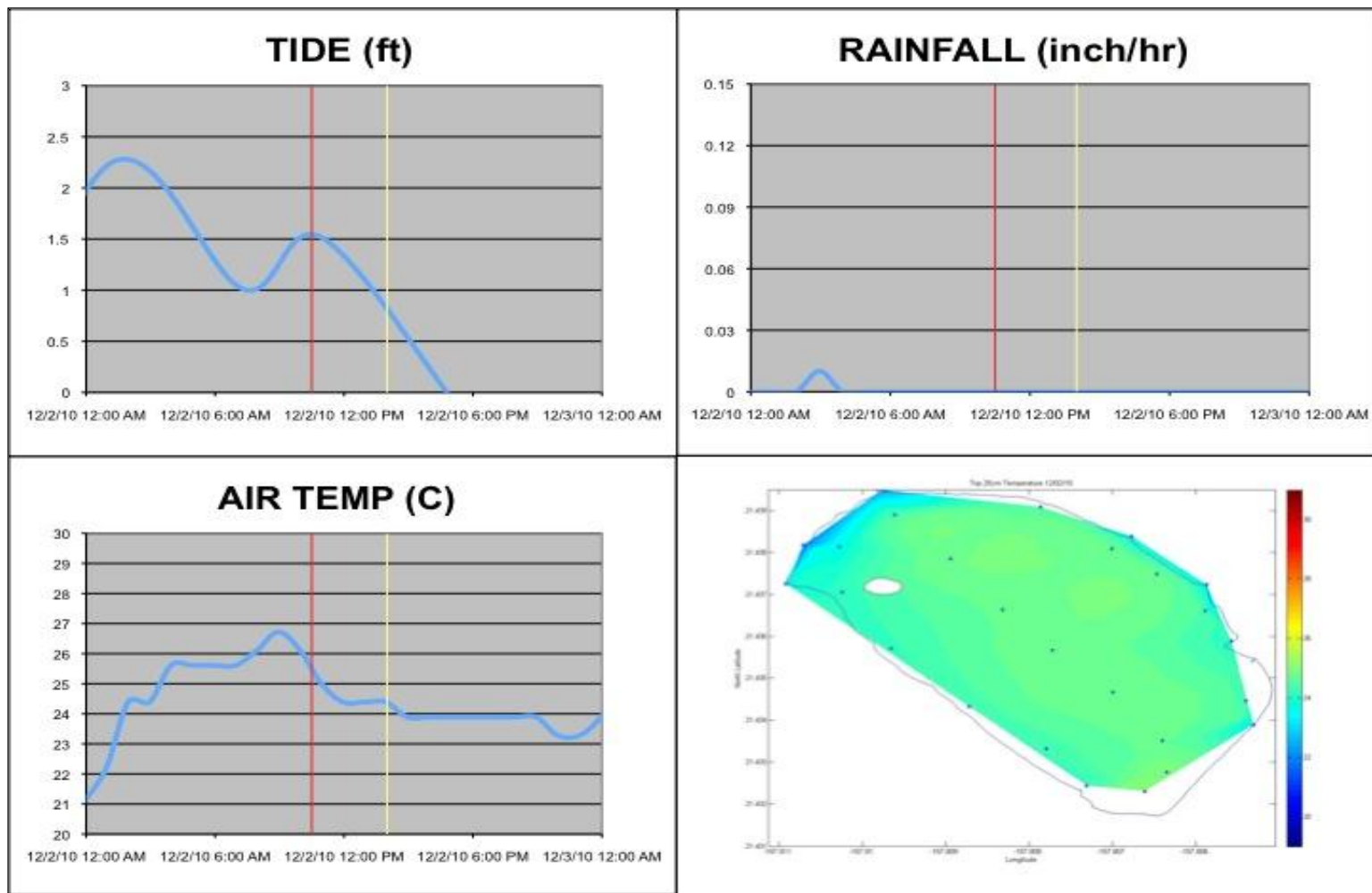
Figure 4.30: Tide, rainfall, and air temperature plots for the 12/02/2010 sampling (data from Mesowest.utah.edu), as well as the surface temperature contour plot from the YSI data. Red line indicates start of sampling, yellow line indicates end of sampling.
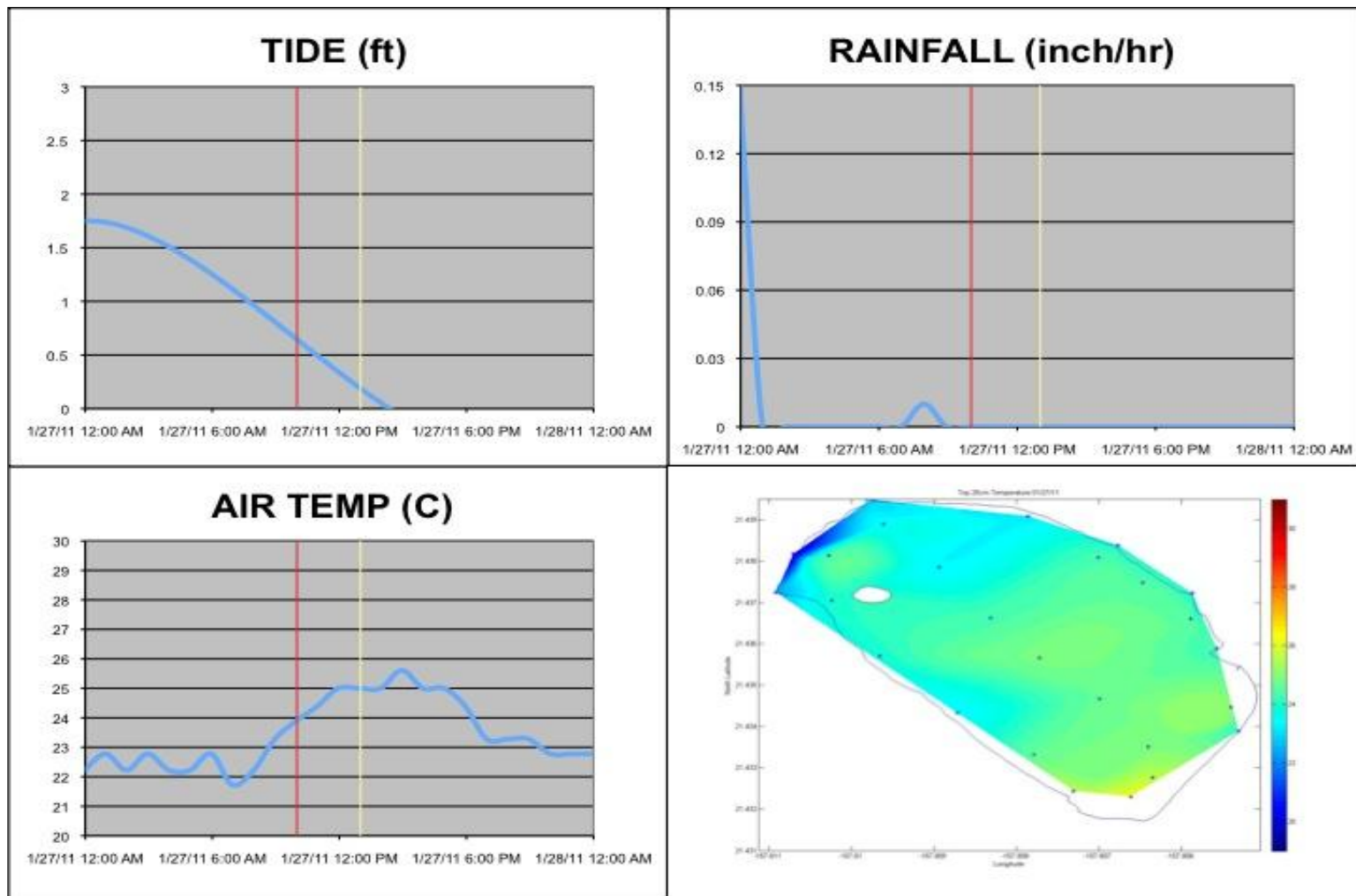
Figure 4.31: Tide, rainfall, and air temperature plots for the 1/27/2011 sampling (data from Mesowest.utah.edu), as well as the surface temperature contour plot from the YSI data. Red line indicates start of sampling, yellow line indicates end of sampling.

135

BIBLIOGRAPHY

Apple, R., and W. Kikuchi. 1975. *Ancient Hawaii Shore Zone Fishponds: An Evaluation of Survivors for Historical Preservation*. National Park Service, Dept. of Interior. Honolulu, HI.

Benjamin, Lindey. 2010. Characterization of the Physical Environment in He'eia Fishpond, O'ahu, Hawai'i. University of Hawaii at Manoa

Chu, Pao-Shin. 1995. Hawaiin Rainfall Anomalies and El Niño. Notes and Correspondence: 1697-1704

Costa-Pierce, B. A. 1987. Aquaculture in Ancient Hawaii. BioScience **37:** 320-330.

Henry, L. B. 1975. An Inventory and Status of Recognizable Fishponds Along the Kaneohe Bay Shoreline. University of Hawaii Urban and Regional Planning Program**:** 1-12.

---. 1993. *He'eia Fishpond (Loko I'a O He'eia): An Interpretive Guide for the He'eia State Park Visitor*. The State Foundation on Culture and the Arts and Ke'Alohi Press.

Jokiel, Paul. 2011. Jokiel's Illustrated Scientific Guide to Kane'ohe Bay, O'ahu. Kane'ohe: Hawaii Institute of Marine Biology.

Kelly, M. 1975. *Loko I'a o He'eia*, Second ed. Bernice Pauahi Bishop Estate.

Kikuchi, W. 1976. Prehistoric Hawaiian Fishponds. Science **193:** 295-299.

McPhadem, M.J., T. Lee, and D. McClurg. 2011. El Niño and Its Relationship to Changing Background Conditions in the Tropical Pacific Ocean. Geophysical Research Letters **38.**

Mesowest. 2011. University of Utah. Department of Atmospheric Sciences. www.mesowest.utah.edu

Noyes, T. James. 2011. El Niño. Oceanography **10 9B.1**

Okumura, Yuko, Masamichi Ohba, Clara Deser, and Hiroaki Ueda. 2011. A Proposed Mechanism for the Asymmetric Duration of El Niño and La Niña. Journal of Climate **24.**

Ostrander, C. E., M. A. Mc Manus, E. H. De Carlo, and F. T. Mackenzie. 2008. Temporal and Spatial Variability of Freshwater Plumes in a Semienclosed Estuarine-bay System. Estuaries and Coasts **31:** 192-203.

Price, Saul. 1983. Climate of Hawaii. National Weather Service Pacific Region Headquarters. http://prh.noaa.gov/hnl/pages/climate_summary.php

Sirvkatka, Paul. 2011. El Niño - Southern Oscillation. ENSO NOTES

YSI Incorporated. 2006. 6-Series Multiparameter Water Quality Sondes User Manual. Revision D. www.ysi.com

Young, Charles. 2011. Perturbation of Nutrient Inventories and Phytoplankton Community Composition During Storm Events in a Tropical Coastal System: He'eia Fishpond, O'ahu, Hawai'i. University of Hawaii at Manoa